

Eastern Kentucky University

Encompass

---

Online Theses and Dissertations

Student Scholarship

---

January 2019

## Influence Of Applied Potential And Metal Ion Concentraion On Metal Electrodeposition At Micron Gap Gold Electrodes

Krista Michel Riggins  
*Eastern Kentucky University*

Follow this and additional works at: <https://encompass.eku.edu/etd>

 Part of the [Physical Chemistry Commons](#)

---

### Recommended Citation

Riggins, Krista Michel, "Influence Of Applied Potential And Metal Ion Concentraion On Metal Electrodeposition At Micron Gap Gold Electrodes" (2019). *Online Theses and Dissertations*. 643.  
<https://encompass.eku.edu/etd/643>

This Open Access Thesis is brought to you for free and open access by the Student Scholarship at Encompass. It has been accepted for inclusion in Online Theses and Dissertations by an authorized administrator of Encompass. For more information, please contact [Linda.Sizemore@eku.edu](mailto:Linda.Sizemore@eku.edu).

INFLUENCE OF APPLIED POTENTIAL AND METAL ION CONCENTRAION ON METAL  
ELECTRODEPOSITION AT MICRON GAP GOLD ELECTRODES

BY

KRISTA MICHEL RIGGINS

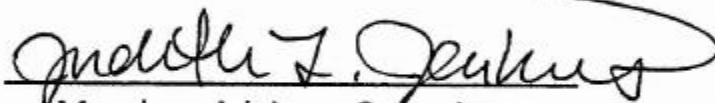
THESIS APPROVED:



D. Radlik

---

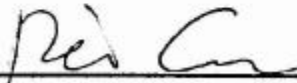
Chair, Advisory Committee



Matthew Z. Jenkins

---

Member, Advisory Committee



Peter C. ...

---

Member, Advisory Committee



Dean, Graduate School

---

Dean, Graduate School



INFLUENCE OF APPLIED POTENTIAL AND METAL ION CONCENTRAION ON METAL  
ELECTRODEPOSITION AT MICRON GAP GOLD ELECTRODES

BY

KRISTA MICHEL RIGGINS

Submitted to the Faculty of the Graduate School of  
Eastern Kentucky University  
in partial fulfillment of the requirements for the degree of

MASTER OF SCIENCE

2019

© Copyright by KRISTA MICHEL RIGGINS 2019  
All Rights Reserved.

## DEDICATION

I dedicate this thesis to my beloved husband, Joshua Riggins, who has supported, loved, and cared for me through this work. I could not have done this without your love, patience, and dedication to our marriage. You have been there since the beginning of this process and I would have never gotten through this without you being by my side. You have showed me what marriage is really about and I just want to thank you for all of the sacrifices you have made for me to pursue my dream of becoming a chemist. I would also like to dedicate this to my parents, David and Dana Harris, who have given me so much to expand my knowledge. You all have also given me so much love and support through my entire education. I would not be here and I would not have achieved this if you all did not push me and give me what I needed to complete this process. Thank you all so much. I would also like to dedicate this to my beloved grandparents, Henry and Naomi VonLinger, and Earl and Deva Harris, for always providing me with love and laughter. You all will forever be in my heart and forever be my best supporters.

## ACKNOWLEDGEMENTS

I would like to acknowledge my mentor, Dr. Radhika Dasari, for her encouragement and mentorship throughout this project, my committee, Dr. Judy Jenkins for her helpful feedback, and Dr. Pei Gao. I would also like to recognize my husband, Joshua Riggins, my parents, David and Dana Harris, my sisters, Lexi and Holli, and my beloved grandparents. Thank you to Eastern Kentucky University for letting me use their facility to do this work.

## ABSTRACT

Zamborini and Coworkers developed, a simple, low cost, and highly parallel electrochemical approach for fabricating nano-scale (metal/metal) or molecular (metal/polymer or self-assembled monolayer (SAM)/metal) junctions that should be useful in preparing working sensors and molecular electronic devices. The fabrication of metal/metal junctions involves metal deposition on one set of electrodes (E1), where the metal grows and becomes connected to a second set of electrodes (E2) of an Au interdigitated array of electrodes with a 5  $\mu\text{m}$  separation. However, when different metals were deposited, they deposited in different fashions. Ag grew in the form of wires and Pd deposited in the form of dendrites. Here we investigated the factors such as applied potential and metal ion concentration on the morphology of the metal electrodeposition across the micron gap electrodes.

## TABLE OF CONTENTS

CHAPTER	PAGE
I. Introduction .....	1
1.1 Main Goal/Summary .....	1
1.2 Motivation/Objective .....	1
1.3 Importance of Nanomaterials .....	1
1.4 Synthesis of 1-D Metal Nanostructures .....	4
II. Experimental .....	10
2.1 Chemicals and Substrates .....	10
2.2 Techniques and Experimental Set-Up .....	11
2.3 Procedures .....	14
2.4 Procedures for preparing various solutions.....	22
III. Ag Electrodeposition .....	25
IV. Pd Electrodeposition.....	45
V. Future Direction.....	62
References .....	63
Appendix .....	87
A. i-V curve graphs before and after metal electrodeposition.....	88

## LIST OF TABLES

TABLE	PAGE
2.1 Different conditions where Ag electrodeposition was performed .....	22
2.2 Different conditions where Pd electrodeposition was performed.....	22
3.1 Time for electrodepositing of Ag at a charge of $6 \cdot 10^{-5}$ C from a solution containing different concentrations of AgNO <sub>3</sub> at various applied potentials .....	34
3.2 Average times for electrodepositing Ag at a charge of $6 \cdot 10^{-5}$ C from a solution containing different concentrations of AgNO <sub>3</sub> at various applied potentials.....	35
3.3a Currents observed at -1 V in air before and after electrodepositing Ag at various potentials from 0.5 mM AgNO <sub>3</sub> solution .....	38
3.3b Currents observed at -1 V in air before and after electrodepositing Ag at various potentials from 5 mM AgNO <sub>3</sub> solution .....	38
3.3c Currents observed at -1 V in air before and after electrodepositing Ag at various potentials from 50 mM AgNO <sub>3</sub> solution .....	39
3.4 Ag connections made or not at different applied potentials and concentrations between the micron gap Au electrodes.....	40
4.1 Time for electrodepositing of Pd at a charge of $1.2 \cdot 10^{-3}$ C from a solution containing different concentrations of K <sub>2</sub> PdCl <sub>4</sub> at various applied potentials.....	51
4.2 Average times for electrodepositing of Pd at a charge of $1.2 \cdot 10^{-3}$ C from a solution containing different concentrations of K <sub>2</sub> PdCl <sub>4</sub> at various applied potentials .....	51

4.3a Currents observed at -1 V before and after electrodeposition of Pd at various applied potentials from 0.5 mM $K_2PdCl_4$ solution.....	54
4.3b Currents observed at -1 V before and after electrodeposition of Pd at various applied potentials 5 mM $K_2PdCl_4$ solution .....	55
4.3c Currents observed at -1 V before and after electrodeposition of Pd at various applied potentials from 50 mM $K_2PdCl_4$ solution.....	55
4.4 Pd ion concentration and applied potentials that lead to the formation of Pd connection between the micron gap Au IDA electrodes.....	56

## LIST OF FIGURES

FIGURE	PAGE
1.1 Pictorial representation showing increase in surface area as the size decreases.....	2
1.2 Pictorial representations showing metal nanoparticles of different structures: a) sphere, b) hexagon, c) cubes, d) triangles, e) branches, f) rods and g) bipyramids. ....	3
1.3 Pictorial representation showing 1-D metal nanostructures: a) nanorods, b) nanobelts, c) nanotubes and d) NWs. ....	4
1.4 Bottom up method for synthesizing nanomaterials by either chemical or electrochemical reduction .....	5
1.5 Pictorial representation showing steps involved in synthesis of 1-D nanostructures in porous polycarbonate membrane .....	6
1.6 Pictorial representation showing steps involved in electrochemical synthesis of 1-D nanostructures at highly oriented pyrolytic (HOPG) .....	7
1.7 Schematic representation of metal electrodeposition from simple salt solution.....	9
2.1 Image showing the conventional three-electrode setup for metal electrodeposition	13
2.2 Image showing two electrode setup for obtaining CV in air. ....	14
2.3 Steps involved in wiring and cleaning the electrodes .....	15
2.4 CV of bare Au IDA in 0.1M H <sub>2</sub> SO <sub>4</sub> vs Ag/AgCl reference electrode.....	16
2.5 CV of Au IDA electrode in 5 mM AgNO <sub>3</sub> in 0.1 M H <sub>2</sub> SO <sub>4</sub> at a scan rate of 100mV/s (scan direction negative to positive). ....	18

2.6 CV of Au IDA electrode in 5 mM $K_2PdCl_4$ in 0.1 M $H_2SO_4$ at a scan rate of 100 mV/s (scan direction negative to positive). .....	19
2.7 Cartoon depicting electrodeposition and stripping.....	20
2.8 Chronocoulometric graph showing Ag electrodeposition from solution containing 5 mM $AgNO_3$ in 0.1 M $H_2SO_4$ at -0.3 V vs. Ag wire reference electrode .....	21
2.9 Chronocoulometric graph showing Pd electrodeposition from solution containing 5 mM $K_2PdCl_4$ in 0.1 M $H_2SO_4$ at -0.1 V vs. Ag/AgCl reference electrode. ....	21
3.1 Overlay plot of chronocoulometric graphs showing Ag electrodeposition from solution containing different concentrations of $AgNO_3$ at a) -0.1 V, b) -0.2 V, c) -0.3 V, d) -0.4 V, and e) -0.5 V vs. Ag wire .....	30
3.2 Overlay plot of chronocoulometric graphs showing electrodeposition at various applied potential vs. Ag wire from solution containing a) 0.5 mM, b) 5 mM, and c) 50 mM $AgNO_3$ . ....	32
3.3 Overlay plot of CV of Au IDA electrode in air before and after Ag electrodeposition at -0.1 V potential from a) 0.5 mM, b) 5 mM and c) 50 mM $AgNO_3$ solution. ....	36
3.4 Scheme showing the diffusion layer structure that leads to the formation of a) no connection and b) connection between micron-gap Au IDA electrode. ....	42
4.1 Overlay plot of chronocoulometric graphs showing electrodeposition of Pd from solution containing different concentrations of $K_2PdCl_4$ at a) +0.1 V, b) 0.0 V, c) -0.1 V, d) -0.2 V, and e) -0.3 V vs. Ag/AgCl reference electrode. ....	47

4.2 Overlay plot of chronocoulometric graphs showing Pd electrodeposition at various applied potential vs. Ag/AgCl reference electrode from solution containing: a) 0.5 mM, b) 5 mM, c) 50 mM  $K_2PdCl_4$ ..... 49

4.3 Overlay plot of CV of Au IDA electrode in air before (black lines) and after (red lines) Pd electrodeposition at +0.1V potential from A) 0.5 mM, B) 5 mM and C) 50 mM  $K_2PdCl_4$  solution. .... 53

## I. Introduction

### **1.1. Main Goal/Summary:**

The main goal of this research was to understand the impacts of applied potential and metal ion concentration on metal electrodeposition on and across micron-gap gold (Au) electrodes.

This dissertation is divided into five main parts. Chapter I is the introduction and Chapter II describes the experimental procedure for the metal electrodeposition. Chapter III describes influence of applied potential and metal ion concentration on silver (Ag) electrodeposition at micron gap Au electrodes. In Chapter IV we describe influence of applied potential and metal ion concentration on palladium (Pd) electrodeposition at micron gap Au electrodes. Chapter V describes future directions for this project.

### **1.2 Motivation/Objective:**

The majority of this work was motivated by the need to understand the factors that affect the morphology of metal electrodeposition at micron gap electrodes. This in turn aids in the development of a simple, fast, and reliable method which would eliminate the use of costly and fancy lithography techniques involved in the fabrication of different functional electronic devices using metal nanostructures as the basic components.

### **1.3 Importance of Nanomaterials**

Nanomaterials are materials that have at least one dimension that is less than approximately 100 nanometers.<sup>1</sup> Due to their small size, nanomaterials have a high

surface to volume ratio as shown in Figure 1.1.<sup>2</sup> This indicates large number of atoms are present on the surface. Surface atoms are more active chemically as they have less adjacent coordinate atoms and unsaturated sites.<sup>3</sup> Hence, nanomaterials exhibit different properties than that of their bulk counterpart.<sup>1</sup> These properties include but are not limited to the following: size-dependent excitation or emission,<sup>4</sup> catalytic,<sup>5-6</sup> electrochemical,<sup>7-8</sup> thermal,<sup>9</sup> and electronic.<sup>10</sup>

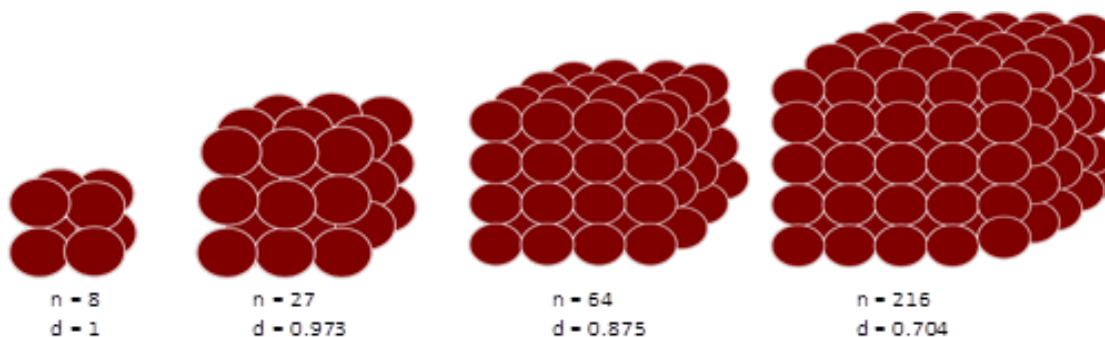


**Figure 1.1.** Pictorial representation showing increase in surface area as the size decreases. Surface-to-volume ratio (d) based upon the number of atoms (n).

Nanomaterials can be made out of several different substances such as carbon,<sup>11-12</sup> polymers,<sup>13</sup> semiconductors,<sup>14-16</sup> biological molecules,<sup>17</sup> and metals.<sup>18</sup> Carbon nanomaterials exhibit unique properties such as the following: are light in weight but strong and hard, can act as a conductor, semi-conductor or insulator, black body.<sup>11</sup> Carbon nanomaterials are also applicable in chemical biosensing.<sup>19</sup> Polymeric nanomaterials, are used in drug delivery systems.<sup>13</sup> Semiconductor nanomaterials have continuous absorption bands, high chemical stability and surface functionality.<sup>14-15</sup> They are used in nano-electronics, energy conversion, and detectors.<sup>16</sup> Bio-molecule nano-

particles are used in many hybrid systems for sensing, synthesis, and fabrication of nano-scale devices.<sup>17</sup>

This research mainly focuses on nanomaterials made of metal. Metal nanomaterials exhibit unique properties such as magnetic, optical and surface Plasmon resonance.<sup>20</sup> For instance, Au solution is golden yellow in color, but solution containing 20nm Au nanospheres has red ruby color and 200nm nanospheres has bluish color.<sup>21</sup> Due to their interesting properties, metal nanomaterials can be used in various applications like fluorescence,<sup>22</sup> sensing,<sup>23</sup> waveguides,<sup>24</sup> surface enhanced Raman spectroscopy,<sup>25</sup> and therapeutics.<sup>26</sup> Portable sensors based on metal nanomaterials for monitoring heavy metals are also reported.<sup>22</sup> Metal nanomaterials exhibit properties which include the following: mechanical,<sup>27</sup> magnetic,<sup>28</sup> catalytic,<sup>29</sup> optical,<sup>30</sup> and electrical.<sup>31</sup> However, this research really focuses on the electrical properties of metal nanomaterials.

Metal nanomaterials can have difference structures such as sphere, hexagon, cubes, triangles, branches, rods and bipyramids (See Figure 1.2).<sup>32</sup> One-dimensional (1-D) metal nanostructures are the interest of this research. 1-D nanostructures are nanostructures where one of the dimensions is outside the nanoscale.<sup>32</sup>

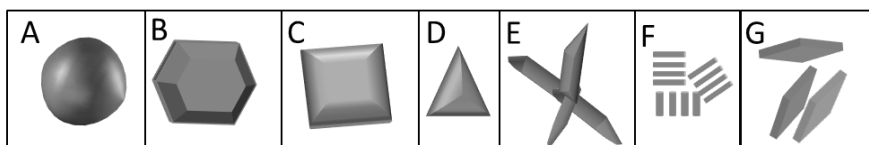


**Figure 1.2.** Pictorial representations showing metal nanoparticles of different structures: a) sphere, b) hexagon, c) cubes, d) triangles, e) branches, f) rods and g) bipyramids.

1-D nanostructures include nanorods,<sup>33</sup> nanobelts,<sup>34</sup> nanotubes,<sup>35</sup> and nanowires (NWs) as shown in Figure 1.3.<sup>36</sup> 1-D nanostructures are used in several applications which include the following: building blocks for circuits,<sup>37</sup> field effect transistors for logic circuits,<sup>38</sup> waveguides,<sup>39</sup> cancer therapy,<sup>40</sup> drug delivery,<sup>41</sup> catalysis,<sup>42</sup> biological sensors,<sup>43</sup> optical sensing,<sup>44</sup> and chemical sensors.<sup>45</sup>

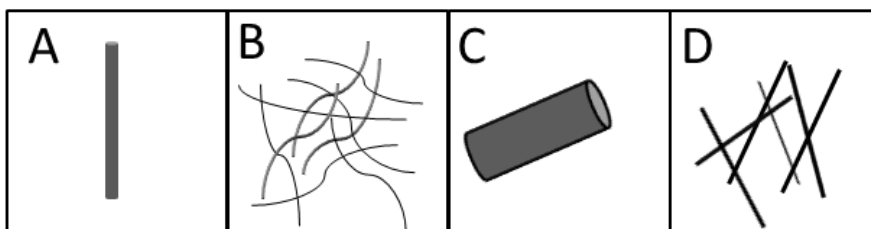


**Figure 1.3.** Pictorial representation showing 1-D metal nanostructures: a) nanorods, b) nanobelts, c) nanotubes and d) NWs.

#### **1.4 Synthesis of 1-D Metal Nanostructures**

Several scientists have reported different methods for synthesizing 1-D metal nanostructures.<sup>46,47</sup> Generally, metal nanostructures synthesis methods can be broadly classified into two methods. The first method is called the top down method. In this method, advance nano-lithographic techniques such as electron beam, focused ion beam writing, proximal probe patterning, x-ray or extreme UV lithography are used to shrink the size of the bulk material to the desired size and shape of the nanostructure.<sup>48</sup> UV lithography is used in making printed circuits and computer boards.<sup>49</sup> These methods are energy intensive and require expensive equipment and facilities. The top down method cannot be used on a wide range of materials and cannot be used for synthesis of large quantities.<sup>50</sup> The second method is called the bottom up method, see Figure 1.4.

In this method of synthesis, solution metal ions are reduced to solid until the solid reaches a desired size and shape. By using a reducing agent, metal ion reduction can either be done chemically<sup>51</sup> or electrochemically.<sup>52</sup>

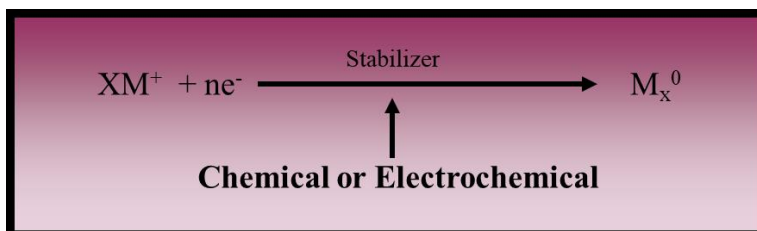


**Figure 1.4.** Bottom up method for synthesizing nanomaterials by either chemical or electrochemical reduction.  $M^+$  represents metal ion, stabilizer serves as the capping agent, and  $ne^-$  is the number of electrons.

Compared to top down method, bottom up method has several advantages such as, better control of size and size distribution of nanoparticles, produces nanoparticles of higher monodispersity and leads to higher concentration.<sup>53</sup> This method is also simple, cost effective, and less tedious relative to the top down method.<sup>53</sup> This research focuses on the bottom up synthesis and electrochemical method for metal ion reduction.

1-D metal nanostructure synthesis in solution (soft template) and hard templates are reported in literature.<sup>46-47</sup> In soft-template method, metal ion is reduced in the presence of capping agent or structure directing molecules such as surfactants, polymers, or ionic species.<sup>54</sup> Structure directing molecules prevent nanomaterial aggregation.<sup>55</sup> They also aid in synthesizing a particular shape of nanostructure either by inhibiting the growth of certain metallic crystals or alter the transport of reagents to certain crystallial faces.<sup>56</sup>

Examples of these capping agents include cylindrical micelles,<sup>57</sup> block copolymers,<sup>58</sup> DNA molecules,<sup>59</sup> and cetyltrimethylammonium bromide (CTAB) surfactant.<sup>60</sup>

In hard template method, the nanostructures growth is restricted within a template.

These templates are usually made up of inorganic or polymer materials.<sup>61-63</sup> Mallouk and coworkers electrodeposited Ag in a porous polycarbonate membrane template to synthesize metal NWs.<sup>61</sup> The size of the NW is related to the pore size of the membrane. Synthesis of NWs of different metal segments, as shown in Figure 1.5, was also reported.

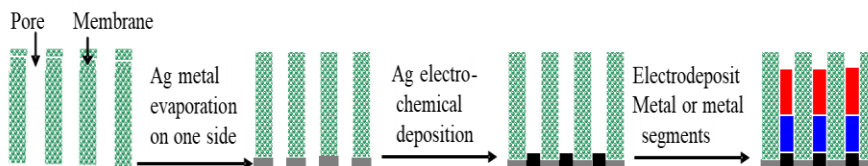


**Figure 1.5.** Pictorial representation showing steps involved in synthesis of 1-D nanostructures in porous polycarbonate membrane.

Penner and coworkers electrodeposited Pd on a highly oriented pyrolytic graphite (HOPG) template to form Pd NWs (see Figure 1.6).<sup>62</sup> To understand why this substrate led to the formation of NWs instead of conformal metal slabs, it is important to consider the different chemical environments of the HOPG surface atoms. HOPG has step edges. These step edges serve as defect sites, and are energetically favorable for the metal electrodeposition.<sup>63</sup> The size of the NWs depends on the size of the step edge of the graphite.

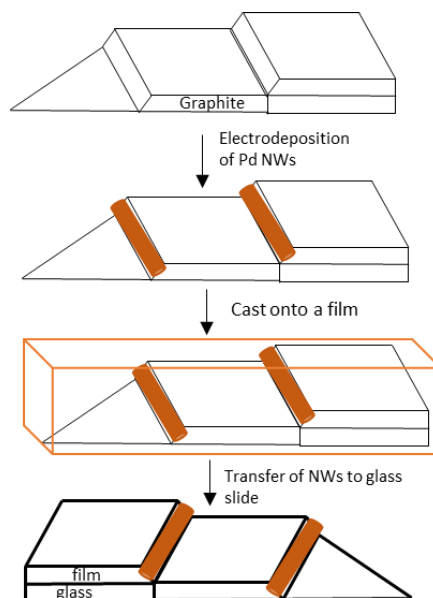


**Figure 1.6.** Pictorial representation showing steps involved in electrochemical synthesis of 1-D nanostructures at highly oriented pyrolytic graphite (HOPG).

The electrochemical methods described above are great for synthesizing metal nanostructures. However, they suffer from several issues with the post-synthesis assembly of the 1-D nanostructures on the desired substrate. . Some of the issues that arise in soft template method are as follows: aggregation of nanostructures, removal of impurities, and transferring the nanostructures on to a desired surface. Whereas in hard template-based methods, the template may need to be removed and/or the nanostructures may need to be transferred to a different substrate to afford device functionality. In either method, once the nanostructures are transferred on to the desired surface, to fabricate an electronic device using 1-D nanostructures, contacts have to be made to the nanostructures.

Different strategies have been reported in the literature for fabricating contacts to nanomaterials in nano-electronic devices.<sup>64-66</sup> These strategies can be generally

classified into two methods: i) where 1-D nanostructures are assembled on a surface first and then the contacts are made<sup>64</sup> and ii) where the 1-D nanostructures are assembled on prefabricated contacts.<sup>65-66</sup> Fabrication of contacts using electron-beam lithography<sup>64</sup> and applying Ag paint manually on the nanostructures are few examples where contacts are made after transferring the nanostructures on to the substrate.<sup>68</sup> Electron-beam lithography is a common way to make contacts, however the process is expensive and tedious.<sup>64</sup> Making reproducible contacts is a challenge when Ag paint manually is applied manually.<sup>67</sup> Nanostructures are assembled on pre-fabricated electrodes either mechanically<sup>65</sup> or with the aid of electric field.<sup>66</sup> The above described methods suffer from making reproducible contacts. To avoid this issue, nanostructures are grown directly at prefabricated electrodes using in-situ-electric field,<sup>68</sup> field emission<sup>69</sup> and electrochemical methods.<sup>70</sup> Electrochemical method is relatively simple, easy to use and is less expensive. Other than Zamborini and coworkers, all the other methods reported used either ion-beam or electron-beam lithography for the fabrication of electrodes.<sup>71</sup> Zamborini and coworkers used photolithography, which is less expensive and highly parallel.<sup>72</sup> Zamborini and coworkers reported electrodeposition of Pd nanostructures and Ag NWs across 5-micron gap interdigitated array (IDA) of Au electrodes fabricated using photolithography. Generally in electrodeposition metallic ions from an electrolyte are reduced to form a solid deposit at the cathode. Metal electrodeposition was performed from simple salt solution in the method reported by Zamborini and coworkers.<sup>73</sup> Figure 1.7 shows the mechanism of

metal electrodeposition from simple salt solutions. In simple salt solution, metal ions exist as hydrated ions. Under the influence of applied field, hydrated ions travel towards cathode. Once they reach the diffusion layer, water molecules align, followed by the removal of water molecules in the Helmholtz layer.

Later, metal ions adsorb at the cathode surface as adatoms which then diffuse on the surface of the cathode and are incorporated into the crystal lattice at the growth point which is where the metal ion is reduced to solid metal. This approach is beneficial as it is simple, versatile, and can quickly prepare NW contacts to any metal, metal oxide or polymer that can be electrodeposited. However, in order to controllably electrodeposit metal electrodes across micron gap electrodes with specific morphologies, it is necessary to determine the impacts of deposition potential and metal ion concentration on the morphology of electrodeposited electrodes, motivating the work described here. Here, we investigated the impact of applied potential and metal ion concentration on metal electrodeposition on and across prefabricated 5 micron-gap Au IDAs.

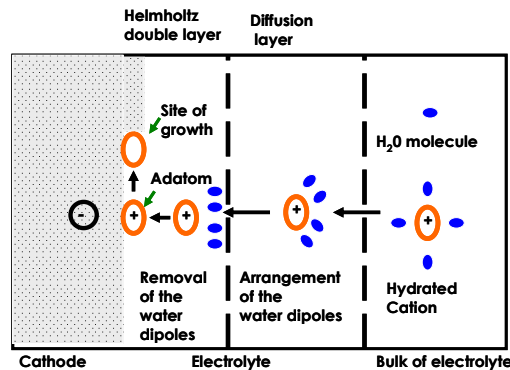


**Figure 1.7.** Schematic representation of metal electrodeposition from simple salt solution.

## II. Experimental

This chapter includes the following four parts: 1) chemicals and substrates used, 2) techniques and experimental set-up used to electrodeposit Ag and Pd, and 3) procedures for Ag and Pd electrodeposition and 4) procedure for preparing various solutions for electrodeposition.

### **2.1 Chemicals and Substrates:**

Chemicals used in this study were as follows: Ag nitrate ( $\text{AgNO}_3$ ) (99%), Potassium tetrachloropalladate ( $\text{K}_2\text{PdCl}_4$ ) (98%), sulfuric acid ( $\text{H}_2\text{SO}_4$ ) (96.0%), isopropanol (99.7%), ethanol (99.8%), nanopure water, and acetone (99.9%), which were purchased from Sigma-Aldrich. Ag epoxy was purchased from Silver ink-HV, Stan Rubinstein Assoc. Inc., Foxboro MA. Loctite E-90FL Hysol epoxy adhesive was purchased from Home Depot. Pt wire, Ag/AgCl (saturated KCl solution) reference electrode and Ag wire quasi reference electrode was purchased from CHI instruments.

In this study, 5 micron gap Au IDA of electrodes were used as substrates for electrodeposition of different metals. The Au IDA electrodes were microfabricated in a cleanroom using photolithography, sputtering and liftoff processes.<sup>74</sup>

**Fabrication of Au IDA's:** The Au IDA electrodes were microfabricated in a cleanroom using photolithography, sputtering and liftoff processes. Photolithography permits one to form a certain pattern of Au IDA electrodes on the silicon/silicon oxide (Si/SiO) substrate.<sup>74</sup> Si was heated to form an  $\text{SiO}_2$  or  $\text{SiO}_x$  layer. Later, hexamethyldisilane

(HMDS) and positive resist were spin coated respectively. Positive resist is a polymer which is relatively insoluble in the developer. However, exposure to light increases its solubility in developer. On the other hand, negative resist's solubility decreases after exposure to light. An aligner is used to align the mask that contains the desired pattern of the electrodes with the wafer to transfer the pattern from the mask to the wafer. The photoresist was exposed through the pattern of the mask to a high intensity UV-light. The wafer was then immersed in developer followed by rinsing with DI water and drying under a N<sub>2</sub> gun. Finally, a hard bake at 115°C for 2.5 min was performed to harden the photoresist and improve adhesion to the wafer. An argon (Ar<sup>+</sup>) ion source was used to sputter Cr, Ti or Ni targets as adhesion layers, followed by Au to form Au IDA electrodes. The photoresist and parts of Au sputtered on top of the photoresist were removed by immersing the Au-coated wafer in an acetone shaking bath for a few hours. Removal of the photoresist and metal on top leaves the patterned Au IDA electrodes on the Si/SiO<sub>x</sub>. This is known as lift-off. Finally, the wafer was diced to separate the individual electrode devices for further use.

### ***2.2 Techniques and Experimental Set-Up:***

All electrochemical measurements were performed using a CHI Instrument electrochemical work station. Following techniques were used in this study: a) cyclic voltammetry (CV) and b) chronocoulometry (CC).

**CV:** CV was used to determine the electrochemical deposition (reduction) potentials for Ag and Pd on Au and to measure Au IDA electrodes resistance before and after metal

electrodeposition (Ag and Pd). In CV method, potential is scanned and the current is monitored.

**CC:** CC was used to perform the metal electrodeposition. CC is an electrochemical technique in which the potential of the working electrode is stepped and the number of coulombs passed at the electrode are monitored as a function of time. This technique was used for the controlled deposition of Ag and Pd onto the Au IDA electrodes. The potential of the working electrode was stepped to a potential negative enough to reduce  $\text{Ag}^+$  or  $\text{Pd}^{2+}$  tetrachloride onto the Au IDA.

#### **Electrochemical Setup:**

**Three-electrode setup:** CV for determining potential for metal reduction/deposition and CC for metal deposition were performed using typical three electrode setup (See Figure 2.1). These experiments were performed at room temperature with a 5 micron gap Au IDA working electrode, Pt wire counter electrode and Ag wire reference electrode for Ag electrodeposition studies and Ag/AgCl in saturated potassium chloride (KCl) reference for Pd electrodeposition studies. Ag/AgCl reference electrode cannot be used in Ag studies. This is because Ag/AgCl reference electrode constitutes Ag wire coated with AgCl which is stored in KCl solution. Cl ions from the reference electrode can leak through the frit into the  $\text{AgNO}_3$  solution from which Ag is electrodeposited and result in the formation of AgCl precipitate (ppt). This would alter the Ag concentration in the  $\text{AgNO}_3$  solution.

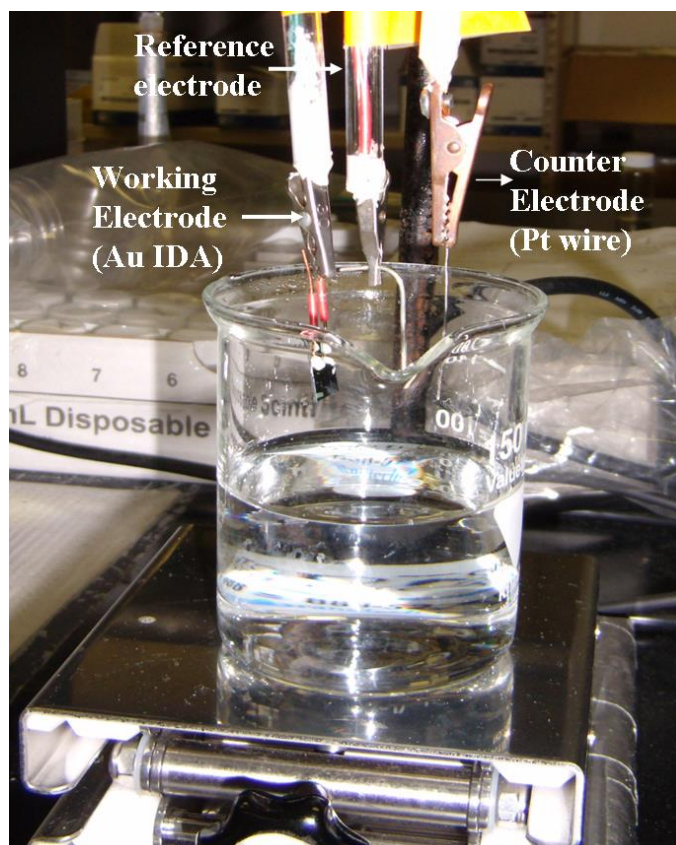


**Figure 2.1** Image showing the conventional three-electrode setup for metal electrodeposition. All three electrodes are suspended above 5 mM  $\text{AgNO}_3$  solution dissolved in 0.1 M sulfuric acid ( $\text{H}_2\text{SO}_4$ ). Electrodes should be submerged in solution before acquisition of the CV. The three electrodes pictured are as follows: reference (AgCl wire), counter (Pt wire), and working (Au IDA).

**Two-electrode setup:** CVs in air or i-V curves for measuring the resistance of electrodes were obtained using two-electrode setup. Here, the reference (white) and the counter (red) electrode cables were clamped together and is connected to one wire lead of the Au IDA. The working electrode cable (green) is connected to the other lead (see Figure 2.2 for setup). All the i-V curves in air were obtained in a Faraday cage.

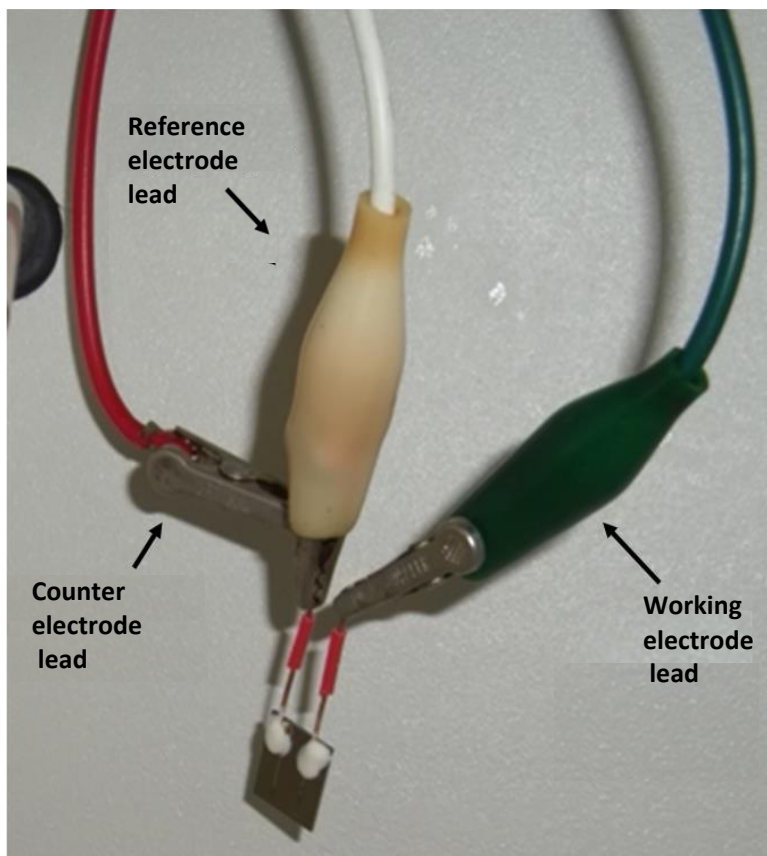


**Figure 2.2.** Image showing two electrode setup for obtaining CV in air. Pictured is the reference electrode cable hooked to the counter electrode cable, which is then connected to one of the wire leads attached to the Au IDA, while the working electrode cable is connected to the other wire lead attached to the Au IDA.

### **2.3 Procedures:**

**Wiring and cleaning of electrodes:** Prior to electrodeposition, Au electrodes were cleaned and wired. Electrodes were cleaned with different solvents. The solvents were as follows: isopropanol (99.7%), ethanol (99.8%), nanopure water, and acetone (99.9%). Each solvent was sprayed from a solvent wash bottle on each electrode for approximately one minute and then air dried. After solvent cleaning, wire leads were

attached to the electrode contact pads. These leads were attached with Ag epoxy and then left to dry in air for at least 24 hours. After Ag epoxy had dried and solidified, an insulating epoxy was applied over the contact pads. Once dried, the electrodes were rinsed with the solvents again and Ozone cleaned for 15 minutes. The steps involved for the cleaning and wiring process of the electrodes are shown in Figure 2.3. Solvent and ozone cleaning are used to remove any organic residues on the Au IDA due to photolithography process.

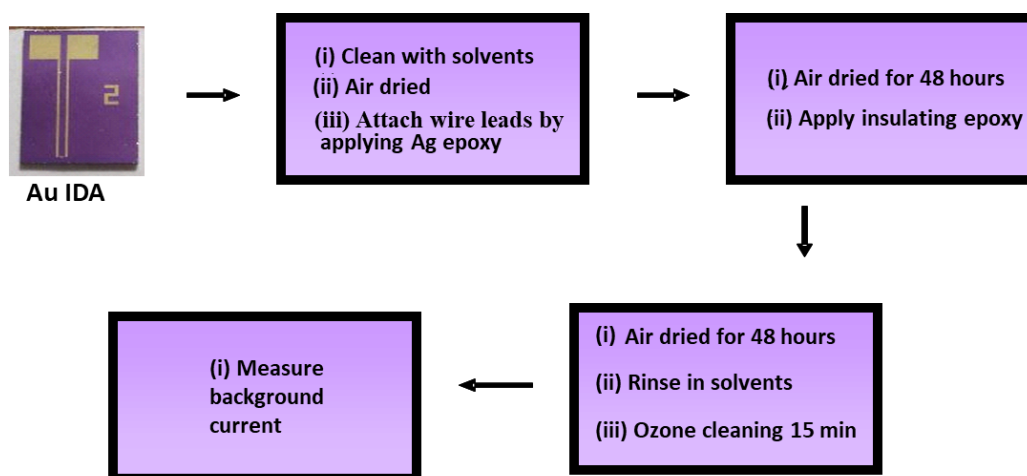


**Figure 2.3.** Steps involved in wiring and cleaning the electrodes.

Organic residues soluble in the solvents are washed away during solvent cleaning. Ozone ( $O_3$ ) is highly reactive gas. Hence, it continually converts back to its most stable form oxygen ( $O_2$ ) by releasing one of its atoms. During this process, it will oxidize any organic matter that it is in contact. A well-pronounced oxidation and reduction peak for Au indicates the cleanliness of the Au surface (See Figure 2.4). The peaks at  $\sim 1.0$  V and  $\sim 0.6$  V represent the Au oxidation and reduction peak, respectively.

If there is any organic residue from the photolithography process on the surface of the Au IDA's after solvent and ozone cleaning, it would hinder electron transfer and redox peaks for Au would not be observe

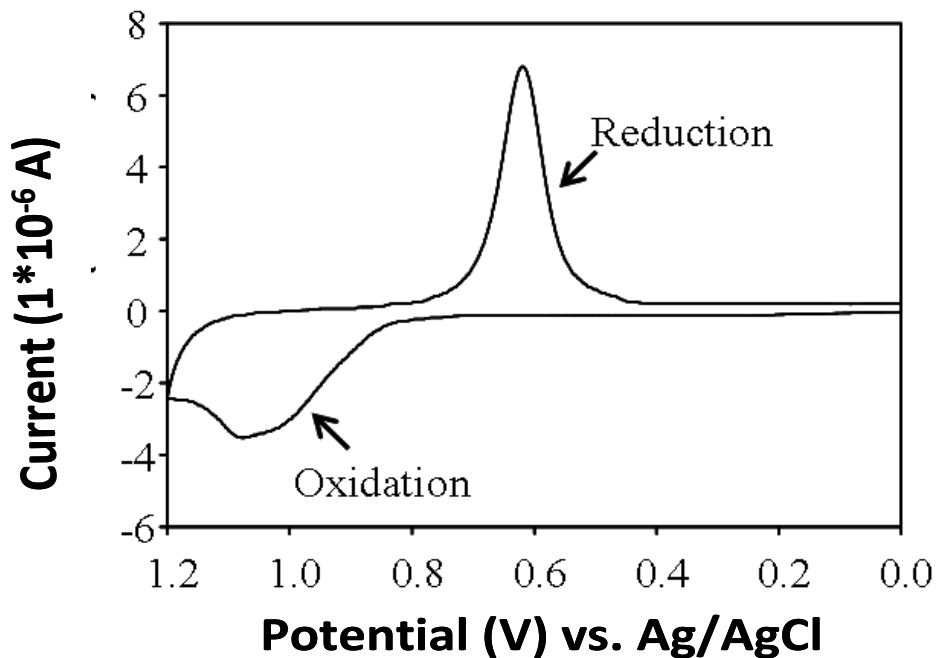


**Figure 2.4.** CV of bare Au IDA in 0.1M H<sub>2</sub>SO<sub>4</sub> vs Ag/AgCl reference electrode. Scan rate was 100 mV/s from 0 to 1.2 (negative to positive direction).

Hence, to ensure the electrodes were clean, CV of Au IDA in 0.1M H<sub>2</sub>SO<sub>4</sub> was obtained after cleaning and wiring the electrodes. Figure 2.5 shows a CV of an Au IDA electrode in 0.1M H<sub>2</sub>SO<sub>4</sub>. Here, Ag/AgCl and a Pt wire were used as reference and counter electrode, respectively. Potential was scanned from 0 to 1.2 V at 100 mV/s in 0.1 M H<sub>2</sub>SO<sub>4</sub>. In case Au oxidation and reduction peaks were not observed, solvent and ozone cleaning were repeated.

After preparing, wiring and cleaning the Au IDA electrodes, several different electrochemical procedures were performed to study the impacts of applied potential and metal ion concentration of metal electrodeposition. The procedures are described in the next sections. Prior to studying the factors that influence the morphology of metal electrodeposition at micron gap Au IDA electrodes, we determined the reduction and oxidation potentials of the metal of interest.<sup>73, 75</sup>

**Procedure for determining oxidation and reduction potential for Ag and Pd:**

**Ag:** CV of Au IDA electrode in 5 mM AgNO<sub>3</sub> in 0.1 M H<sub>2</sub>SO<sub>4</sub> was obtained to determine the reduction and oxidation potential of Ag. Three-electrode setup was used to perform this experiment (see technique section for setup). For this purpose, Ag wire and Pt wire were used as reference and counter electrode respectively. Ag was in the oxidized form. Hence, the potential was scanned in the negative direction from 0.3 V to -0.4 V vs. Ag wire at a scan rate of 100 mV/s. As the potential approaches the characteristic E<sup>0</sup> (~0 V) for the redox process, a cathodic (reduction) current begins to increase, until a peak is reached. After traversing the potential region where the reduction process takes place, the direction of the potential is reversed. Figure 2.5 shows the CV of Au IDA in 5 mM AgNO<sub>3</sub> in aqueous 0.1 M H<sub>2</sub>SO<sub>4</sub>. The peaks at ~0.1 V and ~0.05 V represent Ag reduction/cathodic (Ag<sup>+</sup> to Ag<sup>0</sup>) and oxidation/anodic (Ag<sup>0</sup> to Ag<sup>+</sup>) peaks.

**Pd:** CV of Au IDA in 5mM PdCl<sub>4</sub><sup>2-</sup> in 0.1M H<sub>2</sub>SO<sub>4</sub> at a scan rate of 100 mV/s using Ag/AgCl reference electrode and Pt wire counter electrode was obtained to determine the

oxidation and reduction potential of Pd (see technique section for setup). Figure 2.6 shows CV of the Au IDA in 5mM  $K_2PdCl_4$  in 0.1M  $H_2SO_4$ . The potential was scanned in the negative direction starting from a potential where no reduction occurs (0.8 V) as Pd was in the oxidized form. As the potential approaches the characteristic  $E^0$  ( $\sim 0.1$  V) for

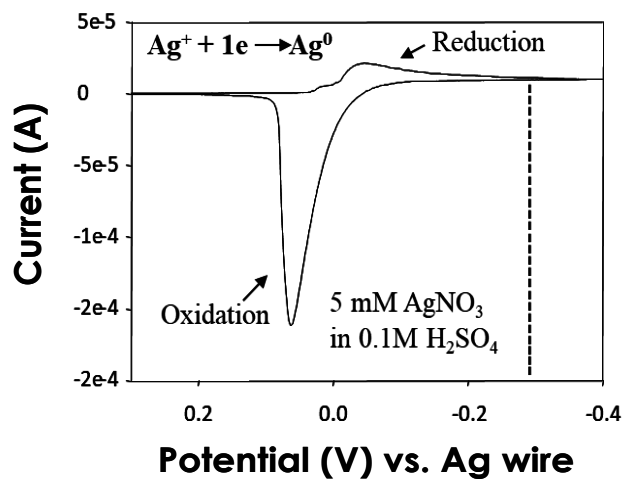


**Figure 2.5.** CV of Au IDA electrode in 5 mM  $AgNO_3$  in 0.1 M  $H_2SO_4$  at a scan rate of 100mV/s (scan direction negative to positive). The dashed line represents the potential at which the Ag reduction and the subsequent electrodeposition begin.

the redox process, a cathodic (reduction) current begins to increase, until a peak is reached. After traversing the potential region where the reduction process takes place, the direction of the potential is reversed. The peaks at  $\sim 0.1$  V and  $\sim 0.5$  V represent the reduction/cathodic ( $Pd^{2+}$  to  $Pd^0$ ) and oxidation/anodic ( $Pd^0$  to  $Pd^{2+}$ ) peaks.

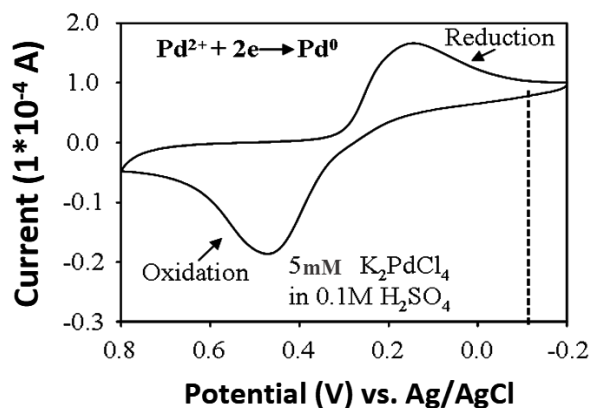


**Figure 2.6.** CV of Au IDA electrode in 5 mM  $\text{K}_2\text{PdCl}_4$  in 0.1 M  $\text{H}_2\text{SO}_4$  at a scan rate of 100 mV/s (scan direction negative to positive). The dashed line represents the potential at which the Pd reduction and the subsequent electrodeposition begin.

**Procedure for studying the influence of metal ion concentration and applied potential on metal electrodeposition:**

Metal (Ag and Pd) electrodeposition was performed using conventional three-electrode set up (see technique section for details). The electrodeposition was performed in chronocoulometric mode by connecting one wire lead of the IDA to the potentiostat as the working electrode. During electrodeposition, metallic ions from an electrolyte are reduced with the aid of applied potential to form a solid deposit on the cathode (see Figure 2.7). In this study, potential was stepped to a desired value where metal ion reduction occurs and was held at that potential until a certain fixed number of coulombs of desired metal were electrodeposited on/across the electrodes.

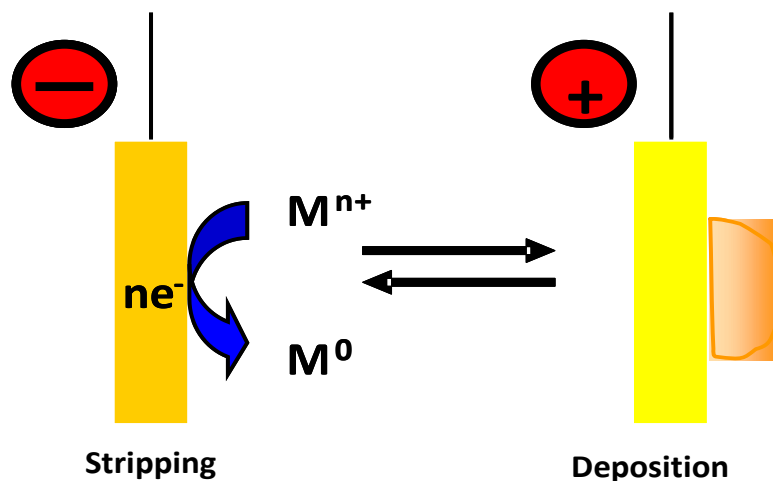


**Figure 2.7.** Cartoon depicting electrodeposition and stripping. The yellow rectangles represent electrodes, red circles represent charge applied: negative (left) and positive (right), metal ion ( $M^{n+}$ ) and solid metal ( $M^0$ ) and  $ne^-$  represents the reducing agent. Arrow pointing to the left represents reduction (deposition) and the arrow pointing to the right represents oxidation (stripping).

$H_2SO_4$ , then a potential was applied and held at that certain value until  $6 \cdot 10^{-5}C$  was passed through and the Ag was electrodeposited (see Figure 2.8). Whereas in case of Pd studies, potential was held at a certain value until  $1.2 \cdot 10^{-3}C$  was passed through and the Pd was electrodeposited from a solution containing  $PdCl_4^{2-}$  in  $0.1M H_2SO_4$  (see Figure 2.9). Deposition was performed at various applied potentials from solutions containing different concentrations of metal of interest (Ag and Pd). Please see Table 2.1 and Table 2.2 for potential and metal concentrations used in Ag and Pd electrodeposition studies.

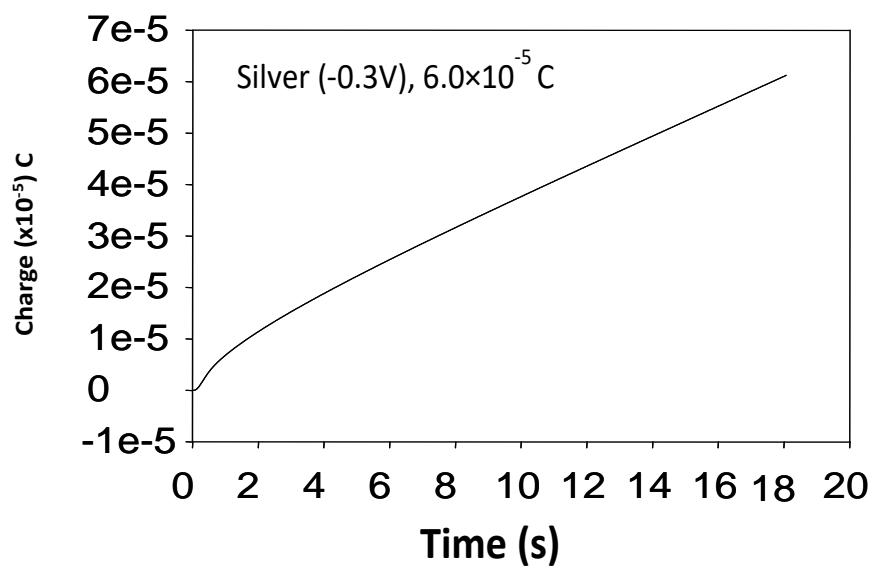


**Figure 2.8.** Chronocoulometric graph showing Ag electrodeposition from solution containing 5 mM AgNO<sub>3</sub> in 0.1 M H<sub>2</sub>SO<sub>4</sub> at -0.3 V vs. Ag wire reference electrode.

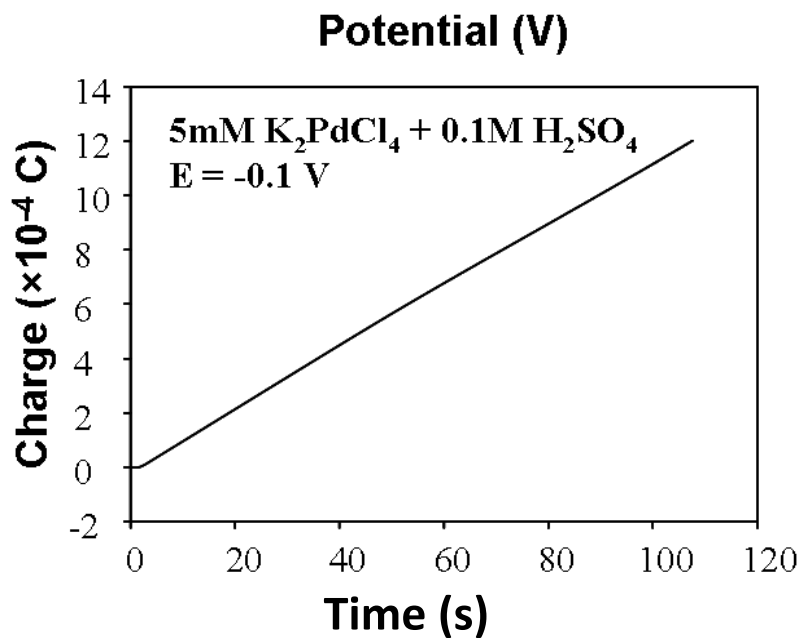


**Figure 2.9.** Chronocoulometric graph showing Pd electrodeposition from solution containing 5 mM K<sub>2</sub>PdCl<sub>4</sub> in 0.1 M H<sub>2</sub>SO<sub>4</sub> at -0.1 V vs. Ag/AgCl reference electrode.

<b>Table 2.1</b> Different conditions where Ag electrodeposition was performed			
	Electrodeposition Ag- charge $6.0 \times 10^{-5}$ C passed		
Concentration	0.5 mM AgNO <sub>3</sub>	5 mM AgNO <sub>3</sub>	50 mM AgNO <sub>3</sub>
Applied potential vs. Ag wire	-0.1 V	-0.1 V	-0.1 V
	-0.2 V	-0.2 V	-0.2 V
	-0.3 V	-0.3 V	-0.3 V
	-0.4 V	-0.4 V	-0.4 V
	-0.5 V	-0.5 V	-0.5 V

<b>Table 2.2</b> Different conditions where Pd electrodeposition was performed			
	Electrodeposition Pd - charge $1.2 \times 10^{-3}$ C passed		
Concentration	0.5 mM K <sub>2</sub> PdCl <sub>4</sub>	5 mM K <sub>2</sub> PdCl <sub>4</sub>	50 mM K <sub>2</sub> PdCl <sub>4</sub>
Applied potential vs. Ag/AgCl wire electrode	+0.1 V	+0.1 V	+0.1 V
	0.0 V	0.0 V	0.0 V
	-0.1 V	-0.1 V	-0.1 V
	-0.2 V	-0.2 V	-0.2 V
	-0.3 V	-0.3 V	-0.3 V

#### **2.4. Procedures for making different solutions:**

**Preparation of 0.1 M H<sub>2</sub>SO<sub>4</sub>:** H<sub>2</sub>SO<sub>4</sub> (96%) was used to make 0.1 M H<sub>2</sub>SO<sub>4</sub>. Since the purity was not 100%, the molarity of the H<sub>2</sub>SO<sub>4</sub> was figured out by using density (1.1 g/mL) and molar mass (98.072 g/mol) of H<sub>2</sub>SO<sub>4</sub>. Then, the dilution equation ( $M_1V_1 = M_2V_2$ ) was used to dilute the stock H<sub>2</sub>SO<sub>4</sub> to 0.1 M H<sub>2</sub>SO<sub>4</sub> (see Equation 2.1).

Equation 2.1:

$$M_1V_1 = M_2V_2$$

$$10.767 \text{ M H}_2\text{SO}_4 * V_1 = 0.1 \text{ M} * 0.5 \text{ L}$$

$$V_1 = 4.64 \text{ ml}$$

**Preparation of 0.5, 5 and 50 mM AgNO<sub>3</sub> in 0.1M H<sub>2</sub>SO<sub>4</sub> solution:** AgNO<sub>3</sub> was dissolved in 0.1 M H<sub>2</sub>SO<sub>4</sub> to make 0.5 mM, 5 mM and 50 mM AgNO<sub>3</sub> (see Equation 2.2).

Equation 2.2:

$$\text{Volume of AgNO}_3 = 20 \text{ mL or } 0.02 \text{ L}$$

*0.5mM*

$$0.0005\text{M} = x \text{ (mol)}/0.02\text{L} \quad x=0.000010 \text{ mol}$$

$$\text{Mass} = 0.000010 \text{ mol} * 169.879 \text{ g/mol}$$

$$\text{Mass of AgNO}_3 \text{ needed is } 0.00170 \text{ g}$$

*5mM*

$$\text{Mass of AgNO}_3 \text{ needed is } 0.0170 \text{ g}$$

*50 mM*

$$\text{Mass of AgNO}_3 \text{ needed is } 0.170 \text{ g}$$

**Preparation of 0.5, 5 and 50 mM PdCl<sub>4</sub><sup>2-</sup> in 0.1M H<sub>2</sub>SO<sub>4</sub> solution:** K<sub>2</sub>PdCl<sub>4</sub> was dissolved in 0.1 M H<sub>2</sub>SO<sub>4</sub> to make 0.5 mM, 5 mM and 50 mM K<sub>2</sub>PdCl<sub>4</sub> (see Equation 2.3).

Equation 2.3:

*Volume of  $K_2PdCl_4$  = 20 mL or 0.02 L*

*0.5mM*

$$0.0005M = x \text{ (mol)}/0.02L \quad x=0.000010 \text{ mol}$$

$$\text{Mass} = 0.000010 \text{ mol} * 326.43 \text{ g/mol}$$

*Mass of  $K_2PdCl_4$  needed is 0.00326 g*

*5mM*

*Mass of  $K_2PdCl_4$  needed is 0.0326 g*

*50 mM*

*Mass of  $K_2PdCl_4$  needed is 0.326 g*

### III. Ag Electrodeposition

There has been an increase in practical and theoretical interest of noble metal deposition in the past few decades.<sup>78-81</sup> Ag deposition is one such metal deposition that has been practiced for many years as it has different applications in various fields. Especially, Ag nanostructures are used in flexible electronics,<sup>82</sup> solar cells,<sup>83-85</sup> capacitors,<sup>86-88</sup> pressure sensing,<sup>89-91</sup> chemical sensing,<sup>92-94</sup> and biological sensing.<sup>95-96</sup>

Hence, various deposition procedures for synthesizing different forms of Ag nanostructures have been reported in the literature and are still being researched.<sup>97-108</sup> The following are few methods that have been reported for Ag deposition: Ag plating,<sup>97</sup> pulsed electrodeposition,<sup>98-100</sup> direct deposition via immersion,<sup>101-104</sup> and chemical vapor deposition (CVD).<sup>105-108</sup> Pulsed electrodeposition of Ag was performed in a template by Schubert and coworkers for synthesizing Ag NWs.<sup>100</sup> Size and shape of the NWs synthesized through this method were determined by the template pore size and shape. Deposition by immersion is a method developed by Nativ-Roth for synthesizing Ag NWs.<sup>103</sup> This method utilizes a template as well and the immersion time varied from one hour to twelve hours. In this method of deposition, Ag did not deeply penetrate the porous silicon template. Hence, length of wires synthesized was shorter than the desired length. Controlling the length of the NWs is not feasible with this method.

However, this method is simple and cost effective. In order to make an electronic device with the NWs synthesized using the above methods, template needs to be sacrificed first, then the NWs are to be transferred on a suitable substrate and

finally electrical contacts are to be made. This involves multiple steps making it tedious. Szczyński and coworkers used CVD to deposit Ag.<sup>106</sup> In CVD, solid material is deposited from a gaseous phase on to metallic, ceramic, alloy or intermetallic substrates. In this method, precursor gas is passed over the surface of the heated substrate, and the chemical reaction between the volatile precursors and the surface of the substrate leads to the formation of a coating on the substrate. This process can be controlled very well. However, the downside of this method is that it runs at very high temperatures and is limited only to the substrates that can tolerate high temperatures. Also, CVD reactor is expensive meaning not every institution can afford a CVD reactor, limiting its application. All of the above described methods require making electrical contacts to NWs to fabricate an electronic device. Making electrical contacts to NWs involves sophisticated procedures and are not very reproducible.

Direct metal deposition across the prefabricated electrodes eliminates multiple steps and also, a direct contact is formed. Campbell and coworkers and Zamborini and coworkers both reported the electrochemical method for direct metal electrodeposition across prefabricated electrodes.<sup>109-110</sup> Campbell and coworkers used two electrodes separated by 20 nm fabricated by e-beam lithography in their study. Approach reported by Zamborini and coworkers is similar to Campbell and coworkers, except that 5- $\mu\text{m}$  gap IDA electrodes fabricated by photolithography were used. Photolithography is cheaper, versatile and massively parallel fabrication method. Zamborini and coworkers

electrodeposited Ag and Pd across 5 micron-gap Au IDA electrodes. Ag grew in the form of wires and Pd grew in the form of dendrites.

In order to deposit any metal that is electroactive with the desired morphology utilizing the procedure reported by Zamborini and coworkers, it is important to understand the factors that affect the morphology of the metal deposited on/across the electrodes. Here we investigated the impact of Ag ion concentration and the applied potential on the morphology of the Ag electrodeposited on/across 5 micron-gap Au IDA electrodes. Electrodeposition was performed in diffusion-controlled regime. Metal ion concentration and applied potential impact the flux of the metal ion to the substrate. This hypothesis is based on *the Fick's 1<sup>st</sup> law* and *Nernst equation*. According to the *Fick's 1st law* flux  $J_A(x, t)$  of substance A due to diffusion at time (t) and position (x) is proportional to the concentration gradient  $\partial C_A(x, t)/\partial x$

$$J_A(x, t) = -D_A \frac{\partial C_A(x, t)}{\partial x}$$

and depends on the diffusion constant  $D_A$  of species A. The minus sign indicates that the direction of flux is opposite to the direction of the gradient. In other words, flux measures the amount of substance that will flow through a unit area during a unit time interval. In simple words, the amount of substance that will flow through a unit area during a unit time interval to the substrate depends on the difference in concentration of the species in bulk and at the surface of the substrate. The higher the difference, the higher the flux. Based on this, we expect the flux of Ag ions to substrate to be higher

when Ag is electrodeposited from solution containing 50 mM followed by 5 and 0.5 mM AgNO<sub>3</sub>.

According to the Nernst equation, in a redox reaction, the ratio  $[R]_{x=0}/[O]_{x=0}$  on the surface of the working electrode ( $x=0$ ) at any time ( $t>0$ ) depends exclusively on its potential (E). R is the reduced form and O is the oxidized form of the species.

$$E = E^0 - \frac{RT}{nF} \log \frac{[R]_{x=0}}{[O]_{x=0}}$$

The ratio of oxidized (Ag<sup>+</sup>) and reduced (Ag<sup>0</sup>) forms of Ag at the surface of the substrate depends on the applied potential. The more negative the applied potential, the smaller this ratio. This indicates, the concentration of Ag ions at the surface of the substrate is lower at more negative applied potentials. This impacts the difference in concentration of Ag ions at surface and the bulk. The more negative the applied potential, the lesser the concentration of Ag ions at the surface of the electrode and the larger the difference in concentration of Ag ions at the surface and the bulk. This leads to a higher flux of Ag ions on the electrode surface from the bulk. We wanted to investigate if the difference in flux of Ag ions to the electrode surface at various conditions such as difference in applied potential and concentration of Ag ions in the bulk leads to different morphology of Ag electrodeposited on/across the micron gap Au electrodes.

Ag electrodeposition was performed using the procedure described in Chapter II. To determine the impact of Ag ion concentration on morphology of the Ag electrodeposited other than the Ag ion concentration in solution, all the other parameters were kept constant. Three different concentrations were tested (0.5 mM, 5

mM and 50 mM). To determine the impact of applied potential on morphology of the Ag deposited, we held the Ag ion concentration and all the other parameters constant and changed the applied potential. Five different potentials were tested (-0.1 V, -0.2 V, -0.3 V, -0.4 V and -0.5 V vs. Ag wire).

Please note, Zamborini and coworkers reported the formation of Ag NW connection between the electrodes when  $6 \times 10^{-5}$  C was reached from 5 mM  $\text{AgNO}_3$  solution at an applied potential of -0.3 V vs. Ag wire. In this study, we electrodeposited Ag until  $6 \times 10^{-5}$  C of charge was passed. Figure 3.1 and 3.2 shows overlay of chronocoulometric plots of Ag electrodeposition from  $\text{AgNO}_3$  solutions at different concentrations and applied potentials. At a particular applied potential, the slope of the chronocoulometric plot of Ag electrodeposition is different when Ag is electrodeposited from different concentrations of  $\text{AgNO}_3$  solutions. The higher the concentration of  $\text{AgNO}_3$ , the higher the slope. At a particular applied potential, the time it took for electrodepositing  $6 \times 10^{-5}$  C of Ag from different solutions containing different concentrations of  $\text{AgNO}_3$  is different.

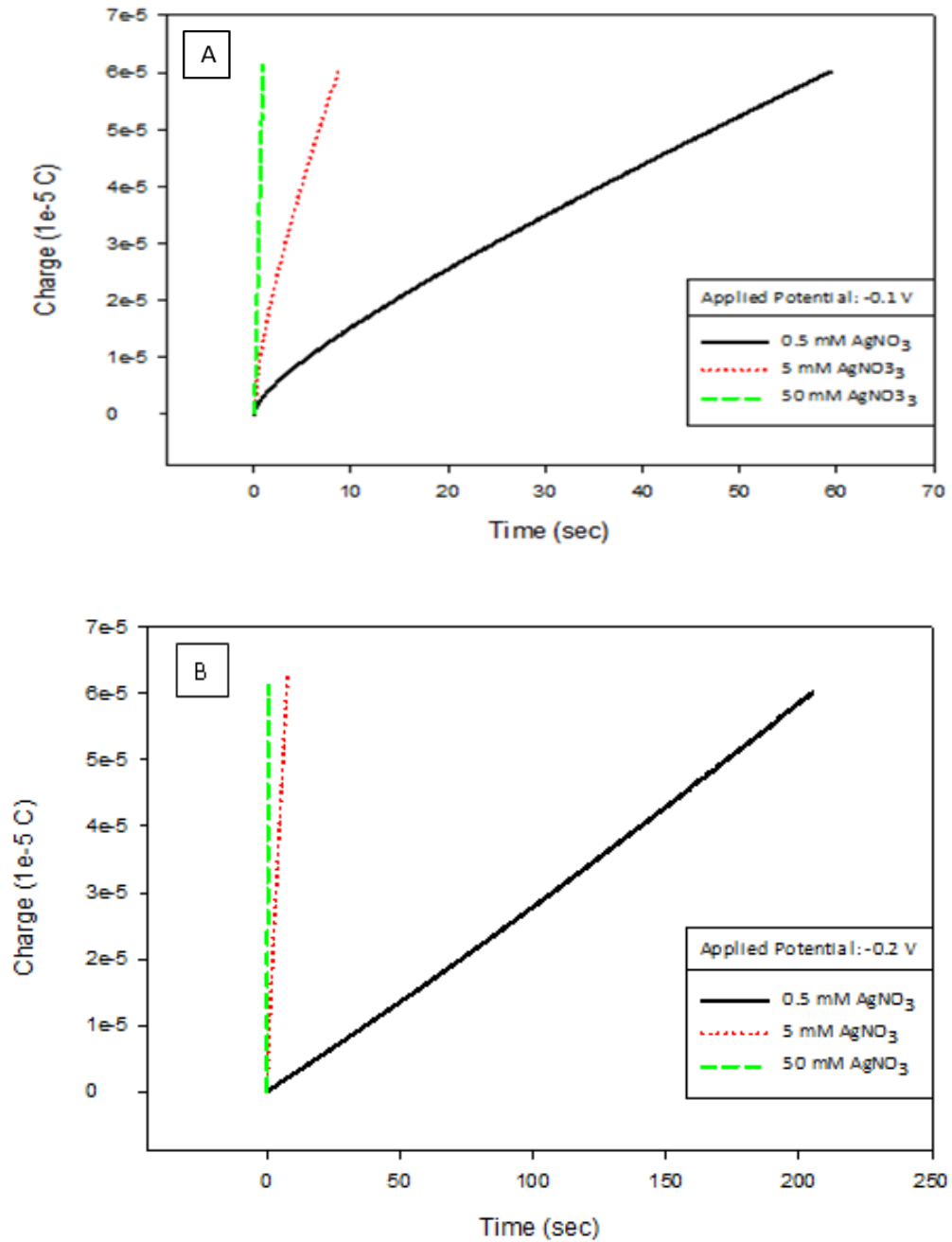


**Figure 3.1.** Overlay plot of chronocoulometric graphs showing Ag electrodeposition from solution containing different concentrations of  $\text{AgNO}_3$  at a) -0.1 V, b) -0.2 V, c) -0.3 V, d) -0.4 V, and e) -0.5 V vs. Ag wire.

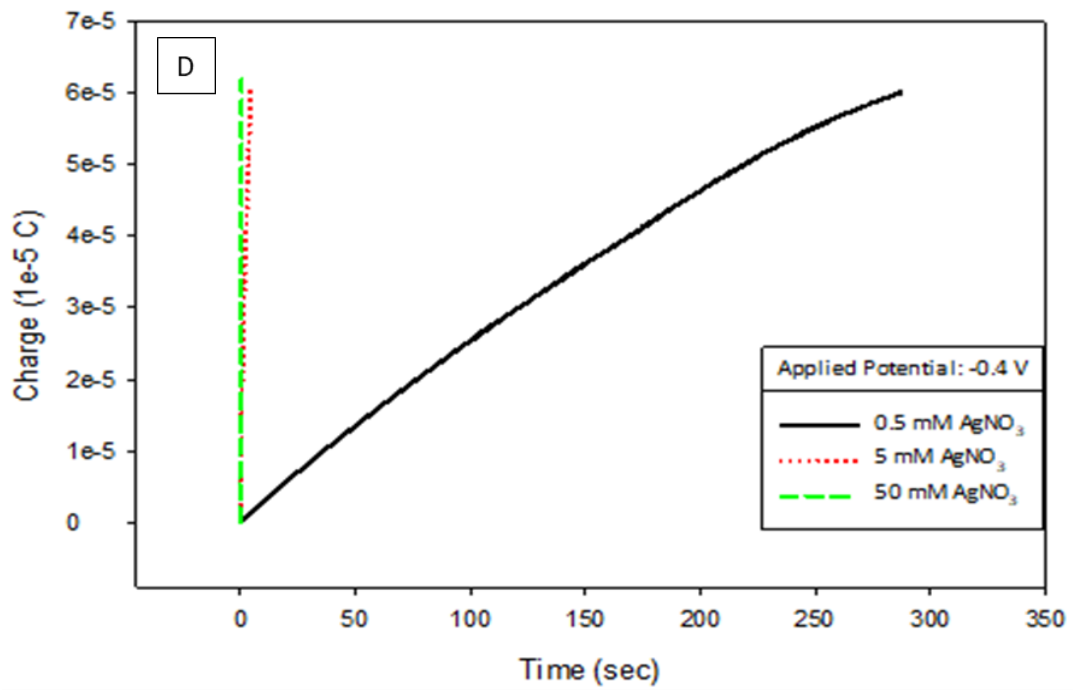
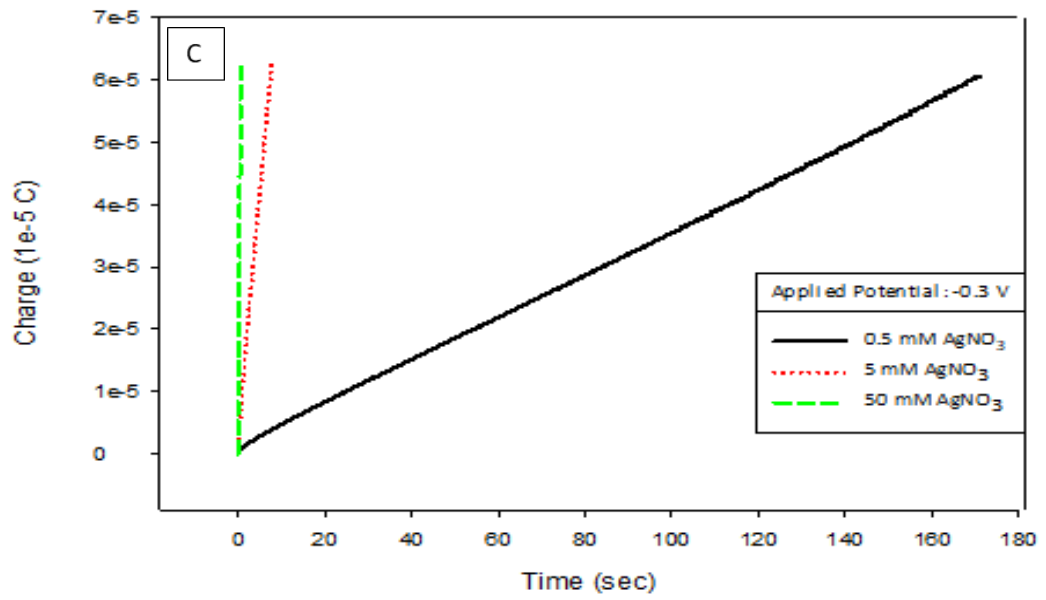


Figure 3.1. (continued).

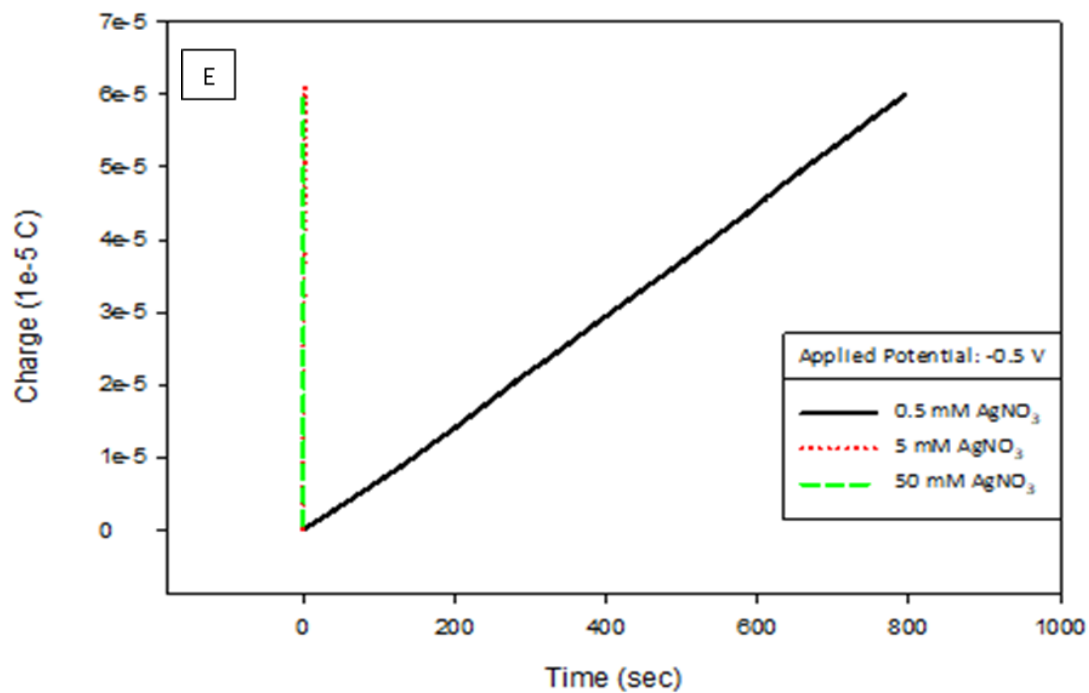


Figure 3.1. (continued).

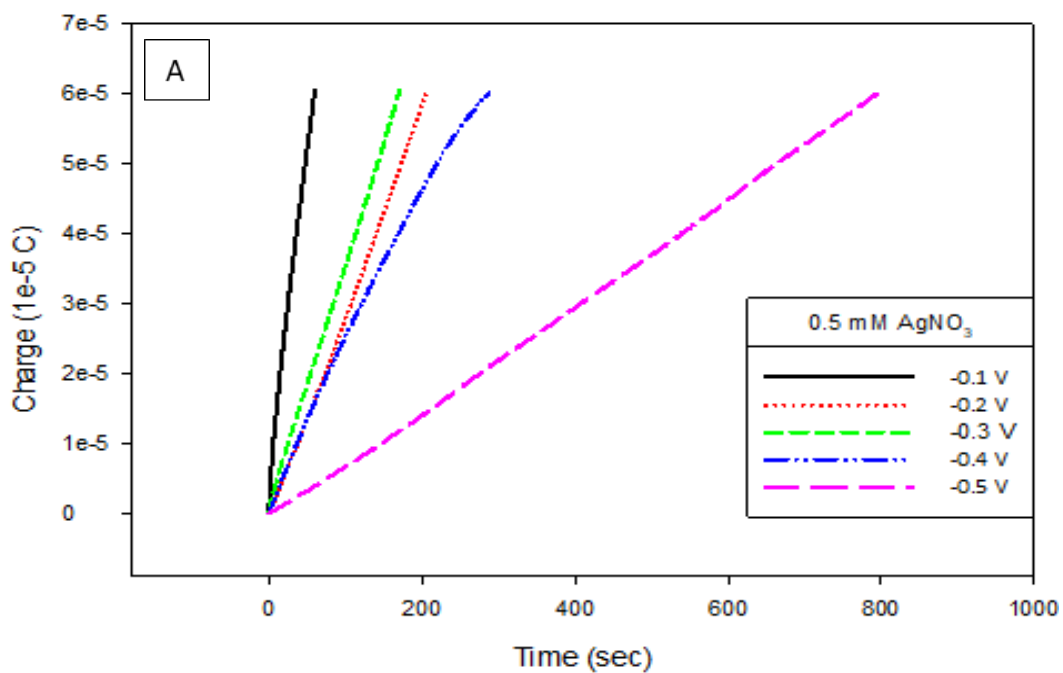
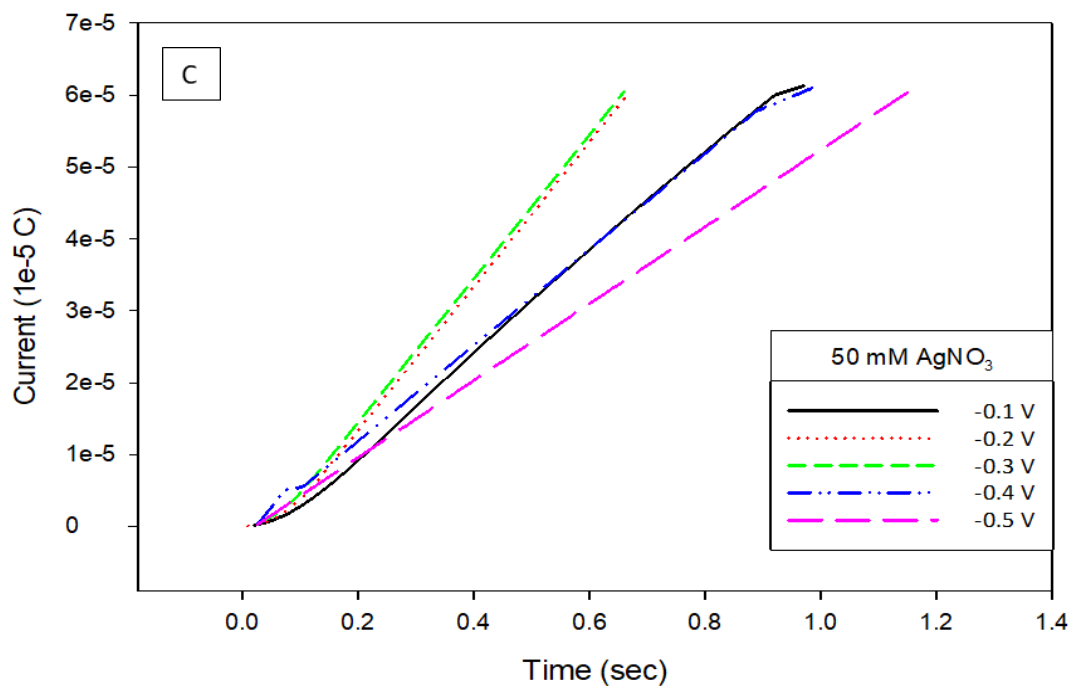
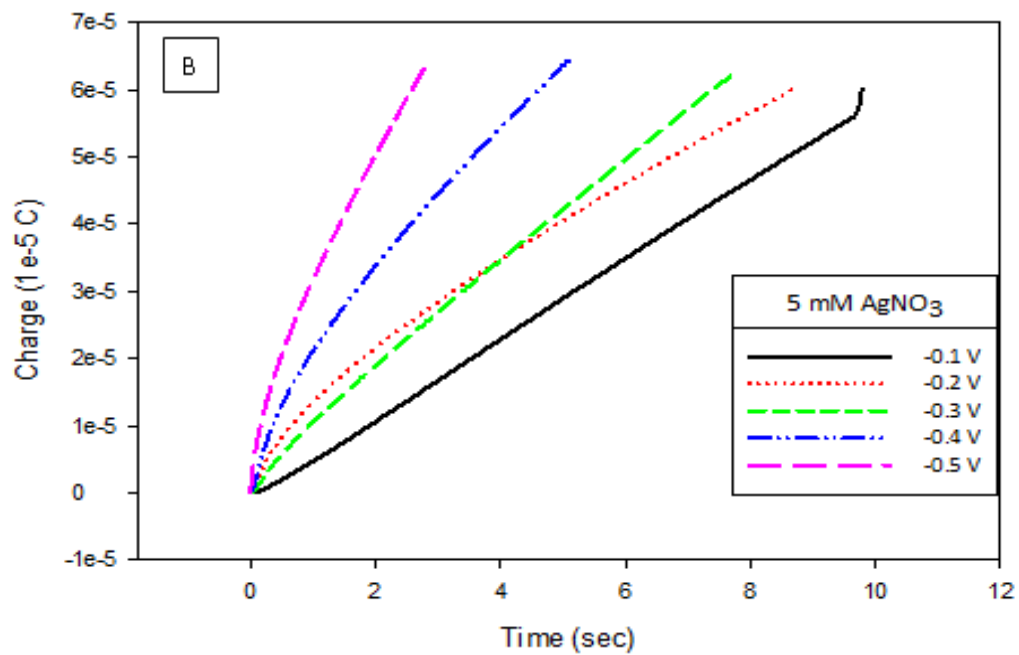


Figure 3.2. Overlay plot of chronocoulometric graphs showing electrodeposition at various applied potential vs. Ag wire from solution containing a) 0.5 mM, b) 5 mM, and c) 50 mM  $\text{AgNO}_3$ .



**Figure 3.2.** (continued).

Table 3.1 shows the time it took to electrodeposit Ag at a charge of  $6 \times 10^{-5}$  C was passed at various potentials from different concentrations of AgNO<sub>3</sub> solution. At a particular potential, the higher the concentration of AgNO<sub>3</sub> solution the lesser time it took to electrodeposit Ag. For instance, at an applied potential of -0.1V vs. Ag wire it took 65, 9 and 1 seconds on average to electrodeposit Ag from 0.5 mM, 5 mM and 50 mM AgNO<sub>3</sub> solution respectively (see Table 3.2).

Table 3.1 Time for electrodepositing of Ag at a charge of $6 \times 10^{-5}$ C from a solution containing different concentrations of AgNO <sub>3</sub> at various applied potentials									
	Concentrations								
	0.5 mM AgNO <sub>3</sub>			5 mM AgNO <sub>3</sub>			50 mM AgNO <sub>3</sub>		
Applied potential vs. Ag wire	Trial 1	Trial 2	Trial 3	Trial 1	Trial 2	Trial 3	Trial 1	Trial 2	Trial 3
-0.1 V	52 sec	60 sec	79 sec	7 sec	9 sec	11 sec	1 sec	1 sec	2 sec
-0.2 V	198 sec	205 sec	228 sec	6 sec	8 sec	12 sec	0.7 sec	0.8 sec	1 sec
-0.3 V	154 sec	170 sec	214 sec	6 sec	8 sec	9 sec	0.6 sec	0.7 sec	0.7 sec
-0.4 V	221 sec	288 sec	298 sec	4 sec	5 sec	6 sec	0.7 sec	1 sec	2 sec
-0.5 V	769 sec	800 sec	814 sec	3 sec	3 sec	4 sec	0.8 sec	1 sec	1 sec

This indicates that at a particular applied potential, the flux of Ag ion to the surface of Au IDA is different when Ag is electrodeposited from different concentrations of AgNO<sub>3</sub> solutions. The higher the Ag ion concentration, the higher the flux of Ag ion to the AuIDA. However, at a particular concentration, the time it took to electrodeposit Ag at a charge of  $6 \times 10^{-5}$  C at various applied potentials was not statistically different from each other (see Figure 3.2 and Table 3.2). This indicates that there is no significant difference

in the flux of Ag ions to the substrate at different applied potentials. This is because deposition potentials used in this study are in diffusion-controlled regime.

After electrodepositing Ag, we obtained i-V curves, to determine whether or not an Ag connection was formed between the Au IDA. Figure 3.3 shows the overlay of CV plots obtained in air before and after electrodeposition of Ag from 0.5 mM, 5 mM and 50 mM AgNO<sub>3</sub> respectively at an applied potential of -0.1 V vs. Ag wire. Before Ag electrodeposition, currents observed in air (background current) at -1 V ranged from 1.05\*10<sup>-7</sup> A to 1.68\*10<sup>-7</sup> A for all three devices. Currents observed in air at -1 V are 1.2\*10<sup>-7</sup> A, 1.6\*10<sup>-7</sup> A and 1.3\*10<sup>-7</sup> A after electrodepositing Ag from 0.5 mM, 5 mM and

Applied potential vs. Ag wire	Concentrations		
	0.5 mM AgNO <sub>3</sub>	5 mM AgNO <sub>3</sub>	50 mM AgNO <sub>3</sub>
-0.1 V	65 sec	9 sec	1 sec
-0.2 V	210 sec	8 sec	0.8 sec
-0.3 V	179 sec	8 sec	0.7 sec
-0.4 V	270 sec	5 sec	1 sec
-0.5 V	794 sec	3 sec	1 sec

50 mM AgNO<sub>3</sub> solution. There was no significant difference in current observed in air at -1 V before and after electrodepositing Ag from 0.5 mM, 5 mM and 50 mM AgNO<sub>3</sub> solution. This indicates that no connections were formed between the 5 micron-gap Au electrodes.

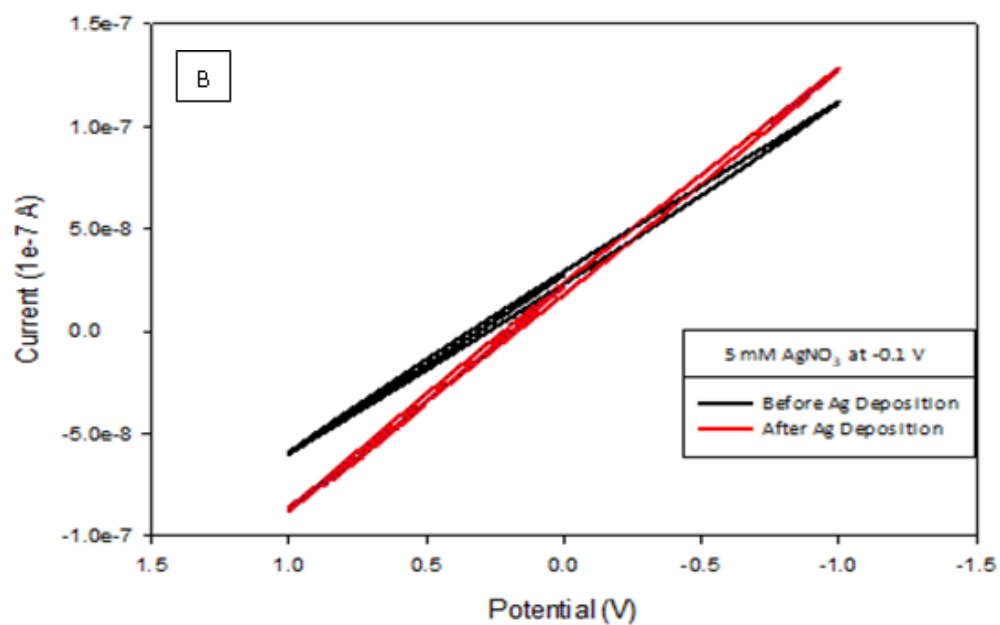
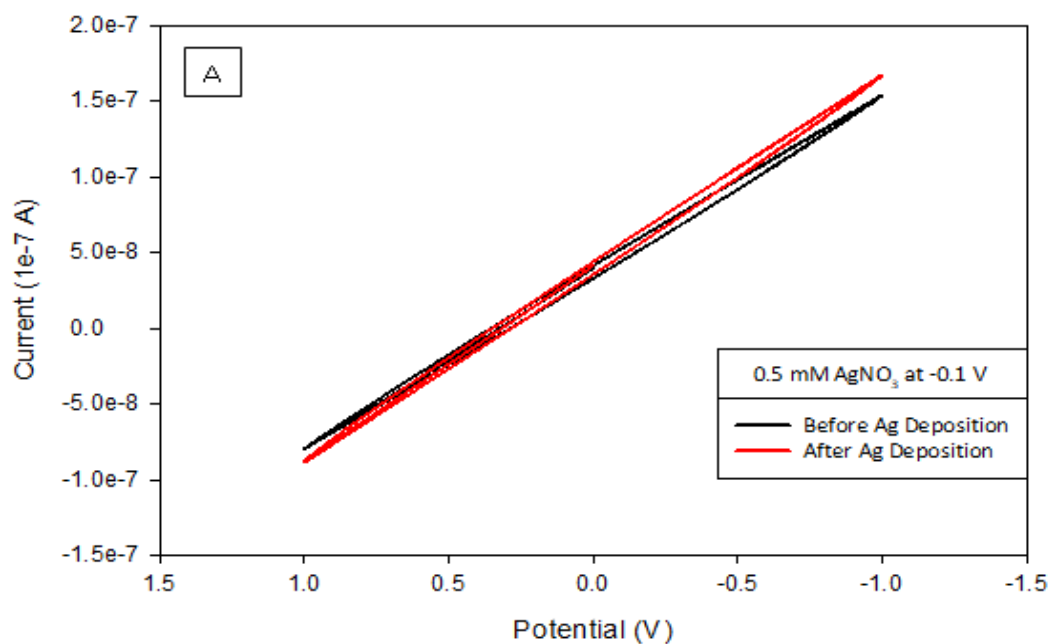


**Figure 3.3.** Overlay plot of CV of Au IDA electrode in air before and after Ag electrodeposition at -0.1 V potential from a) 0.5 mM, b) 5 mM and c) 50 mM AgNO<sub>3</sub> solution.

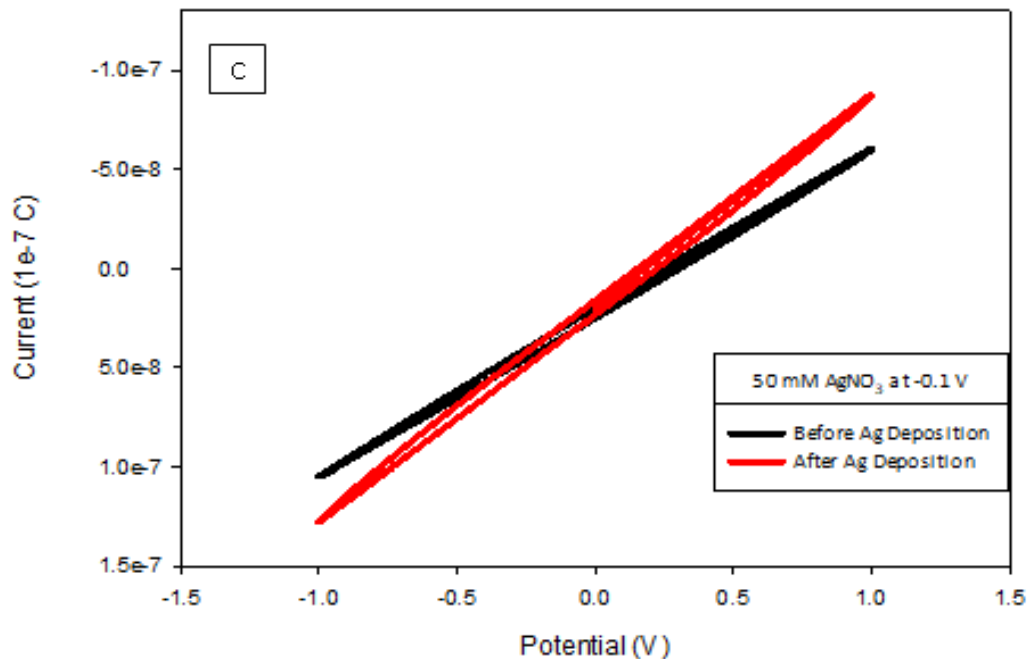


**Figure 3.3.** (continued).

Table 3.3a-c shows the currents observed at -1 V in air before and after electrodepositing Ag at various potentials from different concentrations of  $\text{AgNO}_3$  solution. Ag is more conductive than the  $\text{SiO}_2$  that connects the 5 micron gap Au IDA. If an Ag connection is made between the micron gap Au electrodes, a significant (several orders of magnitude) increase in current would be observed at -1 V due to the formation of metal (Ag)/metal (Au) contact. For instance, currents observed in air at -1 V after electrodepositing Ag from 5 mM and 50 mM  $\text{AgNO}_3$  solution at -0.2 V vs. Ag wire are  $1.4 \times 10^{-2}$  A and  $1.4 \times 10^{-2}$  A respectively (see Table 3.3).

Table 3.3a Currents observed at -1 V before and after electrodeposition of Ag at various applied potentials from 0.5 mM AgNO <sub>3</sub> solution						
Potential vs. Ag wire	0.5 mM AgNO <sub>3</sub>					
	Trial 1		Trial 2		Trial 3	
	Before	After	Before	After	Before	After
-0.1 V	1.32x10 <sup>-7</sup> C	1.27x10 <sup>-2</sup> C	1.29x10 <sup>-7</sup> C	1.22x10 <sup>-7</sup> C	1.26x10 <sup>-7</sup> C	1.27x10 <sup>-7</sup> C
-0.2 V	1.27x10 <sup>-7</sup> C	7.11x10 <sup>-3</sup> C	1.09x10 <sup>-7</sup> C	1.94x10 <sup>-7</sup> C	1.20x10 <sup>-7</sup> C	1.40x10 <sup>-7</sup> C
-0.3 V	1.24x10 <sup>-7</sup> C	6.27x10 <sup>-3</sup> C	1.22x10 <sup>-7</sup> C	3.08x10 <sup>-7</sup> C	1.51x10 <sup>-7</sup> C	1.85x10 <sup>-7</sup> C
-0.4 V	1.43x10 <sup>-7</sup> C	1.06x10 <sup>-2</sup> C	1.32x10 <sup>-7</sup> C	1.80x10 <sup>-7</sup> C	1.21x10 <sup>-7</sup> C	1.39x10 <sup>-7</sup> C
-0.5 V	1.66x10 <sup>-7</sup> C	5.92x10 <sup>-3</sup> C	1.12x10 <sup>-7</sup> C	1.19x10 <sup>-7</sup> C	1.06x10 <sup>-7</sup> C	1.24x10 <sup>-7</sup> C

Table 3.3b Currents observed at -1 V before and after electrodeposition of Ag at various applied potentials from 5 mM AgNO <sub>3</sub> solution						
Potential vs. Ag wire	5 mM AgNO <sub>3</sub>					
	Trial 1		Trial 2		Trial 3	
	Before	After	Before	After	Before	After
-0.1 V	1.16x10 <sup>-7</sup> C	1.56x10 <sup>-7</sup> C	1.14x10 <sup>-7</sup> C	1.64x10 <sup>-7</sup> C	1.12x10 <sup>-7</sup> C	1.62x10 <sup>-7</sup> C
-0.2 V	1.46x10 <sup>-7</sup> C	7.16x10 <sup>-3</sup> C	1.24x10 <sup>-7</sup> C	4.82x10 <sup>-2</sup> C	1.26x10 <sup>-7</sup> C	1.33x10 <sup>-2</sup> C
-0.3 V	1.24x10 <sup>-7</sup> C	4.91x10 <sup>-3</sup> C	1.28x10 <sup>-7</sup> C	5.29x10 <sup>-3</sup> C	1.42x10 <sup>-7</sup> C	1.05x10 <sup>-2</sup> C
-0.4 V	1.16x10 <sup>-7</sup> C	1.51x10 <sup>-2</sup> C	1.19x10 <sup>-7</sup> C	1.07x10 <sup>-2</sup> C	1.62x10 <sup>-7</sup> C	1.17x10 <sup>-2</sup> C
-0.5 V	1.36x10 <sup>-7</sup> C	1.06x10 <sup>-2</sup> C	1.60x10 <sup>-7</sup> C	1.12x10 <sup>-2</sup> C	1.06x10 <sup>-7</sup> C	1.27x10 <sup>-7</sup> C

Table 3.3c Currents observed at -1 V before and after electrodeposition of Ag at various applied potentials from 50 mM AgNO <sub>3</sub> solution						
Potential vs. Ag wire	50 mM AgNO <sub>3</sub>					
	Trial 1		Trial 2		Trial 3	
	Before	After	Before	After	Before	After
-0.1 V	1.35x10 <sup>-7</sup> C	1.25x10 <sup>-7</sup> C	1.18x10 <sup>-7</sup> C	1.28x10 <sup>-7</sup> C	1.19x10 <sup>-7</sup> C	1.30x10 <sup>-7</sup> C
-0.2 V	1.22x10 <sup>-7</sup> C	1.44x10 <sup>-2</sup> C	1.27x10 <sup>-7</sup> C	1.34x10 <sup>-2</sup> C	1.31x10 <sup>-7</sup> C	1.90x10 <sup>-3</sup> C
-0.3 V	1.08x10 <sup>-7</sup> C	1.11x10 <sup>-2</sup> C	1.38x10 <sup>-7</sup> C	1.36x10 <sup>-2</sup> C	1.24x10 <sup>-7</sup> C	6.03x10 <sup>-3</sup> C
-0.4 V	1.21x10 <sup>-7</sup> C	1.38x10 <sup>-2</sup> C	1.13x10 <sup>-7</sup> C	1.85x10 <sup>-7</sup> C	1.16x10 <sup>-7</sup> C	1.28x10 <sup>-7</sup> C
-0.5 V	1.25x10 <sup>-7</sup> C	1.02x10 <sup>-2</sup> C	1.20x10 <sup>-7</sup> C	1.14x10 <sup>-2</sup> C	1.10x10 <sup>-7</sup> C	1.22x10 <sup>-7</sup> C

Approximately five orders of magnitude increase in current was observed, indicating the formation of Ag connection between the micron gap Au IDA electrodes at these conditions. See appendix for the overlay of CV plots obtained in air before and after electrodeposition of Ag from 0.5 mM, 5 mM and 50 mM AgNO<sub>3</sub> respectively at various applied potential vs. Ag wire. When the observed currents in air at -1V are in the range of 10<sup>-2</sup> to 10<sup>-3</sup> A, formation of Ag connection between the micron gap electrode is attributed. Table 3.4 shows Ag ion concentration and the applied potential that favored formation of Ag connections between the micron gap Au IDA electrodes.

Table 3.4 Metal ion concentration and applied potential that lead to the formation of Ag connections between the micron gap Au IDA electrodes									
	0.5 mM AgNO <sub>3</sub>			5 mM AgNO <sub>3</sub>			50 mM AgNO <sub>3</sub>		
Applied potential vs. Ag wire	Trial 1	Trial 2	Trial 3	Trial 1	Trial 2	Trial 3	Trial 1	Trial 2	Trial 3
-0.1 V	Y	N	N	N	N	N	N	N	N
Table 3.4 Metal ion concentration and applied potential that lead to the formation of Ag connections between the micron gap Au IDA electrodes (continued)									
-0.2 V	Y	N	N	Y	Y	Y	Y	Y	Y
-0.3 V	Y	N	N	Y	Y	Y	Y	Y	Y
-0.4 V	Y	N	N	Y	Y	Y	Y	N	N
-0.5 V	Y	N	N	Y	Y	N	Y	Y	N

Results indicate that Ag electrodeposited from solutions containing 5 and 50 mM AgNO<sub>3</sub> solutions favor the formation of connection between the micron gap Au IDA electrodes when the applied potential is at least or more negative than 200 millivolts (mVs) vs. Ag wire reference electrode. Irrespective of the applied potential, the formation of connections was not favored when Ag was electrodeposited from 0.5 mM AgNO<sub>3</sub> solution. At a particular applied potential, flux of Ag ions to the surface of Au IDA electrode is higher when Ag is electrodeposited from solutions containing higher concentrations (5 and 50 mM) of AgNO<sub>3</sub> compared to lower concentration (0.5 mM) of AgNO<sub>3</sub>. Higher flux of the Ag ions to Au IDA electrode surface seems to favor the formation of Ag connection. However, even at high concentrations (5 and 50 mM) of AgNO<sub>3</sub> in solution formation of Ag connections was not observed unless the applied potential is at least or more negative than 200 mVs vs. Ag wire. Higher overpotential seems to favor the formation of Ag connections between the Au Ida electrodes.

However, flux of Ag ion to Au IDA surface at -100 mVs and -200 mVs are not statistically different from each other. Hence, the difference in morphology of electrodeposited Ag at various applied potentials at a particular concentration cannot be attributed to the impact of flux of the Ag ions to the Au IDA electrode surface. Overall, higher flux and higher overpotential seem to favor the formation of Ag connections between the Au IDA electrodes. It has been reported that nucleation rate increases with an increase in applied overpotential.<sup>113</sup> Higher flux also probably increases the nucleation rate as there are more Ag ions colliding with the Au IDA substrate. This difference in nucleation rate at high overpotential and high concentrations probably lead to a difference in the diffusion layer structure as reported earlier<sup>111</sup> which in turn results in different morphologies of Ag electrodeposition at micron gap Au IDAs. This is described in detail in the next section.

Several reports on electrodeposition growth mechanism demonstrate the formation of granules/particles in the initial stages of electrodeposition process. These granules further grow into different structures if the deposition is continued.<sup>111</sup> These growing grains act as individual microelectrodes if they are small (less than 55 micrometers). According to Barton and Bockris, when the distance between the granules is at least 5 times larger than the radius of the growing granule, individual spherical diffusion layer forms around each growing grain (see Figure 3.4).<sup>112</sup> This facilitates the diffusion of ions to all directions of the growing granules. As a result, granule grows in all directions (see Figure 3.4). On the contrary, when the distance between the granules is smaller than 5

times the radius of the growing granule, individual spherical diffusion layer does not form around each growing grain. Rather common diffusion layer of macro electrode is formed. In this scenario, diffusion of ions is facilitated to the tip of the growing grain which favors the connectivity (see Figure 3.4).

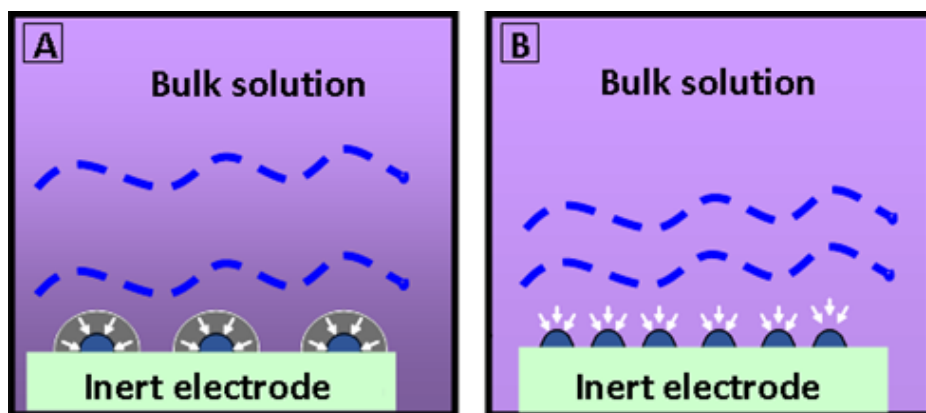


**Figure 3.4.** Scheme showing the diffusion layer structure that leads to the formation of a) no connection and b) connection between micron-gap Au IDA electrode.

Nucleation rate increases with an increase in overpotential and flux. Hence, at less negative applied potential or low over-potential (less negative than 200 mVs vs. Ag wire), probably a smaller number of nuclei form leading to larger distance between the growing granules. The distance between the granules is probably large enough to favor the formation of individual spherical diffusion around each growing grain which facilitates the growth of the granule in all directions resulting in no growth of Ag connections between the micron-gap Au IDA electrodes. This could be the reason that electrodeposition of Ag from 5 and 50 mM AgNO<sub>3</sub> solutions did not result in the formation of connection between micron gap Au

IDA electrodes at low overpotentials (at an applied potential that is less negative than 200 mVs vs. Ag wire). Similarly, when the applied potential or overpotential is more negative than -200 mVs vs. Ag wire reference electrode, more granules might have formed on the surface. The distance between the granules is probably smaller than 5 times the radius of the granule. This does not favor the formation of individual spherical diffusion layer around each growing grain. Rather common diffusion layer of macro electrode is formed quickly. In this scenario, diffusion of Ag ions is facilitated to the tip of the nuclei. This favors the formation of connection between the micron gap electrodes (see Figure 3.4). This is what we propose could be happening when Ag was electrodeposited from 5 and 50 mM AgNO<sub>3</sub> solutions at an applied potential that is more negative than 200 mVs vs. Ag wire reference electrode. We note that, Ag connections were formed in 100 percent of electrodes when Ag was electrodeposited from 5 and 50 mM Ag nitrate solution and the applied potential ranged between -200 mVs and -400 mVs vs. Ag wire. However, when the applied potential is at least or more negative than 400 mVs we observed a decrease in the percentage of electrodes that resulted in connections between the electrodes. To explain these results, more trials would be necessary to statistically validate these results. We note that, irrespective of the applied potential, the formation of connections was not favored when Ag was electrodeposited from 0.5 mM AgNO<sub>3</sub> solution. At these conditions the distance between the nuclei is probably at least 5 times larger than the radius of the growing granule, which favors the formation of individual spherical diffusion layer around each

growing grain resulting in the formation of no Ag connections between the Au IDA electrodes.

In conclusion, Ag ion concentration and applied potential does impact the morphology of electrodeposited Ag at micron gap Au electrodes. Higher Ag concentration leads to larger concentration gradients, higher flux of Ag ions to the Au IDA electrodes and thus higher nucleation rate. High over potential also lead to more nuclei formation. High nucleation on the Au IDA electrode surface does not favor the formation of individual spherical diffusion layer around each growing grain. Rather common diffusion layer of macro electrode is formed quickly. Hence, diffusion of Ag ions is facilitated to the tip of the nuclei and favors the formation of connection between the micron gap electrodes. Combination of higher flux of Ag ions to Au IDA surface and higher over potential promote the formation of Ag connections between the micron gap Au IDA electrodes.

#### IV. Pd Electrodeposition

There has been an increase in practical and theoretical interest of noble metal deposition in the past few decades.<sup>114</sup> Procedures for depositing thin film and different forms of nanostructures have been reported in the literature and are still being researched.<sup>114-128</sup> Pd deposition has been used a lot in hydrogen sensing<sup>115-117</sup> and has been applied in biofuel cells.<sup>118-119</sup> Hydrogen sensing is useful for detecting gas leaks in homes and/ or workplaces. Biofuel cells are currently being studied by many people due to their potential of green energy. However, the method of the Pd deposition varies. The following methods have been used for Pd deposition: electro-less deposition such as direct deposition via immersion,<sup>120-122</sup> galvanic deposition<sup>123-125</sup> and chemical vapor deposition (CVD).<sup>126-128</sup> The advantages and disadvantages for CVD and electro-less deposition methods via immersion have been addressed in Chapter III. Galvanic replacement is the unprompted replacement of surface layers of a metal by a more noble metal when the former is treated with a solution containing the latter in ionic form.<sup>123</sup> As discussed in earlier chapters, post synthesis assembly is an issue with the above described Pd nanostructure synthesis methods. Hence, we used method reported by Zamborini and coworkers as it eliminates the issues associated with post synthesis assembly. Here, we investigated the impacts of Pd ion concentration and applied potential on the morphology of Pd electrodeposition on and across micron gap Au IDA electrodes.

As described in Chapter III, our chemical hypothesis is based on *the Fick's 1<sup>st</sup> law* of diffusion and *Nernst equation* (see Chapter III for details).<sup>129</sup> Based on this, we expect the same results as stated in Chapter III, which is the following: the flux of Pd ions to Au IDA electrode surface is higher when Pd is electrodeposited from solution containing 50 mM, then 5 mM and 0.5 mM K<sub>2</sub>PdCl<sub>4</sub>. Also, applied potential impacts the difference in concentration of Pd ions at the surface of the electrode. Refer to Chapter II for electrodeposition procedure for Pd electrodeposition. To determine the impact of Pd ion concentration on morphology of the Pd electrodeposited other than the Pd ion concentration in solution, all the other parameters were kept constant. Three different concentrations were tested (0.5 mM, 5 mM and 50mM). To determine the impact of applied potential on morphology of the Pd deposited, we held the Pd ion concentration and all the other parameters constant and changed the applied potential. Five different potentials were tested (+0.1 V, 0.0 V, -0.1 V, -0.2 V and -0.3 V vs. Ag/AgCl wire). Please note, Zamborini and coworkers reported the formation of Pd NW connection between Au IDA electrodes when  $1.2 \cdot 10^{-3}$  C was reached from 5 mM K<sub>2</sub>PdCl<sub>4</sub> solution at an applied potential of -0.1 V. In this study, we electrodeposited Pd until  $1.2 \cdot 10^{-3}$  C of charge was passed.

Figure 4.1 and 4.2 shows overlay of chronocoulometric plots of electrodeposition from 0.5, 5, and 50 mM K<sub>2</sub>PdCl<sub>4</sub> solutions at different applied potentials. At a particular applied potential, the slope of the chronocoulometric plot of Pd electrodeposition is different when Pd is electrodeposited from different

concentrations of  $K_2PdCl_4$  solutions. The higher the concentration of  $K_2PdCl_4$ , the higher the slope was. At a particular applied potential, the time it took for  $1.2 \times 10^{-3} C$  to pass for Pd from different concentrations of  $K_2PdCl_4$  solutions was different.

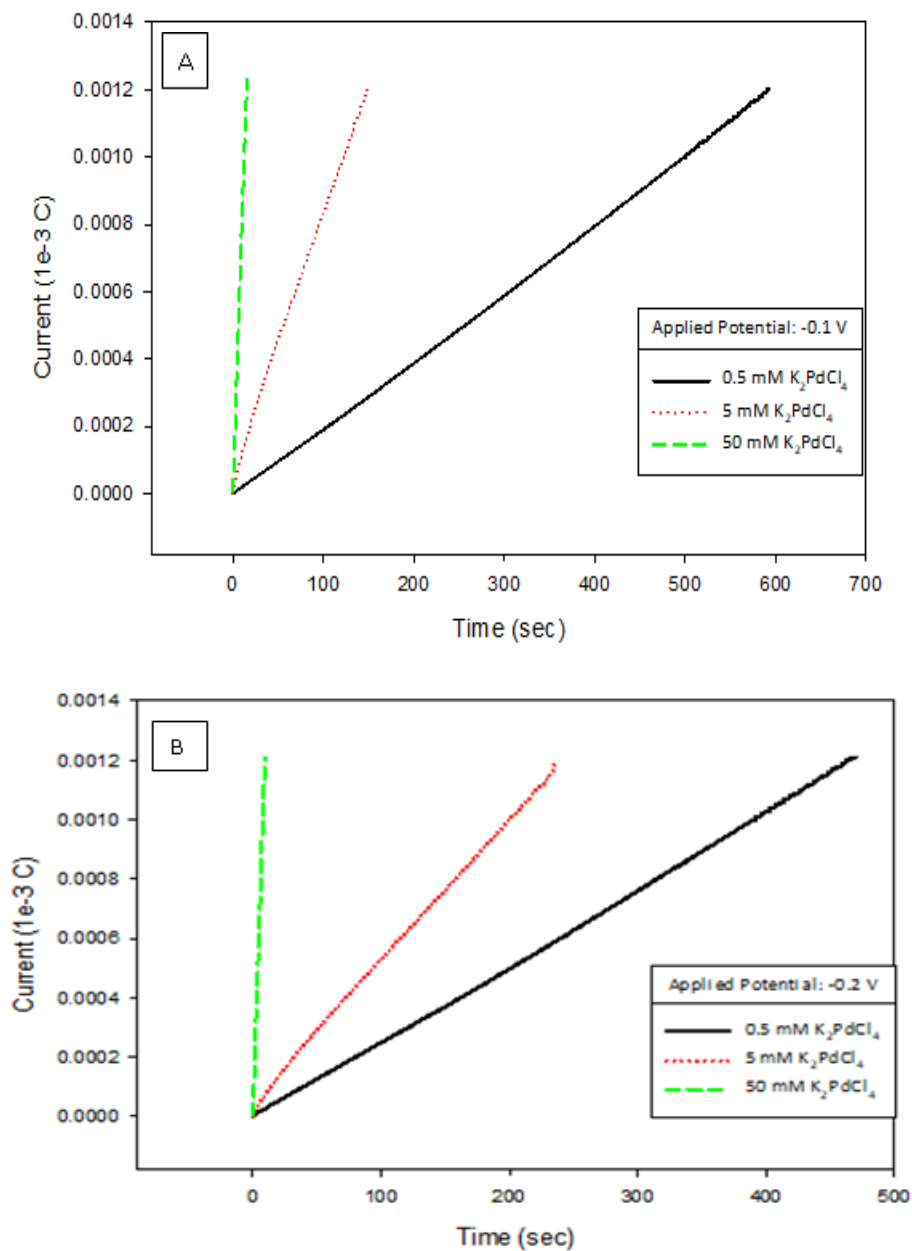


**Figure 4.1.** Overlay plot of chronocoulometric graphs showing electrodeposition of Pd from solution containing different concentrations of  $K_2PdCl_4$  at a) +0.1 V, b) 0.0 V, c) -0.1 V, d) -0.2 V, and e) -0.3 V vs. Ag/AgCl reference electrode.

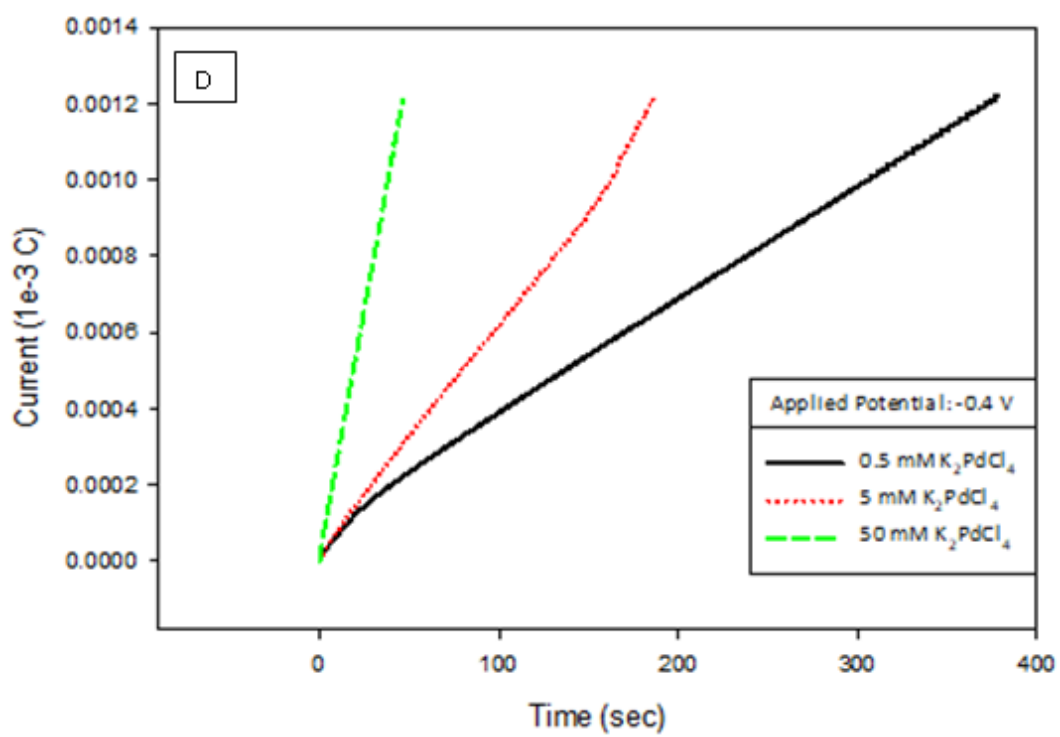
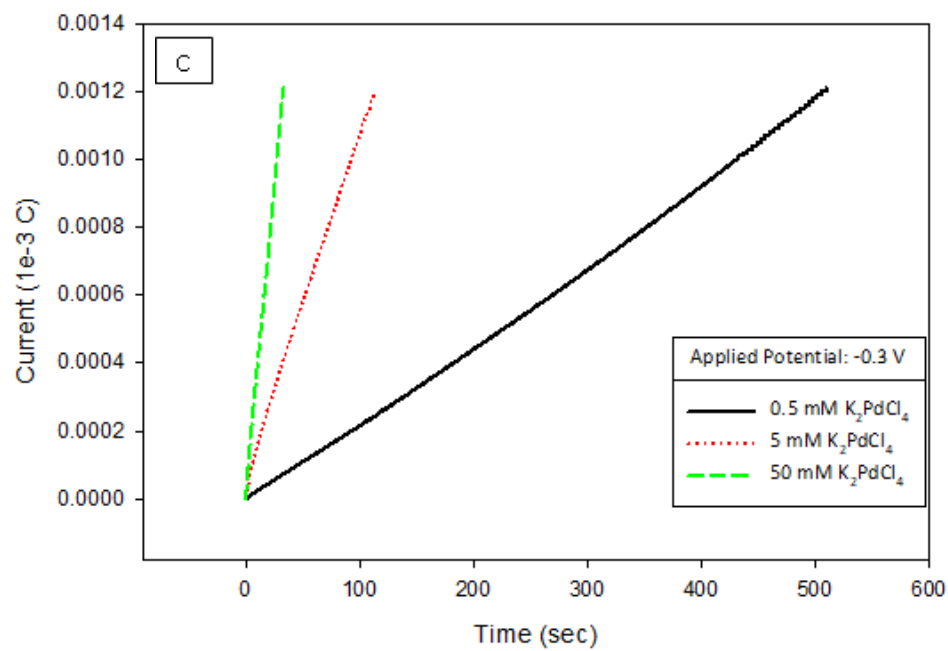


Figure 4.1. (continued).

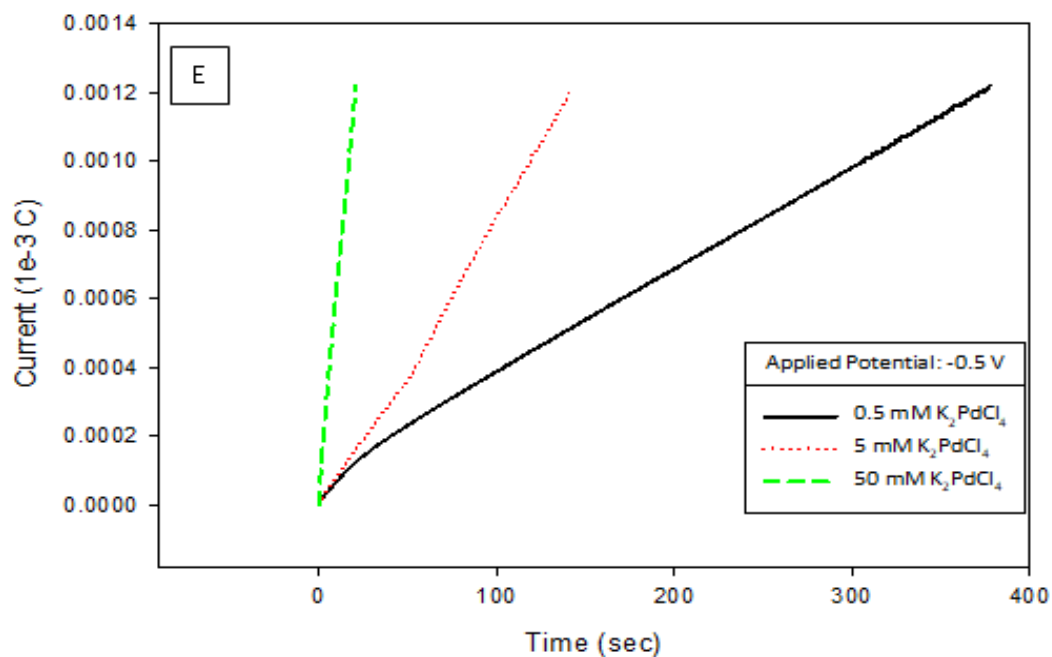


Figure 4.1. (continued).

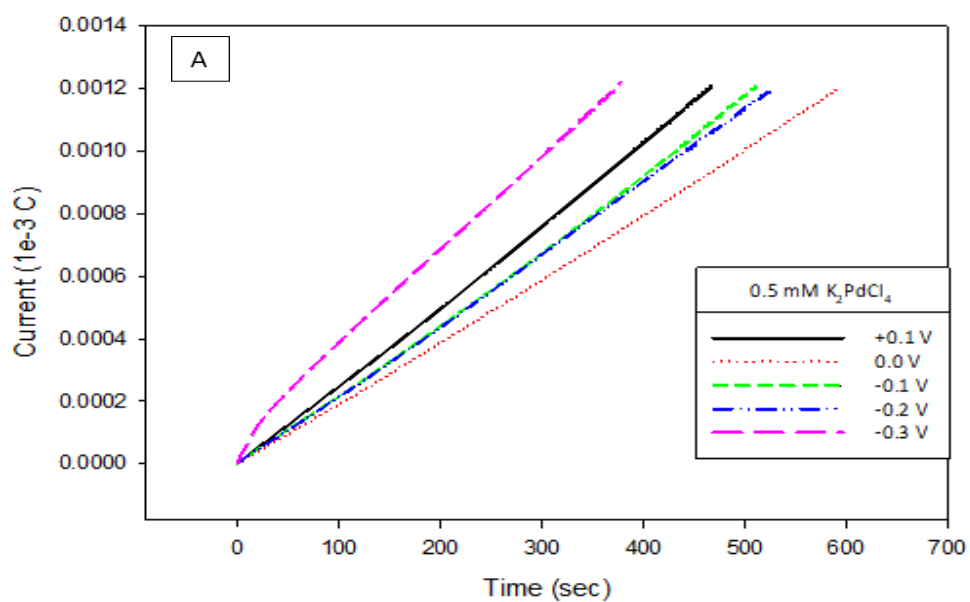


Figure 4.2. Overlay plot of chronocoulometric graphs showing Pd electrodeposition at various applied potential vs. Ag/AgCl reference electrode from solution containing: a) 0.5 mM, b) 5 mM, c) 50 mM  $K_2PdCl_4$ .

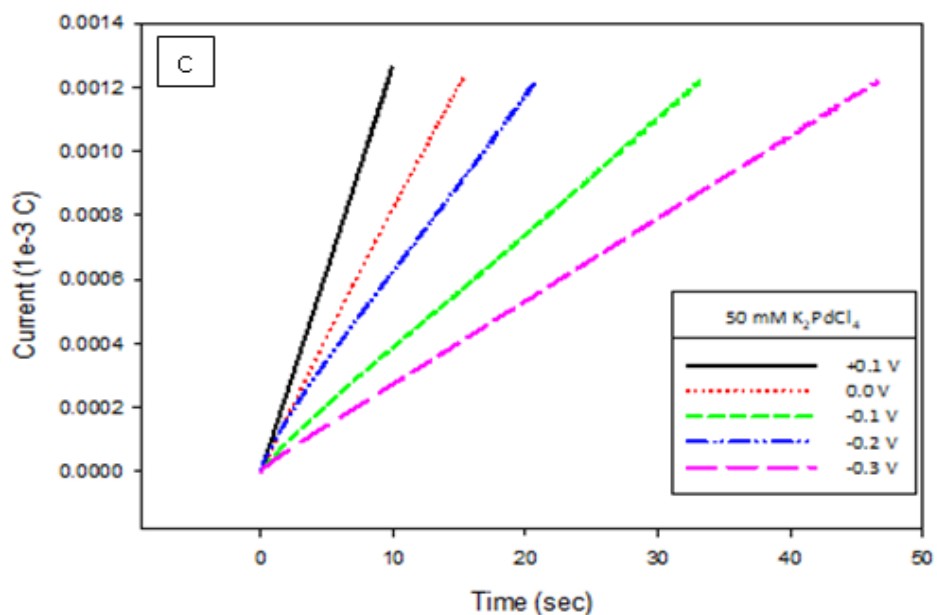
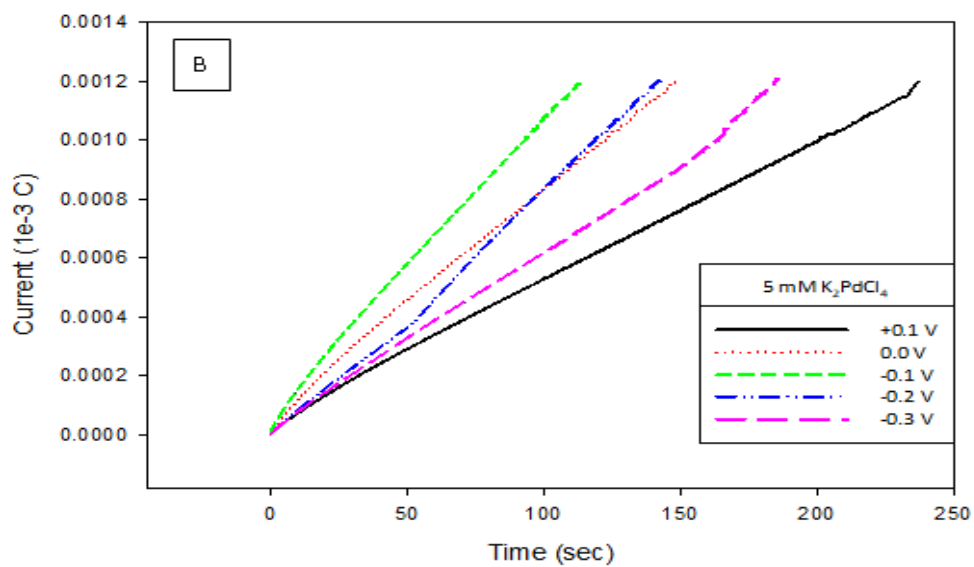


Figure 4.2. (continued).

Table 4.1 shows the times it took to electrodeposit Pd at a charge of  $1.2 \cdot 10^{-3} C$  at various potentials from different concentrations of  $K_2PdCl_4$  solution. At a particular

potential, the higher the concentration of  $K_2PdCl_4$  solution the lesser time it took to electrodeposit Pd. For instance, at an applied potential of +0.1V vs. Ag/AgCl wire it took 595, 150 and 15 seconds on average to electrodeposit  $1.2 \times 10^{-3}$  C of Pd from 0.5 mM, 5 mM and 50 mM  $K_2PdCl_4$  solution respectively (see Table 4.2).

	Concentrations								
	0.5 mM $K_2PdCl_4$			5 mM $K_2PdCl_4$			50 mM $K_2PdCl_4$		
Applied potential vs. Ag/AgCl wire	Trial 1	Trial 2	Trial 3	Trial 1	Trial 2	Trial 3	Trial 1	Trial 2	Trial 3
+0.1 V	585 sec	595 sec	602 sec	147 sec	150 sec	151 sec	12 sec	14 sec	15 sec
0.0 V	525 sec	472 sec	530 sec	228 sec	239 sec	235 sec	9 sec	11 sec	10 sec
-0.1 V	511 sec	515 sec	526 sec	112 sec	115 sec	124 sec	29 sec	33 sec	35 sec
-0.2 V	380 sec	394sec	374sec	178 sec	185 sec	188 sec	42 sec	46 sec	46 sec
-0.3 V	521 sec	532 sec	547 sec	137 sec	143 sec	147 sec	16 sec	21 sec	20 sec

	Concentrations		
Applied potential vs. Ag/AgCl wire	0.5 mM $K_2PdCl_4$	5 mM $K_2PdCl_4$	50 mM $K_2PdCl_4$
+0.1 V	595 sec	150 sec	15 sec
0.0 V	530 sec	234 sec	10 sec
-0.1 V	517 sec	119 sec	32 sec
-0.2 V	382 sec	185 sec	44 sec
-0.3 V	533 sec	142 sec	19 sec

This indicates that at a particular applied potential, the flux of Pd ion to the surface of substrate is different when Pd is electrodeposited from solutions containing different concentrations of  $K_2PdCl_4$ . The higher the Pd ion concentration, the higher the flux of Pd ions to the Au IDA electrode surface. However, at a particular concentration, the time it took to electrodeposit Pd at various applied potentials was not statistically different from each other. This indicates that there is no significant difference in the flux of Pd ions to the substrate at different applied potentials (See Figure 4.2 and Table 4.2).

After electrodepositing Pd we obtained i-V curves, to determine whether or not a Pd connection was formed between the Au IDA. Figure 4.3 shows the overlay of CV plots obtained in air before and after electrodeposition of Pd from 0.5 mM, 5 mM and 50 mM  $K_2PdCl_4$  respectively at an applied potential of +0.1 V vs. Ag/AgCl wire. Before Pd electrodeposition, currents observed in air (background current) at -1 V ranged from  $1.05 \times 10^{-7}$  A to  $1.68 \times 10^{-7}$  A for all three devices. Currents observed in air at -1 V are  $1.4 \times 10^{-7}$  A,  $1.3 \times 10^{-2}$  A and  $1.3 \times 10^{-2}$  A after electrodepositing Pd from 0.5 mM, 5 mM and 50 mM  $K_2PdCl_4$  solution. There was no significant difference in current observed in air at -1 V before and after electrodepositing Pd from 0.5 mM  $K_2PdCl_4$  solution. This indicates that no Pd connections were formed between the 5 micron-gap Au IDA electrodes. However, there was a significant difference in current when Pd was electrodeposited from 5 mM and 50 mM  $K_2PdCl_4$  solution. This indicates that a Pd connection was formed between the 5 micron gap Au IDA electrodes.

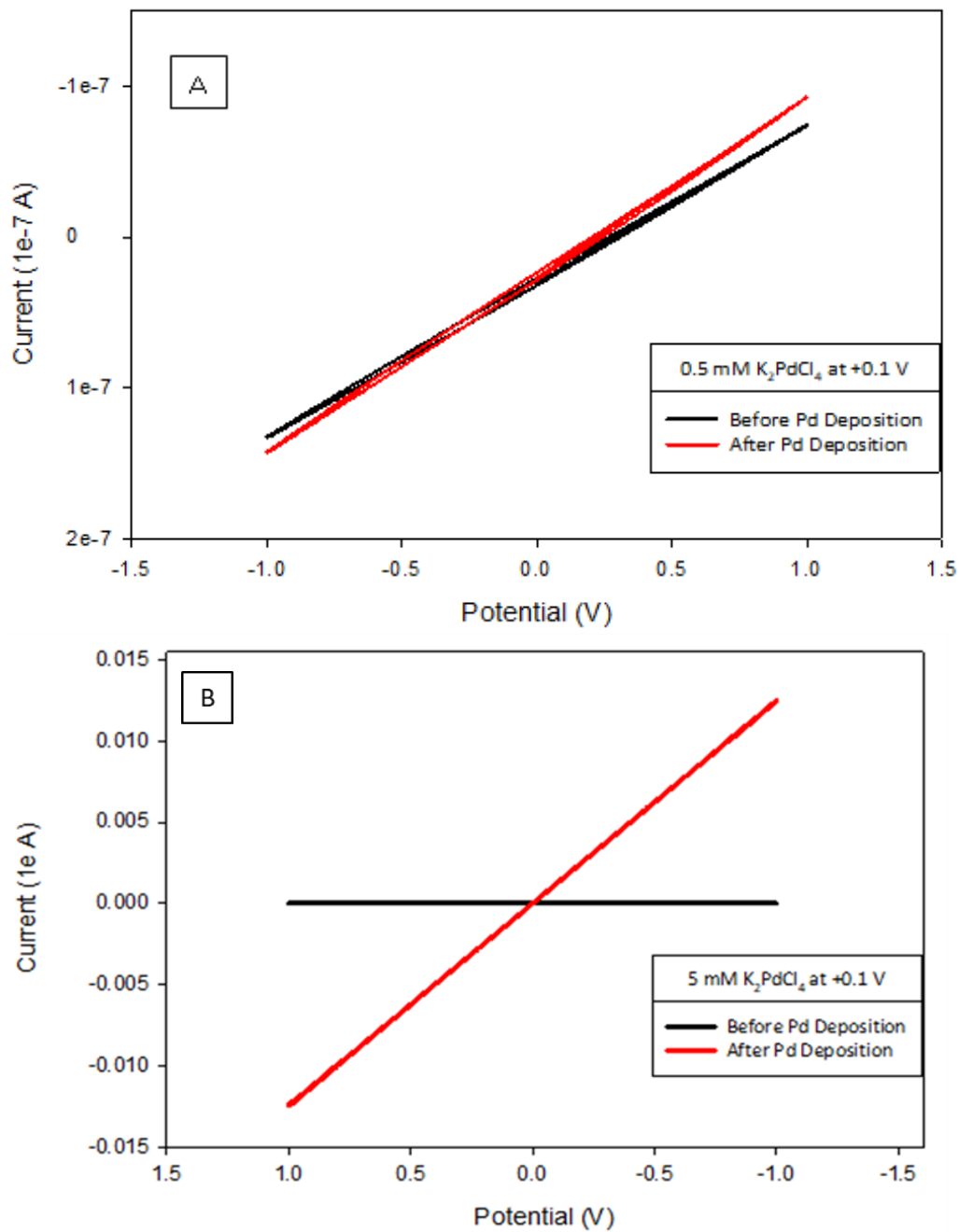


**Figure 4.3.** Overlay plot of CV of Au IDA electrode in air before (black lines) and after (red lines) Pd electrodeposition at +0.1V potential from A) 0.5 mM, B) 5 mM and C) 50 mM  $K_2PdCl_4$  solution.

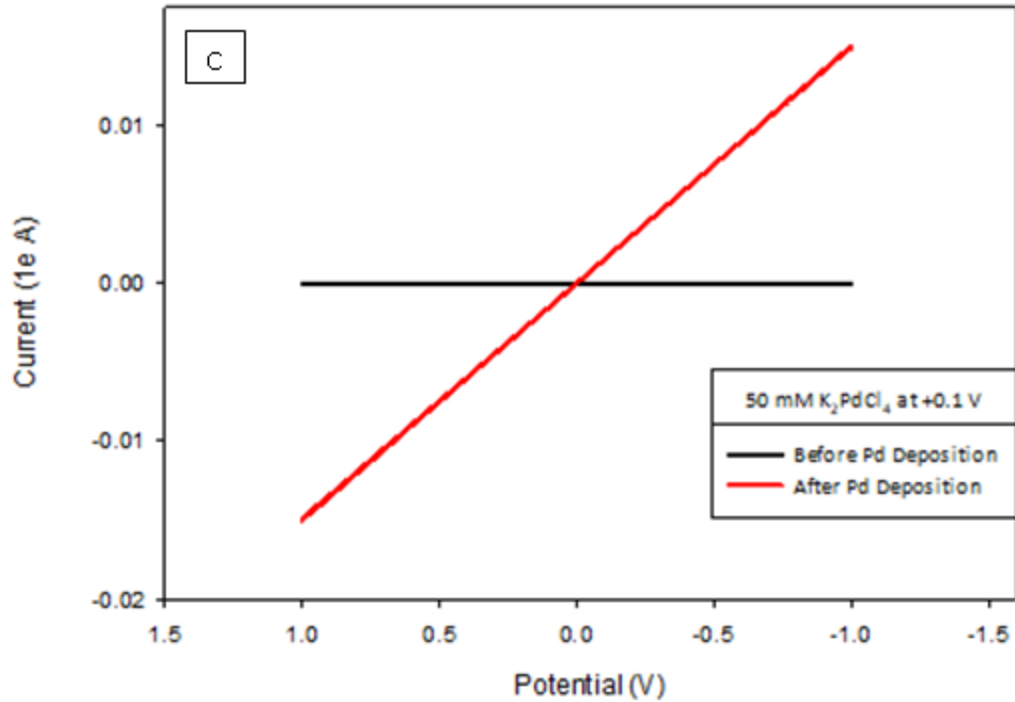


**Figure 4.3.** (continued).

Table 4.3a-c shows the currents observed at -1 V in air before and after electrodepositing Pd at various potentials from different concentrations of  $K_2PdCl_4$  solution. Pd is more conductive than the SiO that connects the 5 micron-gap Au electrodes. If a Pd connection is made between the micron gap Au electrodes, a significant (several orders of magnitude) increase in current would be observed at -1 V due to the formation of metal (Pd)/metal (Au) contact.

Table 4.3a Currents observed at -1 V before and after electrodeposition of Pd at various applied potentials from 0.5 mM $K_2PdCl_4$ solution						
	0.5 mM $K_2PdCl_4$					
	Trial 1		Trial 2		Trial 3	
	Before	After	Before	After	Before	After
+0.1 V	$1.32 \times 10^{-7}$ C	$1.27 \times 10^{-2}$ C	$1.29 \times 10^{-7}$ C	$1.22 \times 10^{-7}$ C	$1.26 \times 10^{-7}$ C	$1.27 \times 10^{-7}$ C

Table 4.3a Currents observed at -1 V before and after electrodeposition of Pd at various applied potentials from 0.5 mM K <sub>2</sub> PdCl <sub>4</sub> solution (continued)						
0.0 V	1.27x10 <sup>-7</sup> C	7.11x10 <sup>-3</sup> C	1.09x10 <sup>-7</sup> C	1.94x10 <sup>-7</sup> C	1.20x10 <sup>-7</sup> C	1.40x10 <sup>-7</sup> C
-0.1 V	1.24x10 <sup>-7</sup> C	6.27x10 <sup>-3</sup> C	1.22x10 <sup>-7</sup> C	3.08x10 <sup>-7</sup> C	1.51x10 <sup>-7</sup> C	1.85x10 <sup>-7</sup> C
-0.2 V	1.43x10 <sup>-7</sup> C	1.06x10 <sup>-2</sup> C	1.32x10 <sup>-7</sup> C	1.80x10 <sup>-7</sup> C	1.21x10 <sup>-7</sup> C	1.39x10 <sup>-7</sup> C
-0.3 V	1.66x10 <sup>-7</sup> C	5.92x10 <sup>-3</sup> C	1.12x10 <sup>-7</sup> C	1.19x10 <sup>-7</sup> C	1.06x10 <sup>-7</sup> C	1.24x10 <sup>-7</sup> C

Table 4.3b Currents observed at -1 V before and after electrodeposition of Pd at various applied potentials 5 mM K <sub>2</sub> PdCl <sub>4</sub> solution						
	5 mM K <sub>2</sub> PdCl <sub>4</sub>					
	Trial 1		Trial 2		Trial 3	
	Before	After	Before	After	Before	After
+0.1 V	1.16x10 <sup>-7</sup> C	1.56x10 <sup>-7</sup> C	1.14x10 <sup>-7</sup> C	1.64x10 <sup>-7</sup> C	1.12x10 <sup>-7</sup> C	1.62x10 <sup>-7</sup> C
0.0 V	1.46x10 <sup>-7</sup> C	7.16x10 <sup>-3</sup> C	1.24x10 <sup>-7</sup> C	4.82x10 <sup>-2</sup> C	1.26x10 <sup>-7</sup> C	1.33x10 <sup>-2</sup> C
-0.1 V	1.24x10 <sup>-7</sup> C	4.91x10 <sup>-3</sup> C	1.28x10 <sup>-7</sup> C	5.29x10 <sup>-3</sup> C	1.42x10 <sup>-7</sup> C	1.05x10 <sup>-2</sup> C
-0.2 V	1.16x10 <sup>-7</sup> C	1.51x10 <sup>-2</sup> C	1.19x10 <sup>-7</sup> C	1.07x10 <sup>-2</sup> C	1.62x10 <sup>-7</sup> C	1.17x10 <sup>-2</sup> C
-0.3 V	1.36x10 <sup>-7</sup> C	1.06x10 <sup>-2</sup> C	1.60x10 <sup>-7</sup> C	1.12x10 <sup>-2</sup> C	1.06x10 <sup>-7</sup> C	1.27x10 <sup>-7</sup> C

Table 4.3c Currents observed at -1 V before and after electrodeposition of Pd at various applied potentials from 50 mM K <sub>2</sub> PdCl <sub>4</sub> solution						
	50 mM K <sub>2</sub> PdCl <sub>4</sub>					
	Trial 1		Trial 2		Trial 3	
	Before	After	Before	After	Before	After
+0.1 V	1.35x10 <sup>-7</sup> C	1.25x10 <sup>-7</sup> C	1.18x10 <sup>-7</sup> C	1.28x10 <sup>-7</sup> C	1.19x10 <sup>-7</sup> C	1.30x10 <sup>-7</sup> C
0.0 V	1.22x10 <sup>-7</sup> C	1.44x10 <sup>-2</sup> C	1.27x10 <sup>-7</sup> C	1.34x10 <sup>-2</sup> C	1.31x10 <sup>-7</sup> C	1.90x10 <sup>-3</sup> C

-0.1 V	1.08x10 <sup>-7</sup> C	1.11x10 <sup>-2</sup> C	1.38x10 <sup>-7</sup> C	1.36x10 <sup>-2</sup> C	1.24x10 <sup>-7</sup> C	6.03x10 <sup>-3</sup> C
-0.2 V	1.21x10 <sup>-7</sup> C	1.38x10 <sup>-2</sup> C	1.13x10 <sup>-7</sup> C	1.85x10 <sup>-7</sup> C	1.16x10 <sup>-7</sup> C	1.28x10 <sup>-7</sup> C
-0.3 V	1.25x10 <sup>-7</sup> C	1.02x10 <sup>-2</sup> C	1.20x10 <sup>-7</sup> C	1.14x10 <sup>-2</sup> C	1.10x10 <sup>-7</sup> C	1.22x10 <sup>-7</sup> C

Approximately five orders of magnitude increase in current was observed, indicating the formation of Pd connection between the micron gap Au IDA electrodes at these conditions. See appendix for the overlay of CV plots obtained in air before and after electrodeposition of Pd from 0.5 mM, 5 mM and 50 mM K<sub>2</sub>PdCl<sub>4</sub> respectively at various applied potential vs. Ag/AgCl reference electrode. When the observed currents in air at -1 V are in the range of 10<sup>-2</sup> to 10<sup>-3</sup> A, formation of Pd connection between the micron gap Au IDAs is attributed. Table 4.4 shows Pd ion concentration and the applied potential that favored formation of Pd connections between the micron gap Au IDA electrodes.

Applied potential vs. Ag/AgCl wire	0.5 mM K <sub>2</sub> PdCl <sub>4</sub>			5 mM K <sub>2</sub> PdCl <sub>4</sub>			50 mM K <sub>2</sub> PdCl <sub>4</sub>		
	Trial 1	Trial 2	Trial 3	Trial 1	Trial 2	Trial 3	Trial 1	Trial 2	Trial 3
+0.1 V	N	N	N	Y	Y	Y	Y	Y	Y
0.0 V	N	N	N	N	N	N	N	N	N
-0.1 V	N	N	N	Y	Y	Y	Y	Y	Y
-0.2 V	N	N	N	Y	Y	Y	Y	Y	N
-0.3 V	N	N	N	Y	Y	Y	Y	Y	Y

Results indicate that Pd electrodeposited from 5 and 50 mM  $K_2PdCl_4$  solutions favor the formation of connection between the micron gap Au electrodes when the applied potential is at least or more negative than 100 mVs vs. Ag/AgCl reference electrode. Irrespective of the applied potential, formation of connections was not favored when Pd was electrodeposited from 0.5 mM  $K_2PdCl_4$  solutions.

At a particular applied potential, flux of Pd ions to the Au IDA electrode surface is higher when Pd is electrodeposited from higher concentrations (5 and 50 mM) of  $K_2PdCl_4$  in solution compared to lower concentration (0.5 mM) of  $K_2PdCl_4$  in solution. Higher flux of the Pd ion to the Au IDA electrode surface seems to favor the formation of Pd connection. However, even at high concentrations (5 and 50 mM) of  $K_2PdCl_4$  in solution formation of connections was not observed unless the applied potential is at least or more negative than 100 mVs vs. Ag/AgCl wire. Flux of Pd ion to the Au IDA electrode surface at -100 mVs and -200 mVs not statistically different from each other. Hence, the difference in morphology of electrodeposited Pd at various applied potentials cannot be solely attributed to the impact of difference in flux of the Pd ion to the Au IDA electrode surface. Higher flux and high overpotentials lead to more nucleation on the Au IDA electrode surface. This in turn leads to a difference in the diffusion layer structure as reported earlier which probably results in different morphologies of Pd electrodeposition at micron gap Au IDA electrodes. This is explained in detail in the next section.

Several reports on electrodeposition growth mechanism demonstrate the formation of granules/particles in the initial stages of electrodeposition process.<sup>111</sup> These granules further grow into different structures if the deposition is continued.<sup>111</sup> These growing grains act as individual microelectrodes if they are small (less than 55 micrometers). According to Barton and Bockris, when the distance between the granules is at least 5 times larger than the radius of the growing granule, individual spherical diffusion layer forms around each growing grain (see Figure 3.4).<sup>112</sup> This facilitates the diffusion of ions to all directions of the growing granules. As a result, granule grows in all directions. On the contrary, when the distance between the granules is smaller than 5 times the radius of the growing granule, individual spherical diffusion layer does not form around each growing grain. Rather common diffusion layer of macro electrode is formed. In this scenario, diffusion of ions is facilitated to the tip of the growing grain which favors the formation of Pd connections between the micron gap Au IDA electrodes.

More number of granules are formed at more negative applied potentials and when Pd is electrodeposited from solutions containing high concentration of Pd ions. Hence, at less negative applied potential or low over-potential (less negative than -100 mVs vs. Ag/AgCl), probably a smaller number of nuclei form leading to larger distance between the growing granules. The distance between the granules is probably large enough to favor the formation of individual spherical diffusion around each growing grain which facilitates the growth of the granule in all directions resulting in no growth

of Pd connections between the micron gap Au electrodes. This could be the reason that electrodeposition of Pd from 5 and 50 mM  $K_2PdCl_4$  solutions did not result in the formation of connection between micron gap electrodes at low over-potentials (at an applied potential that is less negative than 100 mVs vs. Ag/AgCl). Similarly, when the applied potential or over-potential is more negative than -100 mVs vs. Ag/AgCl reference electrode, more granules might have formed on the surface. The distance between the granules is probably smaller than 5 times the radius of the granule. This does not favor the formation of individual spherical diffusion layer around each growing grain. Rather common diffusion layer of macro electrode is formed quickly. In this scenario, diffusion of Pd ions is facilitated to the tip of the nuclei. This favors the formation of connection between the micron gap electrodes. This is what we propose could be happening when Pd was electrodeposited from 5 and 50 mM  $K_2PdCl_4$  solutions at an applied potential that is more negative than 100 mVs vs. Ag/AgCl reference electrode. We note that 100% of electrodes resulted in connections when Pd was electrodeposited from 5 and 50 mM  $K_2PdCl_4$  solution and the applied potential at +100 mVs, -100 mVs and -300 mVs vs. Ag/AgCl. However, when the applied potential is at -200 mVs we observed a decrease in the percentage of electrodes that resulted in connections between the electrodes. This could be due to the difference in the surfaces of the micron gap Au electrodes. Micron gap Au electrodes are not atomically smooth and nucleation occurs preferentially at the active sites or defects on the surface of the micron gap Au electrode. The electrodes that did not result in the formation of Pd

connection between the micron gap Au IDA electrodes probably had a smaller number of active sites on the surface. This probably resulted in formation of a smaller number of nuclei on the surface which facilitates the formation of individual spherical diffusion layer which favors the growth of granules in all directions resulting in no Pd connection between the micron-gap Au IDA electrodes. At this point, we do not fully understand what is going on when the applied potential is 0 V vs. Ag/AgCl. These trials should be repeated to further investigate why no connection was formed. We note that, irrespective of the applied potential, the formation of connections was not favored when Pd was electrodeposited from solution containing 0.5 mM Pd. At these conditions the distance between the nuclei is probably at least 5 times larger than the radius of the growing granule, which favors the formation of individual spherical diffusion layer around each growing grain resulting in the formation of no Pd connections between the Au IDA electrodes.

In conclusion, Pd ion concentration and applied potential does impact the morphology of electrodeposited Pd at micron gap Au electrodes. Higher Pd concentration leads to larger concentration gradients, higher flux of Pd ions to the Au IDA electrodes and thus higher nucleation rate. High over potential also leads to more nuclei formation. High nucleation on the Au IDA electrode surface does not favor the formation of individual spherical diffusion layer around each growing grain. Rather common diffusion layer of macro electrode is formed quickly. Hence, diffusion of Pd ions is facilitated to the tip of the nuclei and favors the formation of connection

between the micron gap electrodes. Combination of higher flux of Pd ions to Au IDA surface and higher over potential promote the formation of Pd connections between the micron gap Au IDA electrodes.

## **V. Future Direction**

In future, scanning electron microscope (SEM) image of every Au IDA electrode after Ag and Pd electrodeposition would be obtained. Correlation of i-V curves and SEMs would be performed to better understand the impact of metal ion concentration and applied potential on morphology of Ag and Pd electrodeposition at micron gap Au IDA electrodes.

## References

1. MyaKhin, M., Nair, A., Babu, V., Murugana, R., & Ramakrishna, S. (n.d.). A review on nanomaterials for environmental remediation ... Retrieved from [https://www.researchgate.net/publication/235907565\\_A\\_review\\_on\\_nanomaterials\\_for\\_environmental\\_remediation](https://www.researchgate.net/publication/235907565_A_review_on_nanomaterials_for_environmental_remediation)
2. Murray, R. W. Murray, R. (n.d.). Nanoelectrochemistry: Metal Nanoparticles, Nanoelectrodes, and Nanopores. Retrieved from <https://pubs.acs.org/doi/10.1021/cr068077e>
3. Chemistry in Nanotechnology: Particles, Bonds and Structure. (2015, November 27). Retrieved from <http://www.biologydiscussion.com/nanotechnology-2/chemistry-in-nanotechnology-particles-bonds-and-structure/16109>
4. Sylvestre, J. (2004, October 06). Surface Chemistry of Gold Nanoparticles Produced by Laser Ablation in Aqueous Media. Retrieved from <https://pubs.acs.org/doi/10.1021/jp047134>
5. Size and Shape Dependent Second Order Nonlinear Optical Properties of Nanomaterials and Their Application in Biological and Chemical Sensing. (n.d.). Retrieved from <https://pubs.acs.org/doi/abs/10.1021/cr900335g>
6. Shui, J., Chen, C., & Li, J. C. (2011, July 11). Evolution of Nanoporous Pt–Fe Alloy Nanowires by Dealloying and their Catalytic Property for Oxygen Reduction Reaction - Shui - 2011 - Advanced Functional Materials - Wiley Online Library. Retrieved from <https://onlinelibrary.wiley.com/doi/abs/10.1002/adfm.201100723>

6. Maier, S. A., Kik, P. G., Atwater, H. A., Meltzer, S., Harel, E., Koel, B. E., & Requicha, A. A. (2016, March 20). Local detection of electromagnetic energy transport below the diffraction limit in metal nanoparticle plasmon waveguides. Retrieved from <https://www.scholars.northwestern.edu/en/publications/local-detection-of-electromagnetic-energy-transport-below-the-dif>
7. Tao, A.; Kim, F.; Hess, C.; Goldberger, J.; He, R.; Sun, Y.; Xia, Y.; Yang, P.(n.d.). Langmuir–Blodgett Silver Nanowire Monolayers for Molecular Sensing Using Surface-Enhanced Raman Spectroscopy. Retrieved from <https://pubs.acs.org/doi/10.1021/nl0344209>Huang, X.; El-Sayed, I. H.; Qian, W.; El-Sayed, M. A. J. Am. Chem. Soc. 2006, *128*, 2115-2120.
8. Schwartzberg, A. M.; Zhang, J. Z. (n.d.). Facile Fabrication and Unexpected Electrocatalytic Activity of Palladium Thin Films with Hierarchical Architectures. Retrieved from <https://pubs.acs.org/doi/abs/10.1021/jp804828k>
9. Chen, M.; Goodman, D. W. (n.d.). Catalytically Active Gold: From Nanoparticles to Ultrathin Films. Retrieved from <https://pubs.acs.org/doi/10.1021/ar040309d>
10. Marinakos, S., Chen, S., & Chilkoti, A. (n.d.). Plasmonic Detection of a Model Analyte in Serum by a Gold Nanorod Sensor. Retrieved from <https://pubs.acs.org/doi/abs/10.1021/ac0706527>

11. Zhu, J., Holmen, A., & Chen, D. (2013, January 25). Carbon Nanomaterials in Catalysis: Proton Affinity, Chemical and Electronic Properties, and their Catalytic Consequences - Zhu - 2013 - ChemCatChem - Wiley Online Library. Retrieved from <https://onlinelibrary.wiley.com/doi/abs/10.1002/cctc.201200471>
12. Yang, W., Ratinac, K., Ringer, S., Thordarson, P., Gooding, J., & Braet, F. (2010, February 24). Carbon Nanomaterials in Biosensors: Should You Use Nanotubes or Graphene? - Yang - 2010 - Angewandte Chemie International Edition - Wiley Online Library. Retrieved from <https://onlinelibrary.wiley.com/doi/abs/10.1002/anie.200903463>
13. Hubbell, J. A., & Chilkoti, A. (2012, July 20). Nanomaterials for Drug Delivery. Retrieved from <https://science.sciencemag.org/content/337/6092/303> Kavosh, M., Moallemian, H., Molaei, H., Mehranniya, H., Salami, M., & Dehdashti, M. E. (2016). Study of Optical and Structural Properties of Zinc Oxide Nanofibers by Using Zn(ac) 2 /PVA Precursors. *Synthesis & Reactivity in Inorganic, Metal-Organic, & Nano-Metal Chemistry*, 46(2), 225–229. <https://doi.org/10.1080/15533174.2014.963248>
14. Bera, D., Lei Qian, Teng-Kuan Tseng, & Holloway, P. H. (2010). Quantum Dots and Their Multimodal Applications: A Review. *Materials (1996-1944)*, 3(4), 2260–2345. <https://doi.org/10.3390/ma3042260>
15. Pitto-Barry, A., Sadler, P. J., & Barry, N. P. (2015, December 24). Dynamics of formation of Ru, Os, Ir and Au metal nanocrystals on doped graphitic surfaces. Retrieved from <https://pubs.rsc.org/en/content/articlelanding/2015/cc/c5cc09564f#ldivAbstract>

16. Biomolecule-Based Nanomaterials and Nanostructures. (n.d.). Retrieved from <https://pubs.acs.org/doi/10.1021/nl102083j>
17. Murray, R. W. Murray, R. (n.d.). Nanoelectrochemistry: Metal Nanoparticles, Nanoelectrodes, and Nanopores. Retrieved from <https://pubs.acs.org/doi/10.1021/cr068077e>
18. Chen, M., & Goodman, D. W. (2008, July 10). Catalytically active gold on ordered titania supports. Retrieved from <https://pubs.rsc.org/en/content/articlelanding/2008/cs/b707318f#!divAbstract>
19. Mohamed, M., Volkov, V., Link, S., & El-Sayed, M. (2000, February 14). The 'lightning' gold nanorods: Fluorescence enhancement of over a million compared to the gold metal. Retrieved from <https://www.sciencedirect.com/science/article/abs/pii/S0009261499014141?via=ihub>
20. Luk'yanchuk, B., Zheludev, N. I., Maier, S. A., Halas, N. J., Nordlander, P., Giessen, H., & Chong, C. T. (2010, August 23). The Fano resonance in plasmonic nanostructures and metamaterials. Retrieved from <https://www.nature.com/articles/nmat2810>
21. Gold Nanoparticles: Properties and Applications. (n.d.). Retrieved from <https://www.sigmaaldrich.com/technical-documents/articles/materials-science/nanomaterials/gold-nanoparticles.html>

22. Zhang, L., Wang, J., & Tian, Y. (2014, February 28). Electrochemical in-vivo sensors using nanomaterials made from carbon species, noble metals, or semiconductors. Retrieved from <https://link.springer.com/article/10.1007/s00604-014-1203-z>
23. Li, M., Gou, H., Al-Ogaidi, I., & Wu, N. (n.d.). Nanostructured Sensors for Detection of Heavy Metals: A Review. Retrieved from <https://pubs.acs.org/doi/abs/10.1021/sc400019a>
24. Ji, C., & Park, H. S. (1970, January 01). The coupled effects of geometry and surface orientation on the mechanical properties of metal nanowires - Semantic Scholar. Retrieved from <https://www.semanticscholar.org/paper/The-coupled-effects-of-geometry-and-surface-on-the-Ji-Park/a8d92dc198bc9eb1cf7fd5c1a49bdcbf8d2b8611> Pan, H., Liu, B., Yi, J., Poh, C., Lim, S., & Ding, J. (n.d.). Growth of Single-Crystalline Ni and Co Nanowires via Electrochemical Deposition and Their Magnetic Properties. Retrieved from <https://pubs.acs.org/doi/10.1021/jp0451997>
25. Alavian, F., & Shams, N. (2019, July 04). Oral and intranasal administration of nanoparticles in the cerebral ischemia treatment; Considering the advantages and disadvantages. Retrieved from <https://www.ncbi.nlm.nih.gov/pubmed/31272358>

26. Ji, C., & Park, H. S. (1970, January 01). The coupled effects of geometry and surface orientation on the mechanical properties of metal nanowires - Semantic Scholar. Retrieved from <https://www.semanticscholar.org/paper/The-coupled-effects-of-geometry-and-surface-on-the-Ji-Park/a8d92dc198bc9eb1cf7fd5c1a49bdcbf8d2b8611>
27. Silver-Coated Engineered Magnetic Nanoparticles Are Promising for the Success in the Fight against Antibacterial Resistance Threat. (n.d.). Retrieved from <https://pubs.acs.org/doi/abs/10.1021/nn300042m>
28. Mimura, N., Hiyoshi, N., Daté, M., Fujitani, T., & Dumeignil, F. (2014). Microscope Analysis of Au-Pd/TiO Glycerol Oxidation Catalysts Prepared by Deposition-Precipitation Method. *Catalysis Letters*, 144(12), 2167–2175. <https://doi.org/10.1007/s10562-014-1382-6>
29. Schider, G., Krenn, J. R., Gotschy, W., Lamprecht, B., Ditlbacher, H., Leitner, A., & Aussenegg, F. R. (2001, October 15). Optical properties of Ag and Au nanowire gratings. Retrieved from <https://aip.scitation.org/doi/10.1063/1.1404425>
30. Aliev, A., & Aliev, A. (n.d.). Improved Electrical Conductivity of Graphene Films Integrated with Metal Nanowires. Retrieved from [https://www.academia.edu/24226461/Improved\\_Electrical\\_Conductivity\\_of\\_Graphene\\_Films\\_Integrated\\_with\\_Metal\\_Nanowires](https://www.academia.edu/24226461/Improved_Electrical_Conductivity_of_Graphene_Films_Integrated_with_Metal_Nanowires)
31. Banadaki, A. D., & Kajbafvala, A. (2014). Recent Advances in Facile Synthesis of Bimetallic Nanostructures: An Overview. *Journal of Nanomaterials*, 1–28. <https://doi.org/10.1155/2014/985948>

32. Chau, Y.-F. C., Chao, C.-T. C., Chiang, H.-P., Lim, C. M., Voo, N. Y., & Mahadi, A. H. (2018). Plasmonic effects in composite metal nanostructures for sensing applications. *Journal of Nanoparticle Research*, 20(7), 1. <https://doi.org/10.1007/s11051-018-4293-4>
33. Jin Huang, & Qing Wan. (2009). Gas Sensors Based on Semiconducting Metal Oxide One-Dimensional Nanostructures. *Sensors (14248220)*, 9(12), 9903–9924. <https://doi.org/10.3390/s91209903>
34. Lebukhova, N., Karpovich, N., Pyachin, S., Kirichenko, E., Makarevich, K., & Pugachevskii, M. (2017). Synthesis and optic properties of titanium dioxide nanostructures doped with alkali metals. *Theoretical Foundations of Chemical Engineering*, 51(5), 820–824. <https://doi.org/10.1134/S0040579517050141>
35. Lee, B. C., Kim, M. H., Chandran, J., Kim, S. K., Shin, H. J., & Moon, S. (2008). Metal nanostructures fabricated by selective metal nanoscale etch method. *Journal of Experimental Nanoscience*, 3(1), 87–94. <https://doi.org/10.1080/17458080802139892>
36. Chilstedt, S., Dong, C., & Chen, D. (2009). Design and Evaluation of a Carbon Nanotube-Based Programmable Architecture. *International Journal of Parallel Programming*, 37(4), 389–416. <https://doi.org/10.1007/s10766-009-0105-x>
37. Ravalia, A., Vagadia, M., Solanki, P. S., Asokan, K., & Kuberkar, D. G. (2015). Role of strain and nanoscale defects in modifying the multiferroicity in nanostructured BiFeO<sub>3</sub> films. *Journal of Experimental Nanoscience*, 10(14), 1057–1067. <https://doi.org/10.1080/17458080.2014.953608>

38. Soleimani H, Abbas Z, Yahya N, Shamel K, Soleimani H, Shabanzadeh P. Reflection and Transmission Coefficient of Yttrium Iron Garnet Filled Polyvinylidene Fluoride Composite Using Rectangular Waveguide at Microwave Frequencies. *International Journal of Molecular Sciences*. 2012;13(7):8540-8548. doi:10.3390/ijms13078540.
39. Zottel, A., Videtič Paska, A., & Jovčevska, I. (2019). Nanotechnology Meets Oncology: Nanomaterials in Brain Cancer Research, Diagnosis and Therapy. *Materials (1996-1944)*, 12(10), 1588. <https://doi.org/10.3390/ma12101588>
40. Zhao, Q., Lin, Y., Han, N., Li, X., Geng, H., Wang, X., ... Wang, S. (2017). Mesoporous carbon nanomaterials in drug delivery and biomedical application. *Drug Delivery*, 24(2), 94–107. <https://doi.org/10.1080/10717544.2017.1399300>
41. Rioux, R. M., & Kim, S. H. (2018). Molecular Surface Science, Nanomaterials & Catalysis: Symposium in Honor of Gabor Somorjai at 80. *Topics in Catalysis*, 61(9–11), 711–713. <https://doi.org/10.1007/s11244-018-0958-6>
42. Della Pelle, F., & Compagnone, D. (2018). Nanomaterial-Based Sensing and Biosensing of Phenolic Compounds and Related Antioxidant Capacity in Food. *Sensors (14248220)*, 18(2), 462. <https://doi.org/10.3390/s18020462>
43. Xu, Z., Lu, M., Jin, H., Chen, T., & Bond, T. C. (2015). Nanomaterials for Optical Sensing and Sensors: Plasmonics, Raman, and Optofluidics. *Journal of Nanomaterials*, 1–3. <https://doi.org/10.1155/2015/162537>

44. Shtykov, S. N., & Rusanova, T. Y. (2008). Nanomaterials and nanotechnologies in chemical and biochemical sensors: Capabilities and applications. *Russian Journal of General Chemistry*, 78(12), 2521–2531. <https://doi.org/10.1134/S1070363208120323>
45. Coville, J., N., Mhlanga, Nxumalo, N., E., & Ahmed. (n.d.). A review of shaped carbon nanomaterials. Retrieved from [http://www.scielo.org.za/scielo.php?script=sci\\_arttext&pid=S0038-23532011000200013](http://www.scielo.org.za/scielo.php?script=sci_arttext&pid=S0038-23532011000200013) Nanomaterials in Actuators—A Review Roxana Shabani and Hyoung J. Cho\* - carbon Nanomaterials
46. Liu, C. Y., Zhang, Y. S., Kao, C. K., & Liu, J. H. (2018). Fabrication of silver nanowires via a  $\beta$ -cyclodextrin-derived soft template. *Express Polymer Letters*, 12(7), 591–599. <https://doi.org/10.3144/expresspolymlett.2018.50>
47. Advances in top–down and bottom–up surface nanofabrication: Techniques, applications & future prospects. (2011, November 16). Retrieved from <https://www.sciencedirect.com/science/article/pii/S0001868611001904>
48. FABRICATION OF NANOMATERIALS BY TOP-DOWN AND BOTTOM-UP ... (n.d.). Retrieved from <https://pdfs.semanticscholar.org/34f8/921434fb256c9c8cca886722b5c920a1e4d2.pdf>
49. Wang, Y. (n.d.). Bottom-Up and Top-Down Approaches to the Synthesis of Monodispersed Spherical Colloids of Low Melting-Point Metals. Retrieved from <https://pubs.acs.org/doi/abs/10.1021/nl048689j>

50. AZoNano, W. B. (2018, November 16). Bottom-Up Methods for Making Nanotechnology Products. Retrieved from <https://www.azonano.com/article.aspx?ArticleID=1079>
51. Bottom-Up and Top-Down Approaches to the Synthesis of Monodispersed Spherical Colloids of Low Melting-Point Metals. (n.d.). Retrieved from <https://pubs.acs.org/doi/10.1021/nl048689j>
52. Tour, J. M. (2013, August 23). Top-Down versus Bottom-Up Fabrication of Graphene-Based Electronics. Retrieved from <https://pubs.acs.org/doi/abs/10.1021/cm402179h>
53. Synthesis of high-concentration Cu nanoparticles in aqueous CTAB solutions. (2004, March 02). Retrieved from <https://www.sciencedirect.com/science/article/pii/S0021979704001432>
54. Jana, N. R., Gearheart, L., & Murphy, C. J. (2001, September 05). Seed-Mediated Growth Approach for Shape-Controlled Synthesis of Spheroidal and Rod-like Gold Nanoparticles Using a Surfactant Template - Jana - 2001 - Advanced Materials - Wiley Online Library. Retrieved from [https://onlinelibrary.wiley.com/doi/abs/10.1002/1521-4095\(200109\)13:183.0.CO;2-F](https://onlinelibrary.wiley.com/doi/abs/10.1002/1521-4095(200109)13:183.0.CO;2-F)
55. Role of Capping Agent in Wet Synthesis of Nanoparticles. (n.d.). Retrieved from <https://pubs.acs.org/doi/abs/10.1021/acs.jpca.7b02186>

56. Cortes, M. de los A., de la Campa, R., Valenzuela, M. L., Díaz, C., Carriedo, G. A., & Presa Soto, A. (2019). Cylindrical Micelles by the Self-Assembly of Crystalline-b-Coil Polyphosphazene-b-P2VP Block Copolymers. Stabilization of Gold Nanoparticles. *Molecules*, 24(9), 1772. <https://doi.org/10.3390/molecules24091772>
57. ÖZTÜRK, S., ÇAKMAK, İ., TEKEŞ, A. T., & YILDIKO, Ü. (2019). Synthesis and Characterization of Poly (lactic acid-b-e-caprolactone) Block Copolymers. *Journal of the Institute of Science & Technology / Fen Bilimleri Estitüsü Dergisi*, 9(2), 1035–1045. <https://doi.org/10.21597/jist.543626>
58. P, S. P., & Tharayil, N. J. (n.d.). DNA Assisted Synthesis, Characterization and Optical ... Retrieved from <http://ijmse.net/uploadfile/2014/0519/20140519033454644.pdf>
59. Selvi, S. S. T., Linet, J. M., & Sagadevan, S. (2018). Influence of CTAB surfactant on structural and optical properties of CuS and CdS nanoparticles by hydrothermal route. *Journal of Experimental Nanoscience*, 13(1), 130–143. <https://doi.org/10.1080/17458080.2018.1445306>
60. Martin, B. R., Dermody, D. J., Reiss, B. D., Fang, M., Lyon, L. A., Natan, M. J., & Mallouk, T. E. (2017, January 11). Orthogonal self-assembly on colloidal gold-platinum nanorods. Retrieved from <https://pennstate.pure.elsevier.com/en/publications/orthogonal-self-assembly-on-colloidal-gold-platinum-nanorods>

61. Murray, B., Walter, E. C., Penner, R. M. (n.d.). Noble and Coinage Metal Nanowires by Electrochemical Step Edge Decoration. Retrieved from <https://pubs.acs.org/doi/abs/10.1021/jp026389p>
62. Walter, E. C., Zach, M. P., Favier, F., Murray, B. J., Inazu, K., Hemminger, J. C., & Penner, R. M. (2003, February 17). Metal nanowire arrays by electrodeposition. Retrieved from <https://www.ncbi.nlm.nih.gov/pubmed/12619411>
63. Huang, Y., Duan, X., Cui, Y., Lauhon, L. J., Kim, K. H., & Lieber, C. M. (2001, November 09). Logic gates and computation from assembled nanowire building blocks. Retrieved from <https://www.ncbi.nlm.nih.gov/pubmed/11701922>
64. Roschier, L., Penttilä, J., Martin, M., Hakonen, P., Paalanen, M., Tapper, U., ... Bernier, P. (1999). Singleelectron transistor made of multiwalled carbon nanotube using scanning probe manipulation. *Applied Physics Letters*, 75(5), 728-730. <https://doi.org/10.1063/1.124495>
65. Mayer, T. S., Mayer, J. S., & Keating, C. D. (1970, January 01). Electric-Field-Assisted Deterministic Nanowire Assembly. Retrieved from [https://link.springer.com/referenceworkentry/10.1007/978-90-481-9751-4\\_188](https://link.springer.com/referenceworkentry/10.1007/978-90-481-9751-4_188)
66. Tans, S. J., Verschueren, A. R., & Dekker, C. (n.d.). Room-temperature transistor based on a single carbon nanotube. Retrieved from [https://www.nature.com/articles/29954?error=cookies\\_not\\_supported&code=d4277988-6548-4118-b558-201b39dd52d1](https://www.nature.com/articles/29954?error=cookies_not_supported&code=d4277988-6548-4118-b558-201b39dd52d1)

67. Yueli Liu, Lei Zhong, Zhuoyin Peng, Yanbao Song, & Wen Chen. (2010). Field emission properties of one-dimensional single CuO nanoneedle by in situ microscopy. *Journal of Materials Science*, 45(14), 3791–3796.  
<https://doi.org/10.1007/s10853-010-4433-4>
68. Akram, M., Bashir, S., Jalil, S. A., Rafique, M. S., Hayat, A., & Mahmood, K. (2018). Investigation of field emission properties of laser irradiated tungsten. *Applied Physics A: Materials Science & Processing*, 124(2), 0. <https://doi.org/10.1007/s00339-018-1612-7>
69. Chang, C., Gonela, R. K., Gu, Q., & Haynie, D. T. (2004, November 26). Self-Assembly of Metallic Nanowires from Aqueous Solution. Retrieved from <https://pubs.acs.org/doi/10.1021/nl048240q>
70. Asghar, W., Ramachandran, P. P., Adewumi, A., Noor, M. R., & Iqbal, S. M. (2010). Rapid Nanomanufacturing of Metallic Break Junctions Using Focused Ion Beam Scratching and Electromigration. *Journal of Manufacturing Science & Engineering*, 132(3), 030911:1-030911:4. <https://doi.org/10.1115/1.4001664>
71. Dasari, R., & Zamborini, F. (n.d.). Hydrogen Switches and Sensors Fabricated by Combining Electropolymerization and Pd Electrodeposition at Microgap Electrodes. Retrieved from <https://pubs.acs.org/doi/abs/10.1021/ja806428y>

72. Takashi Usui, Sinjiro Miyake, Toshio Iwata, Takero Otsuka, So Koizumi, Nobukazu Shirakawa, & Toshitsugu Kawata. (2017). Aesthetic characteristics of the orthodontic wire with silver plating. *Biomedical Research (0970-938X)*, 28(11), 4937–4941. Retrieved from

<http://search.ebscohost.com/login.aspx?direct=true&AuthType=shib&db=a9h&AN=124198434&site=ehost-live&scope=site>

73. Pattadar, Dhruva & N. Sharma, Jay & Mainali, Badri & Zamborini, Francis. (2018). Structural, Physical, and Chemical Characterization of Metal Nanoparticles by Anodic Stripping Electrochemical Analysis. *Current Opinion in Electrochemistry*. 13. 10.1016/j.coelec.2018.12.006.

74. Radhika Dasari, Francisco J. Ibañez, & Francis P. Zamborini. (2011). Electrochemical Fabrication of Metal/Organic/Metal Junctions for Molecular Electronics and Sensing Applications. *Langmuir*, 27(11), 7285–7293.

<https://doi.org/10.1021/la103559p>

75. Libretexts. (2019, June 05). P1: Standard Reduction Potentials by Element. Retrieved from

[https://chem.libretexts.org/Ancillary\\_Materials/Reference/Reference\\_Tables/Electrochemistry\\_Tables/P1: Standard Reduction Potentials by Element](https://chem.libretexts.org/Ancillary_Materials/Reference/Reference_Tables/Electrochemistry_Tables/P1:_Standard_Reduction_Potentials_by_Element)

76. What is Faraday's law? (n.d.). Retrieved from

<https://www.khanacademy.org/science/physics/magnetic-forces-and-magnetic-fields/magnetic-flux-faradays-law/a/what-is-faradays-law>

77. Kozadaev, K. (2016). A device for atmospheric laser deposition of noble metal nanostructures. *Instruments & Experimental Techniques*, 59(6), 865–869.  
<https://doi.org/10.1134/S0020441216060178>
78. Singh, J. A., Thissen, N. F. W., Kim, W.-H., Johnson, H., Kessels, W. M. M., Bol, A. A., ... Mackus, A. J. M. (2018). Area-Selective Atomic Layer Deposition of Metal Oxides on Noble Metals through Catalytic Oxygen Activation. *Chemistry of Materials*, 30(3), 663–670. <https://doi.org/10.1021/acs.chemmater.7b03818>
79. Straney, P. J., Diemler, N. A., Smith, A. M., Eddinger, Z. E., Gilliam, M. S., & Millstone, J. E. (2018). Ligand-Mediated Deposition of Noble Metals at Nanoparticle Plasmonic Hotspots. *Langmuir*, 34(3), 1084–1091.  
<https://doi.org/10.1021/acs.langmuir.7b03309>
80. Allmond, C. E., Sellinger, A. T., Gogick, K., & Fitz-Gerald, J. M. (2007). Photochemical synthesis and deposition of noble metal nanoparticles. *Applied Physics A: Materials Science & Processing*, 86(4), 477–480. <https://doi.org/10.1007/s00339-006-3780-0>
81. Tu, L., Yuan, S., Zhang, H., Wang, P., Cui, X., Wang, J., ... Zheng, L.-R. (2018). Aerosol jet printed silver nanowire transparent electrode for flexible electronic application. *Journal of Applied Physics*, 123(17), N.PAG.  
<https://doi.org/10.1063/1.5028263>

82. Yang-Yen Yu, Yo-Jen Ting, Chung-Lin Chung, Tzung-Wei Tsai, & Chih-Ping Chen. (2017). Comprehensive Study on Chemical and Hot Press-Treated Silver Nanowires for Efficient Polymer Solar Cell Application. *Polymers (20734360)*, 9(11), 635.  
<https://doi.org/10.3390/polym9110635>
83. Kong, P., Wang, R., Zhang, C., Du, Z., Li, H., & Zou, W. (2017). Synthesis of 4-aminothiophenol functionalized quantum dots to sensitize silver nanowires and its application for solar cells. *Synthetic Metals*, 226, 50–55.  
<https://doi.org/10.1016/j.synthmet.2017.02.004>
84. Zhang, X., Wu, J., Liu, H., Wang, J., Zhao, X., & Xie, Z. (2017). Efficient flexible polymer solar cells based on solution-processed reduced graphene oxide–Assisted silver nanowire transparent electrode. *Organic Electronics*, 50, 255–263.  
<https://doi.org/10.1016/j.orgel.2017.07.055>
85. Zhong-Ai Hu, Yao-Xian Wang, Yu-Long Xie, Yu-Ying Yang, Zi-Yu Zhang, & Hong-Ying Wu. (2010). Ag nanowires and its application as electrode materials in electrochemical capacitor. *Journal of Applied Electrochemistry*, 40(2), 341–344.  
<https://doi.org/10.1007/s10800-009-0002-4>
86. Yuan-Jun Song, Jing Chen, Jing-Yuan Wu, Tong Zhang. Applications of Silver Nanowires on Transparent Conducting Film and Electrode of Electrochemical Capacitor. *Journal of Nanomaterials*. January 2014:1-7. doi:10.1155/2014/193201.

87. Wu, J. B., Li, Z. G., & Lin, Y. (2011). Porous NiO/Ag composite film for electrochemical capacitor application. *Electrochimica Acta*, 56(5), 2116–2121. <https://doi.org/10.1016/j.electacta.2010.11.029>
88. Wang, J., Jiu, J., Araki, T., Nogi, M., Sugahara, T., Nagao, S., ... Suganuma, K. (2015). Silver Nanowire Electrodes: Conductivity Improvement Without Post-treatment and Application in Capacitive Pressure Sensors. *Nano-Micro Letters*, 7(1), 51–58. <https://doi.org/10.1007/s40820-014-0018-0>
89. Jeong, H., Noh, Y., Ko, S. H., & Lee, D. (2019). Flexible resistive pressure sensor with silver nanowire networks embedded in polymer using natural formation of air gap. *Composites Science & Technology*, 174, 50–57. <https://doi.org/10.1016/j.compscitech.2019.01.028>
90. Baozhang Li, Chengyi Xu, Jianming Zheng, & Chunye Xu. (2014). Sensitivity of Pressure Sensors Enhanced by Doping Silver Nanowires. *Sensors* (14248220), 14(6), 9889–9899. <https://doi.org/10.3390/s140609889>
91. Xu, A., Chao, L., Xiao, H., Sui, Y., Liu, J., Xie, Q., & Yao, S. (2018). Ultrasensitive electrochemical sensing of Hg<sup>2+</sup> based on thymine-Hg<sup>2+</sup>-thymine interaction and signal amplification of alkaline phosphatase catalyzed silver deposition. *Biosensors & Bioelectronics*, 104, 95–101. <https://doi.org/10.1016/j.bios.2018.01.005>

92. Yang, S., Wang, G., Li, G., & Qu, L. (2015). One step controllable electrochemical deposition of silver hexacyanoferrate nanoparticles/multi-wall carbon nanotubes/Nafion modified electrode for the sensing of phenol. *Journal of Analytical Chemistry*, 70(9), 1116–1122. <https://doi.org/10.1134/S1061934815090154>
93. Jiang, Y., Zheng, B., Du, J., Liu, G., Guo, Y., & Xiao, D. (2013). Electrophoresis deposition of Ag nanoparticles on TiO<sub>2</sub> nanotube arrays electrode for hydrogen peroxide sensing. *Talanta*, 112, 129–135. <https://doi.org/10.1016/j.talanta.2013.03.015>
94. Shahriary, L., & Athawale, A. (2015). Electrochemical deposition of silver/silver oxide on reduced graphene oxide for glucose sensing. *Journal of Solid State Electrochemistry*, 19(8), 2255–2263. <https://doi.org/10.1007/s10008-015-2865-0>
95. Lin, Y., Tao, Y., Ren, J., Pu, F., & Qu, X. (2011). Highly sensitive and selective detection of thiol-containing biomolecules using DNA-templated silver deposition. *Biosensors & Bioelectronics*, 28(1), 339–343. <https://doi.org/10.1016/j.bios.2011.07.040>
96. Chen, J.-J., Liu, S.-L., Wu, H.-B., Sowade, E., Baumann, R. R., Wang, Y., ... Feng, Z.-S. (2018). Structural regulation of silver nanowires and their application in flexible electronic thin films. *Materials & Design*, 154, 266–274. <https://doi.org/10.1016/j.matdes.2018.05.018>

97. Schubert, I., Burr, L., Trautmann, C., & Toimil-Molares, M. E. (2015, June 08). Growth and morphological analysis of segmented AuAg alloy nanowires created by pulsed electrodeposition in ion-track etched membranes. Retrieved from <https://www.ncbi.nlm.nih.gov/pmc/articles/PMC4505191/>
98. Dhanapal, K., Vasumathi, M., Santhi, K., Narayanan, V., & Stephen, A. (2014, January 28). Double dumbbell shaped AgNi alloy by pulsed electrodeposition. Retrieved from <https://aip.scitation.org/doi/abs/10.1063/1.4861991>
99. Santhi, K. (2011, November 19). Microstructure analysis of the ferromagnetic Ag–Ni system synthesized by pulsed electrodeposition. Retrieved from <https://www.sciencedirect.com/science/article/pii/S0169433211018009>
100. Simonet, J. (2009). Novel and efficient electrochemical way for silver nanoparticles deposition onto solid conductors: a new concept of metal-silver cathodes. *Journal of Applied Electrochemistry*, 39(9), 1625–1632. <https://doi.org/10.1007/s10800-009-9853-y>
101. Emma L. Smith, Andrew P. Abbott, Jason Griffin, Robert C. Harris, Cecil O'Connor, & Karl S. Ryder. (2010). Pilot trials of immersion silver deposition using a choline chloride based ionic liquid. *Circuit World*, 36(1), 3–9. <https://doi.org/10.1108/03056121011015031>
102. Nativ-Roth, E., Rechav, K., & Porat, Z. (2016). Deposition of gold and silver on porous silicon and inside the pores. *Thin Solid Films*, 603, 88–96. <https://doi.org/10.1016/j.tsf.2016.01.020>

103. Milazzo, R. G., Mio, A. M., D'Arrigo, G., Grimaldi, M. G., Spinella, C., & Rimini, E. (2015). Coalescence of silver clusters by immersion in diluted HF solution. *Journal of Chemical Physics*, 143(2), 1–6. <https://doi.org/10.1063/1.4926530>
104. Szczęsny, R., Szymańska, I., Piszczek, P., Dobrzańska, L., & Sztyk, E. (2005). Chemical Vapour Deposition (CVD) of metallic layers prepared from silver carboxylates complexes with tertiary phosphines. *Materials Science (0137-1339)*, 23(3), 671–676.  
Retrieved from  
<http://search.ebscohost.com/login.aspx?direct=true&AuthType=shib&db=a9h&AN=20983754&site=ehost-live&scope=site>
105. VASILESCU, E., VASILESCU, V. G., & DIMA, D. (2015). Research on Chemical Deposition of Silver with Antibacterial Role in Implantology. *Annals of the University Dunarea de Jos of Galati: Fascicle IX, Metallurgy & Materials Science*, 33(4), 52–57.  
Retrieved from  
<http://search.ebscohost.com/login.aspx?direct=true&AuthType=shib&db=a9h&AN=130367210&site=ehost-live&scope=site>
106. Olenius, T., Yli-Juuti, T., Elm, J., Kontkanen, J., & Riipinen, I. (2018, June 08). New Particle Formation and Growth: Creating a New Atmospheric Phase Interface. Retrieved from <https://www.sciencedirect.com/science/article/pii/B978012813641600011X>
107. Barton, J. L., & Bockris, O. (1997, January 01). The electrolytic growth of dendrites from ionic solutions. Retrieved from  
<https://royalsocietypublishing.org/doi/abs/10.1098/rspa.1962.0154>

108. Kim, B.; Ahn, S. J.; Park, J. G.; Lee, S. H.; Park, Y. W. *Appl. Phys. Lett.* 2004, 85, 4756-4758.
109. Kim, B.; Ahn, S. J.; Park, J. G.; Lee, S. H.; Park, Y. W.; Campbell, E. E. B. *Thin Solid Films* 2006, 499, 196-200.
110. Scharifker, B. R. (2019, June 24). Electrochemical nucleation and growth of Zn-Ni alloys from chloride citrate-based electrolyte. Retrieved from <https://www.sciencedirect.com/science/article/pii/S1572665719305296>
111. Mikac, L., Ivanda, M., Gotić, M., Maksimović, A., Trusso, S., D'Andrea, C., ... Gucciardi, P. G. (2015). Metal Nanoparticles Deposited on Porous Silicon Templates as Novel Substrates for SERS. *Croatica Chemica Acta*, 88(4), 437–444. <https://doi.org/10.5562/cca2769>
112. Rill, M. S., Plet, C., Thiel, M., Staude, I., von Freymann, G., Linden, S., & Wegener, M. (2008). Photonic metamaterials by direct laser writing and silver chemical vapour deposition. *Nature Materials*, 7(7), 543–546. <https://doi.org/10.1038/nmat2197>
113. Piszczek, P., Lewandowska, Ż., Radtke, A., Jędrzejewski, T., Kozak, W., Sadowska, B., ... Fiori, F. (2017). Biocompatibility of Titania Nanotube Coatings Enriched with Silver Nanograins by Chemical Vapor Deposition. *Nanomaterials* (2079-4991), 7(9), 274. <https://doi.org/10.3390/nano7090274>
114. Z H Chen, J S Jie, L B Luo, H Wang, C S Lee, & S T Lee. (2007). Applications of silicon nanowires functionalized with palladium nanoparticles in hydrogen sensors. *Nanotechnology*, 18(34), 45502. <https://doi.org/10.1088/0957-4484/18/34/345502>

115. Alfano, B., Massera, E., Polichetti, T., Miglietta, M. L., & Di Francia, G. (2017). Effect of palladium nanoparticle functionalization on the hydrogen gas sensing of graphene based chemi-resistive devices. *Sensors & Actuators B: Chemical*, 253, 1163–1169. <https://doi.org/10.1016/j.snb.2017.07.146>
116. Atashbar, M. Z., Banerji, D., Singamaneni, S., & Bliznyuk, V. (2005). Polystyrene Palladium Nanocomposite for Hydrogen Sensing. *Molecular Crystals & Liquid Crystals*, 427(1), 529–536. <https://doi.org/10.1080/15421400590892299>
117. Slaughter, G., & Kulkarni, T. (2016). Fabrication of palladium nanowire array electrode for biofuel cell application. *Microelectronic Engineering*, 149, 92–96. <https://doi.org/10.1016/j.mee.2015.09.019>
118. Wen, D., Liu, W., Herrmann, A., & Eychmüller, A. (2014). A Membraneless Glucose/O<sub>2</sub> Biofuel Cell Based on Pd Aerogels. *Chemistry - A European Journal*, 20(15), 4380–4385. <https://doi.org/10.1002/chem.201304635>
119. Hoik Lee, Duy-Nam Phan, Myungwoong Kim, Daewon Sohn, Seong-Geun Oh, Seong Hun Kim, & Ick Soo Kim. (2016). The Chemical Deposition Method for the Decoration of Palladium Particles on Carbon Nanofibers with Rapid Conductivity Changes. *Nanomaterials (2079-4991)*, 6(12), 226. <https://doi.org/10.3390/nano6120226>
120. Ye, X. R., Wai, C. M., Lin, Y., Young, J. S., & Engelhard, M. H. (2005). Supercritical fluid immersion deposition: a new process for selective deposition of metal films on silicon substrates. *Surface & Coatings Technology*, 190(1), 25–31. <https://doi.org/10.1016/j.surfcoat.2004.06.023>

121. Pap, A. E., Kordás, K., Peura, R., & Leppävuori, S. (2002). Simultaneous chemical silver and palladium deposition on porous silicon; FESEM, TEM, EDX and XRD investigation. *Applied Surface Science*, 201(1–4), 56. [https://doi.org/10.1016/S0169-4332\(02\)00489-0](https://doi.org/10.1016/S0169-4332(02)00489-0)
122. Rezaei, B., Mokhtarianpour, M., & Ensafi, A. A. (2015). Fabricated of bimetallic Pd/Pt nanostructure deposited on copper nanofoam substrate by galvanic replacement as an effective electrocatalyst for hydrogen evolution reaction. *International Journal of Hydrogen Energy*, 40(21), 6754–6762. <https://doi.org/10.1016/j.ijhydene.2015.03.122>
123. Zhang, X., Zhou, Y., Zhang, B., & Zhang, J. (2017). An improved galvanic replacement deposition method for synthesis of compact palladium coatings on copper substrates. *Materials Letters*, 197, 75–78. <https://doi.org/10.1016/j.matlet.2017.03.119>
124. Masnadi, M., Yao, N., Braidy, N., & Moores, A. (2015). Cu(II) Galvanic Reduction and Deposition onto Iron Nano- and Microparticles: Resulting Morphologies and Growth Mechanisms. *Langmuir*, 31(2), 789–798. <https://doi.org/10.1021/la503598b>
125. Abdullah Mirzaie R, Eshghi A. Study of methanol electro-oxidation on Ni and Ni-Pt/carbon paper electrodes for direct methanol fuel cell applications. *Surface Engineering*. 2014;30(4):263-267. doi:10.1179/1743294414Y.0000000248.
126. Dobrovets'ka, O., Kuntzy, O., Zozulya, G., Saldan, I., & Reshetnyak, O. (2015). Galvanic Deposition of Gold and Palladium on Magnesium by the Method of Substitution. *Materials Science*, 51(3), 418–423. <https://doi.org/10.1007/s11003-015-9857-1>

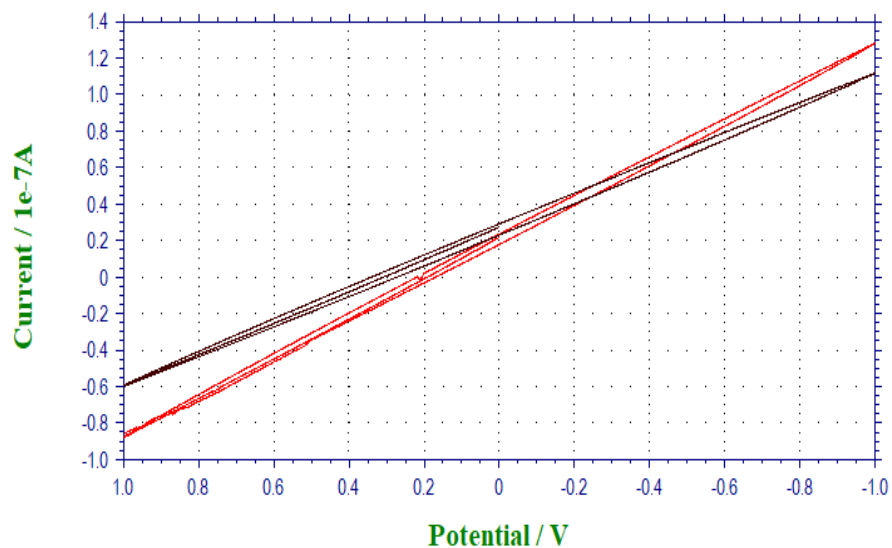
127. Sanjay, S., Prabakaran, K., Singh, S., & Baskar, K. (2018). Growth of gold-palladium alloy catalyzed gallium nitride nanowires by chemical vapour deposition. *Materials Letters*, 217, 100–103. <https://doi.org/10.1016/j.matlet.2018.01.059>
128. Krisyuk, V. V., Urkasym Kyzy, S., Baidina, I. A., Romanenko, G. V., Korolkov, I. V., Koretskaya, T. P., ... Turgambaeva, A. E. (2017). Structure and thermal properties of heterometallic complexes for chemical vapor deposition of Cu-Pd films. *Journal of Structural Chemistry*, 58(8), 1522–1529. <https://doi.org/10.1134/S0022476617080078>
129. Safavi, A., Maleki, N., & Doroodmand, M. M. (2012). Comparative Investigation of Chemical Vapor Deposition of Palladium Nanoparticles on Different Carbon Substrates. *Fullerenes, Nanotubes & Carbon Nanostructures*, 20(1), 56–71. <https://doi.org/10.1080/1536383X.2010.533301>

## APPENDIX

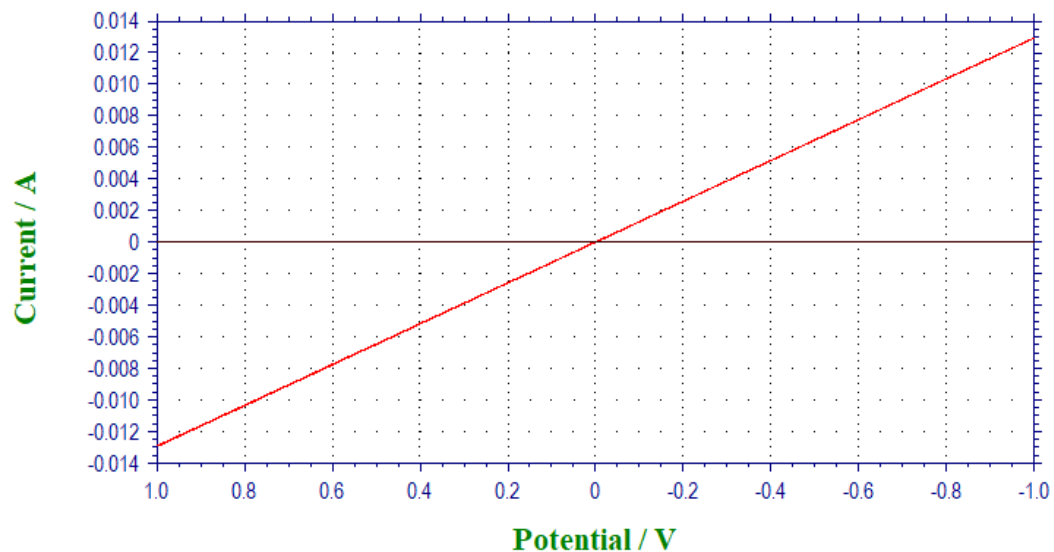
Appendix A: i-V curve graphs before and after metal electrodeposition

Appendix A: i-V curve graphs before and after metal electrodeposition

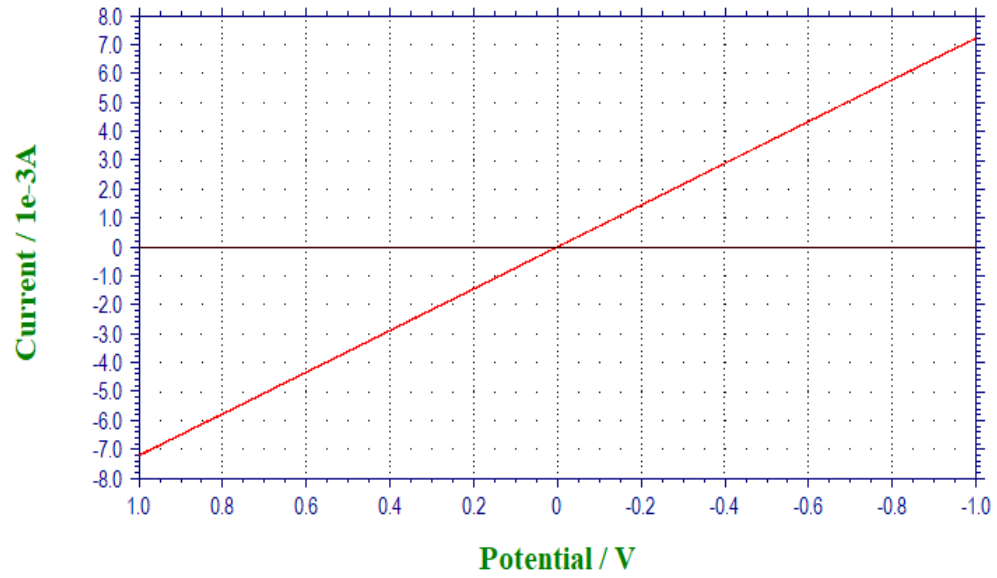
i-V curve obtained in air before (black) and after (red) electrodepositing Ag from 0.5 mM AgNO<sub>3</sub> in 0.1 M H<sub>2</sub>SO<sub>4</sub> at -0.1 V potential.



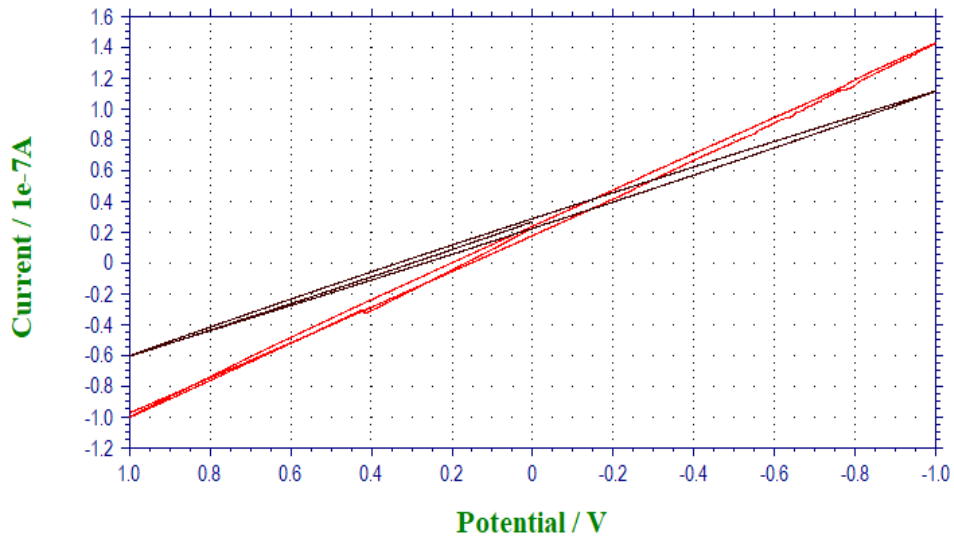
i-V curve obtained in air before (black) and after (red) electrodepositing Ag from 0.5 mM AgNO<sub>3</sub> in 0.1 M H<sub>2</sub>SO<sub>4</sub> at -0.1 V potential.



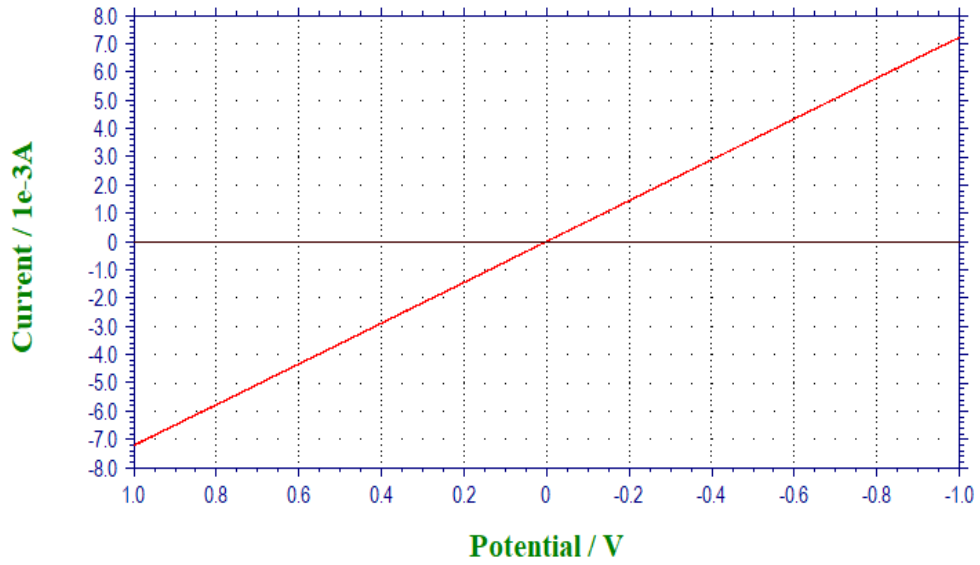
i-V curve obtained in air before (black) and after (red) electrodepositing Ag from 0.5 mM AgNO<sub>3</sub> in 0.1 M H<sub>2</sub>SO<sub>4</sub> at -0.2 V potential.



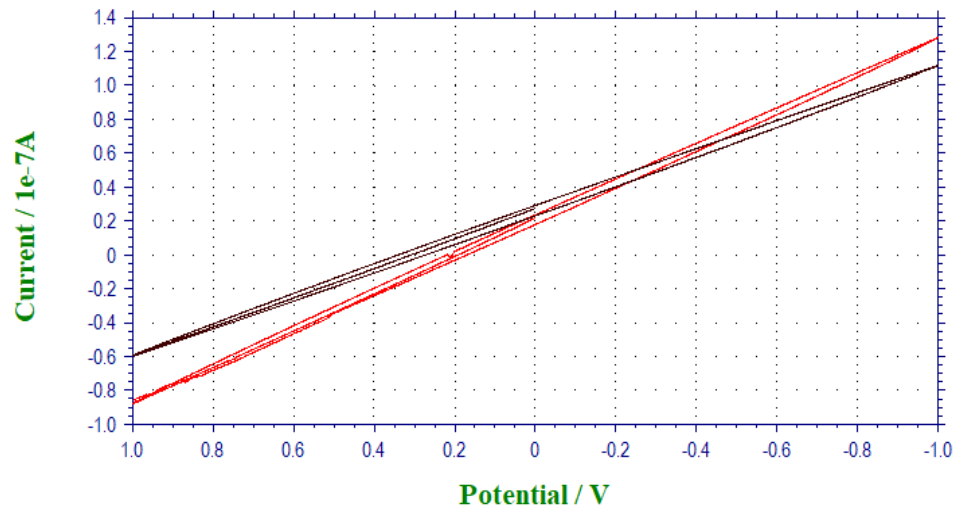
i-V curve obtained in air before (black) and after (red) electrodepositing Ag from 0.5 mM AgNO<sub>3</sub> in 0.1 M H<sub>2</sub>SO<sub>4</sub> at -0.2 V potential.



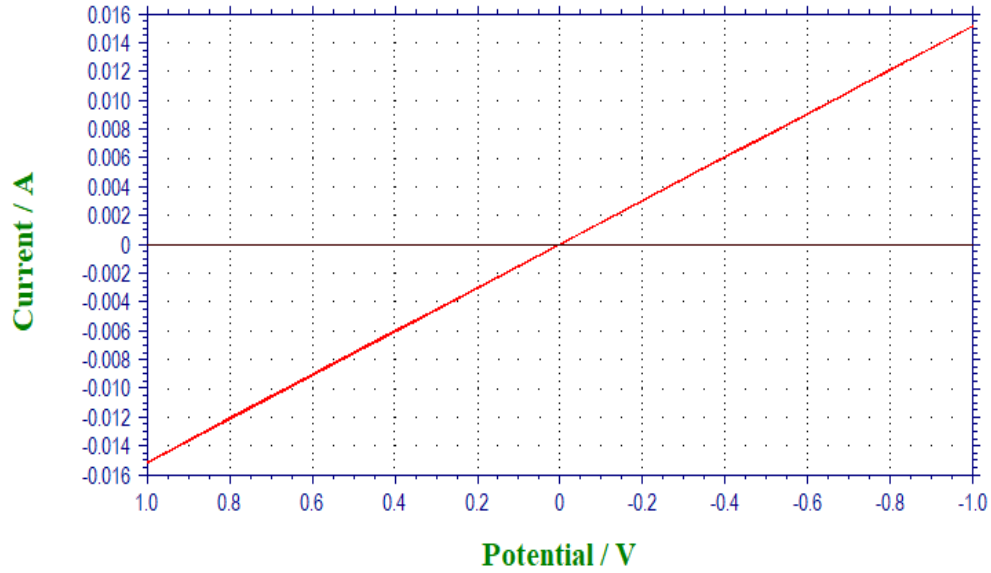
i-V curve obtained in air before (black) and after (red) electrodepositing Ag from 0.5 mM AgNO<sub>3</sub> in 0.1 M H<sub>2</sub>SO<sub>4</sub> at -0.3 V potential.



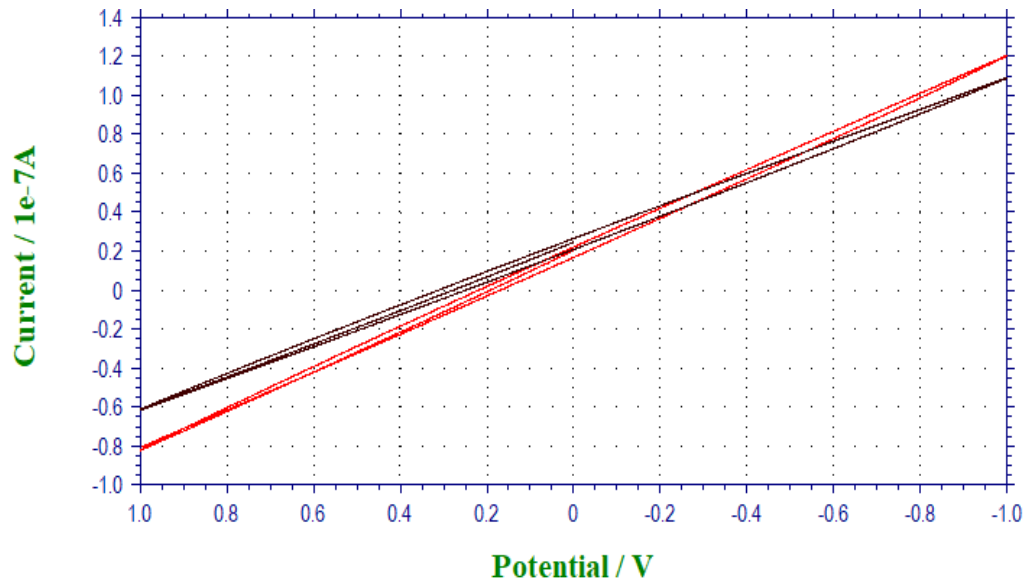
i-V curve obtained in air before (black) and after (red) electrodepositing Ag from 0.5 mM AgNO<sub>3</sub> in 0.1 M H<sub>2</sub>SO<sub>4</sub> at -0.3 V potential.



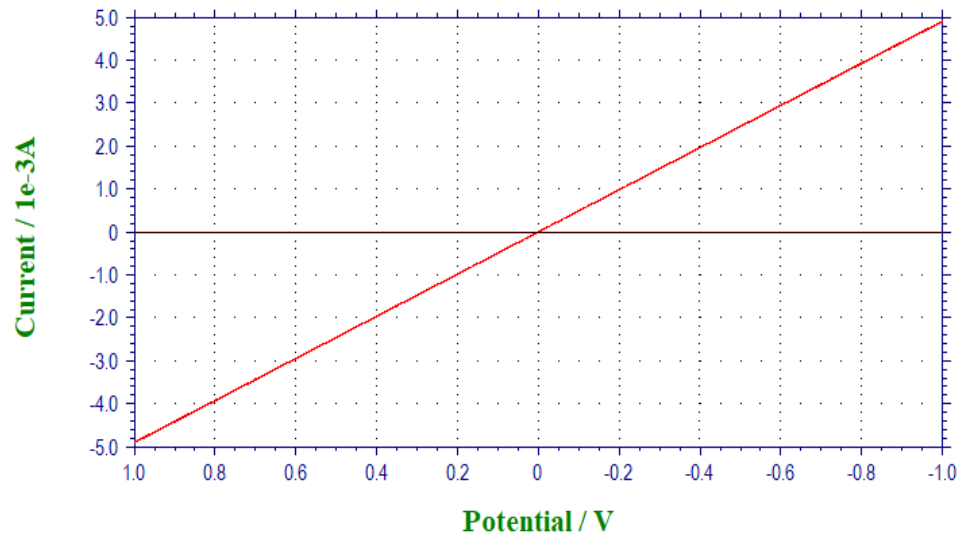
i-V curve obtained in air before (black) and after (red) electrodepositing Ag from 0.5 mM AgNO<sub>3</sub> in 0.1 M H<sub>2</sub>SO<sub>4</sub> at -0.4 V potential.



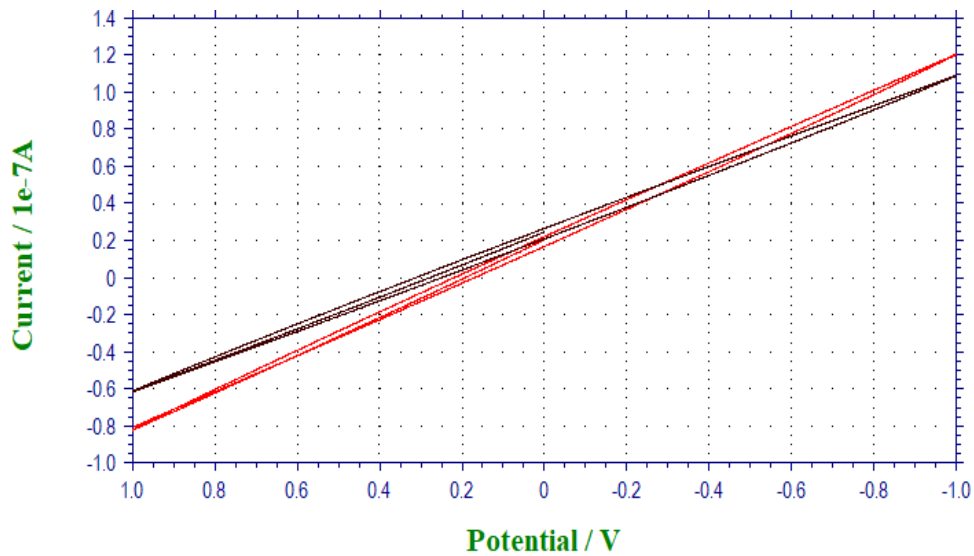
i-V curve obtained in air before (black) and after (red) electrodepositing Ag from 0.5 mM AgNO<sub>3</sub> in 0.1 M H<sub>2</sub>SO<sub>4</sub> at -0.4 V potential.



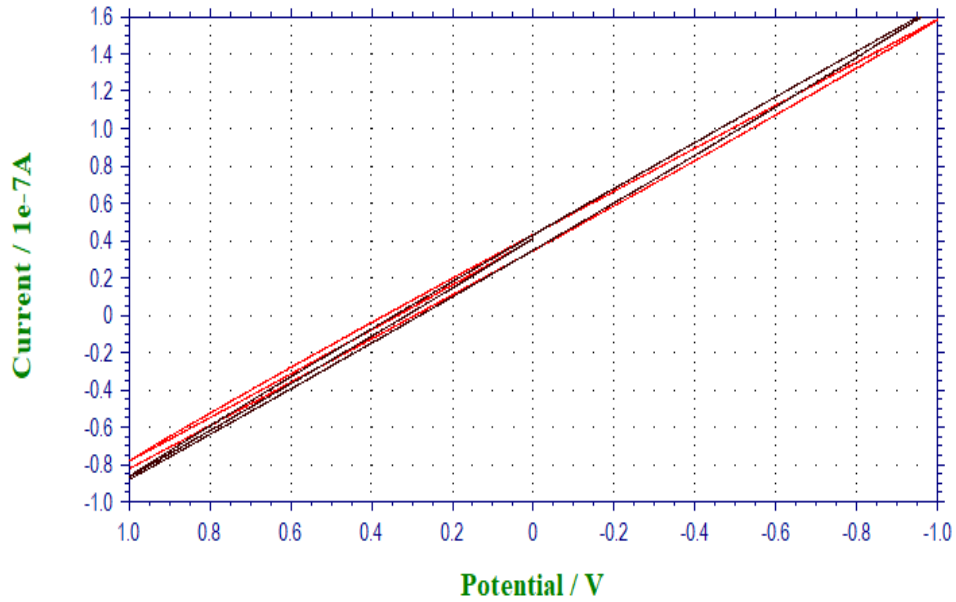
i-V curve obtained in air before (black) and after (red) electrodepositing Ag from 0.5 mM AgNO<sub>3</sub> in 0.1 M H<sub>2</sub>SO<sub>4</sub> at -0.5 V potential.



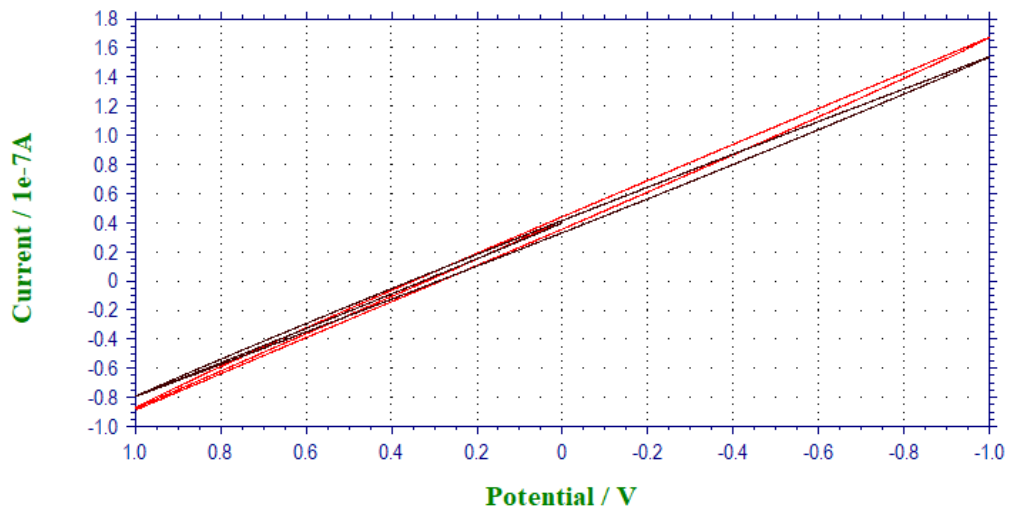
i-V curve obtained in air before (black) and after (red) electrodepositing Ag from 0.5 mM AgNO<sub>3</sub> in 0.1 M H<sub>2</sub>SO<sub>4</sub> at -0.5 V potential.



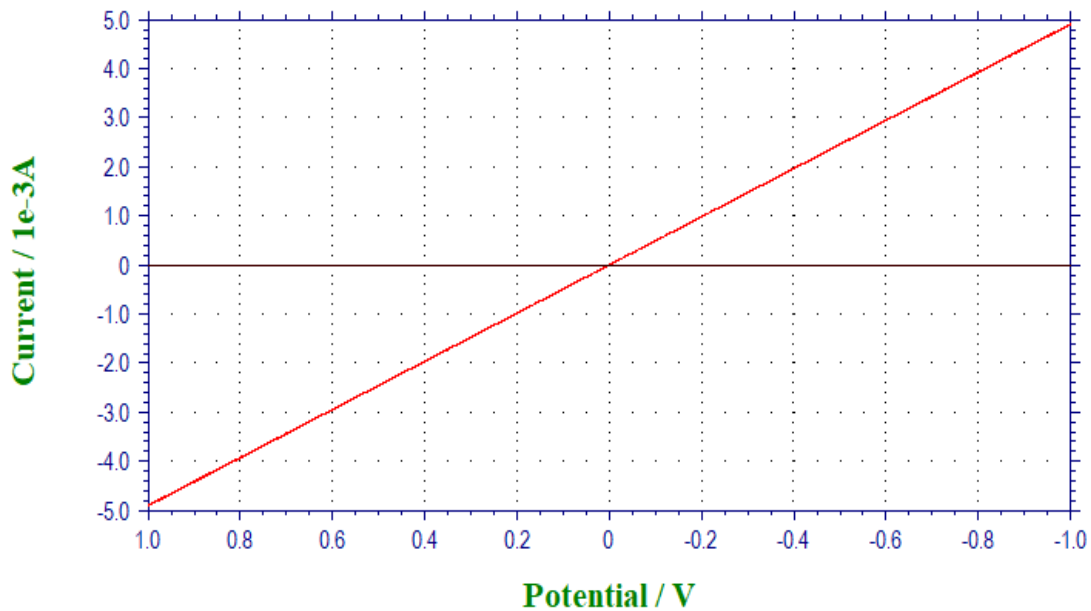
i-V curve obtained in air before (black) and after (red) electrodepositing Ag from 5 mM AgNO<sub>3</sub> in 0.1 M H<sub>2</sub>SO<sub>4</sub> at -0.1 V potential.



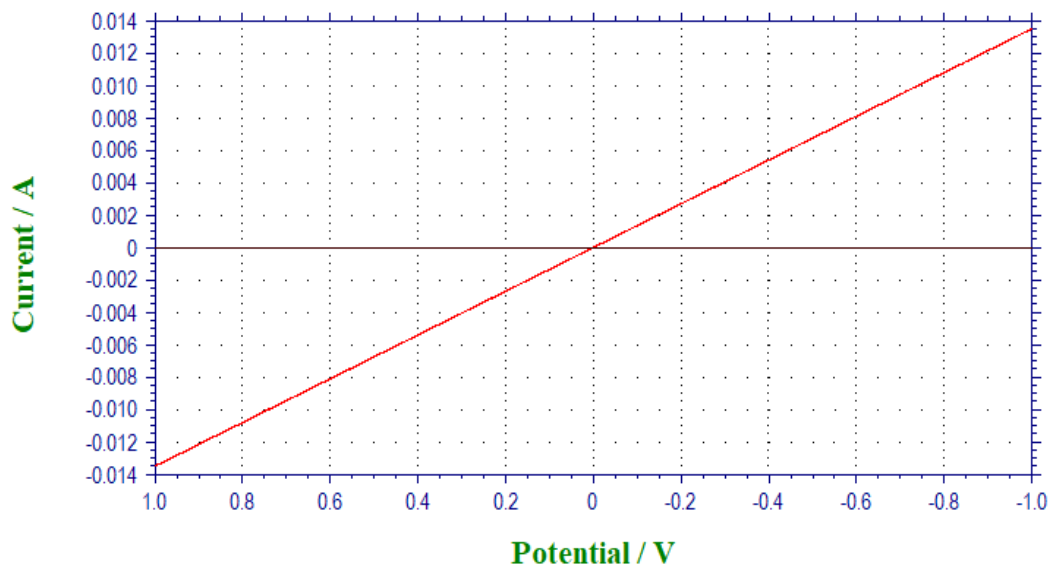
i-V curve obtained in air before (black) and after (red) electrodepositing Ag from 5 mM AgNO<sub>3</sub> in 0.1 M H<sub>2</sub>SO<sub>4</sub> at -0.1 V potential.



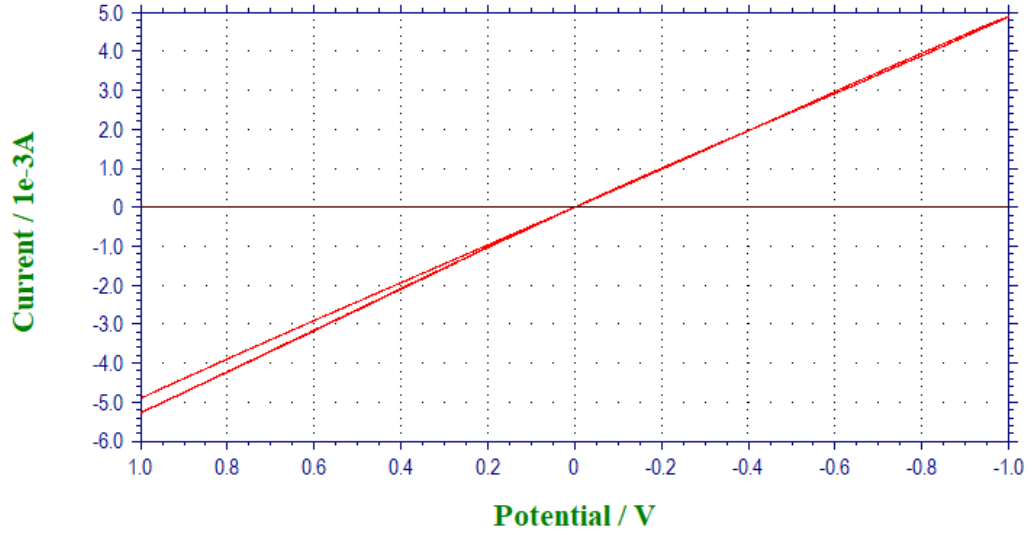
i-V curve obtained in air before (black) and after (red) electrodepositing Ag from 5 mM AgNO<sub>3</sub> in 0.1 M H<sub>2</sub>SO<sub>4</sub> at -0.2 V potential.



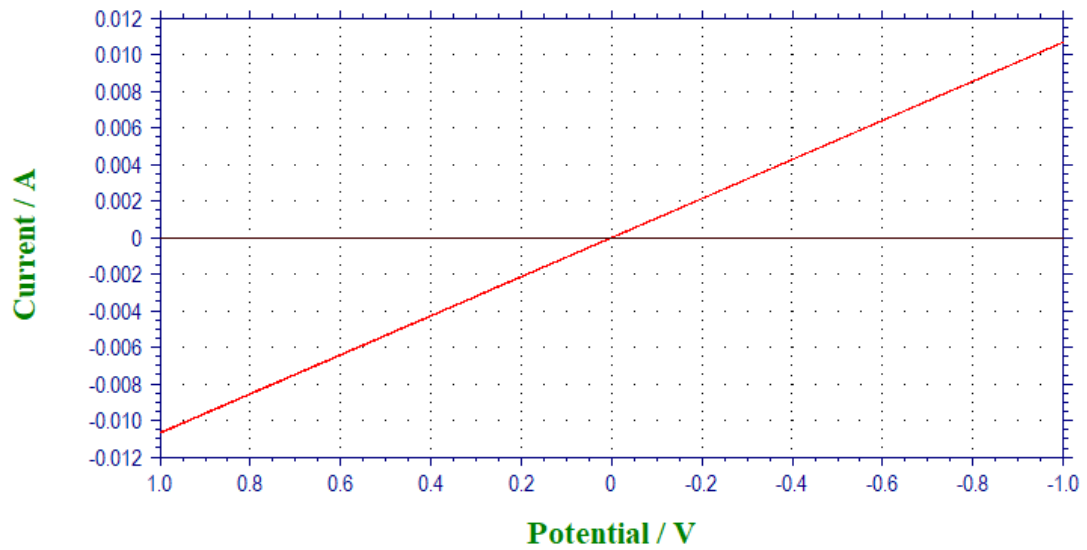
i-V curve obtained in air before (black) and after (red) electrodepositing Ag from 5 mM AgNO<sub>3</sub> in 0.1 M H<sub>2</sub>SO<sub>4</sub> at -0.2 V potential.



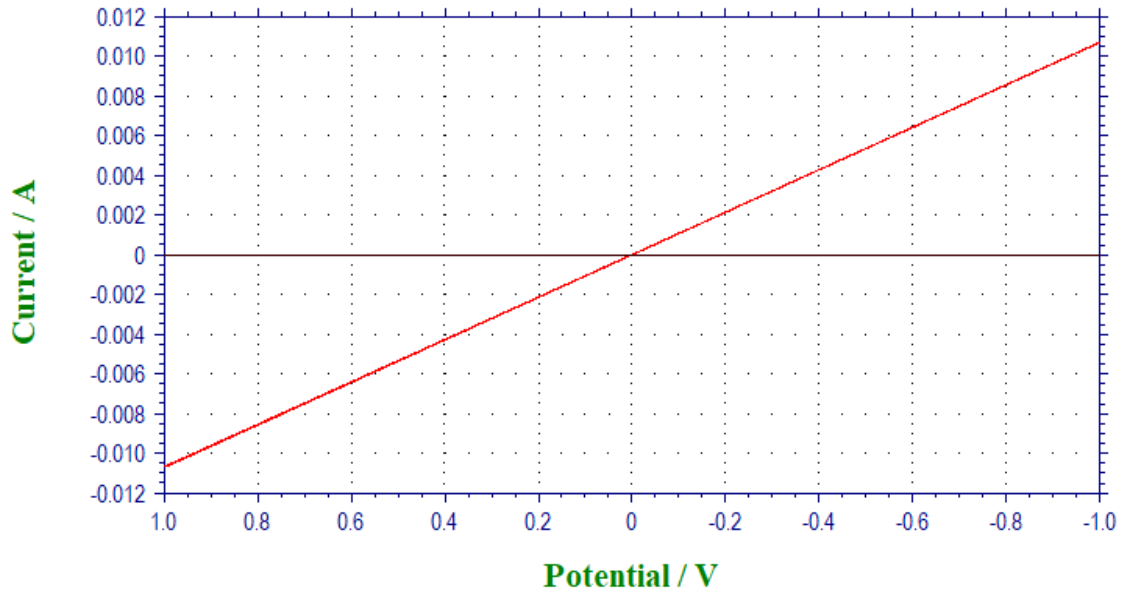
i-V curve obtained in air before (black) and after (red) electrodepositing Ag from 5 mM AgNO<sub>3</sub> in 0.1 M H<sub>2</sub>SO<sub>4</sub> at -0.3 V potential



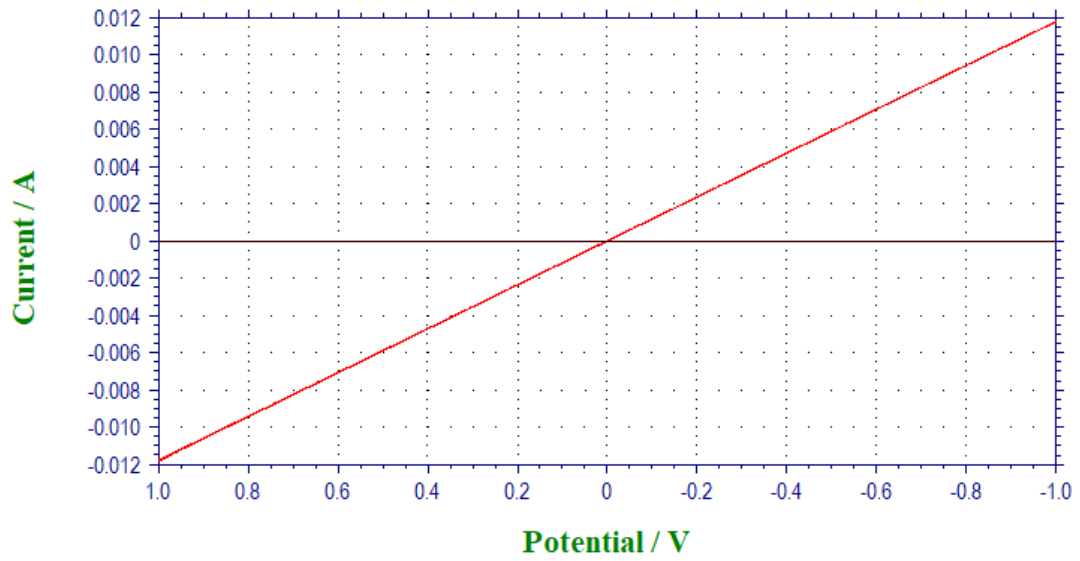
i-V curve obtained in air before (black) and after (red) electrodepositing Ag from 5 mM AgNO<sub>3</sub> in 0.1 M H<sub>2</sub>SO<sub>4</sub> at -0.3 V potential



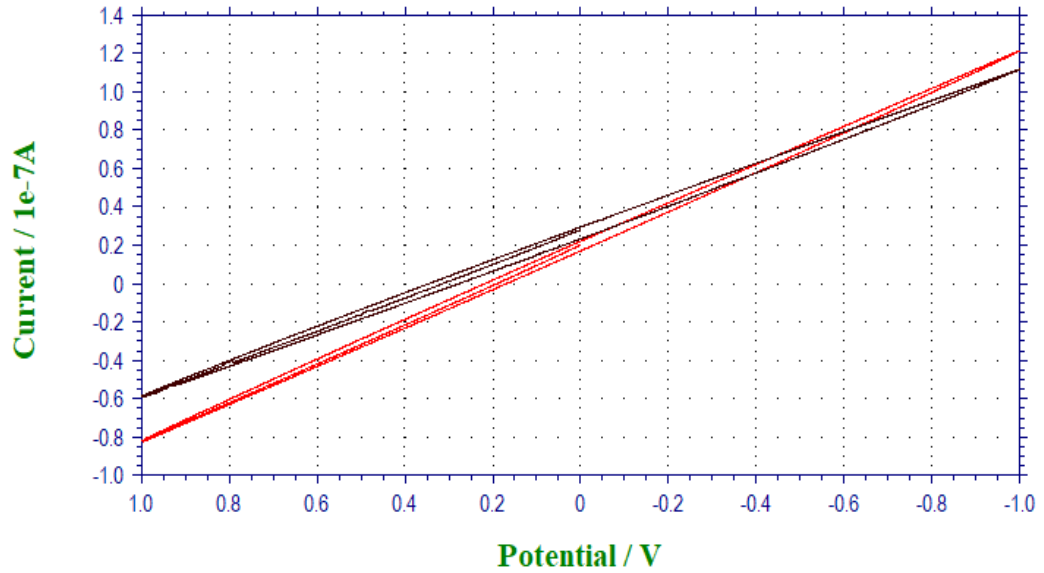
i-V curve obtained in air before (black) and after (red) electrodepositing Ag from 5 mM AgNO<sub>3</sub> in 0.1 M H<sub>2</sub>SO<sub>4</sub> at -0.4 V potential.



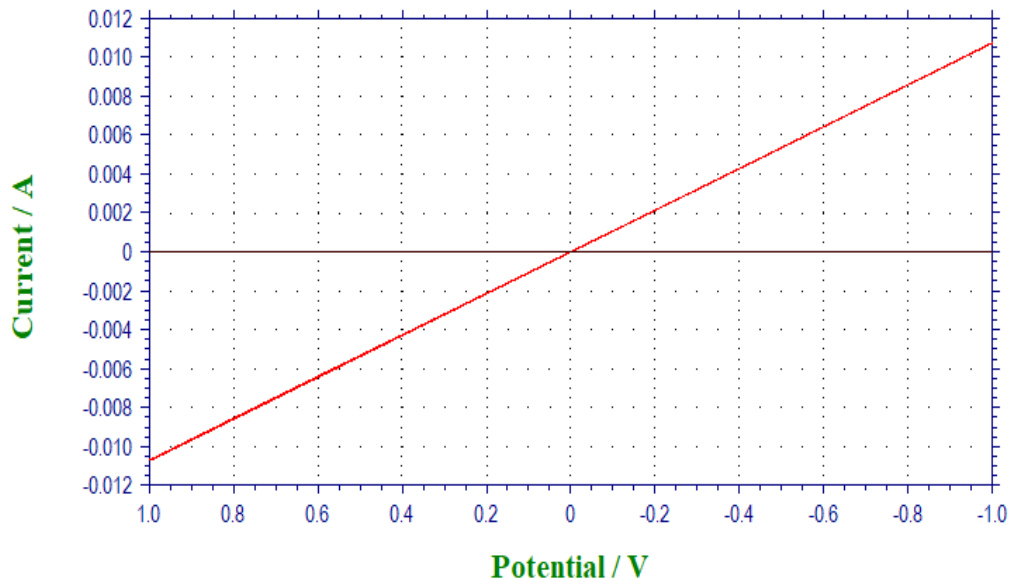
i-V curve obtained in air before (black) and after (red) electrodepositing Ag from 5 mM AgNO<sub>3</sub> in 0.1 M H<sub>2</sub>SO<sub>4</sub> at -0.4 V potential.



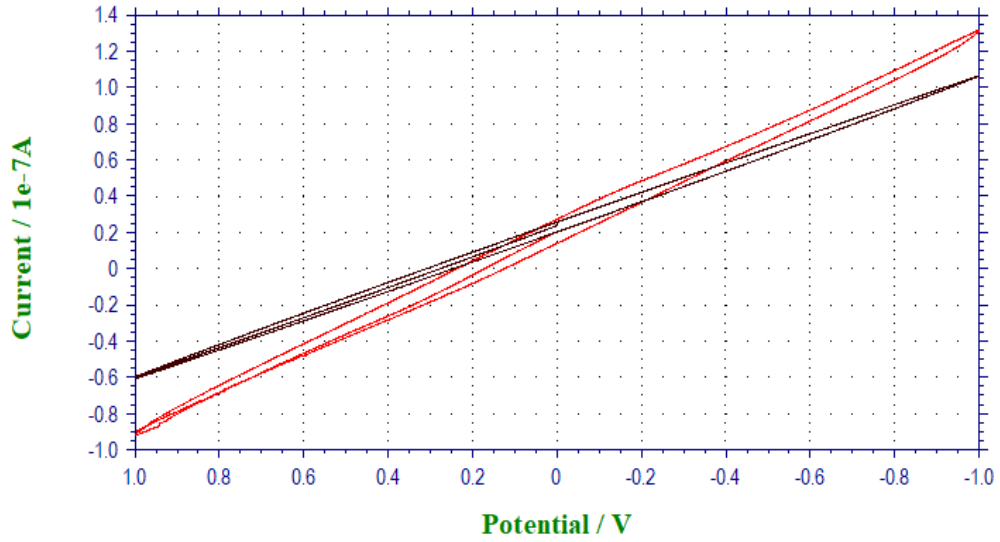
i-V curve obtained in air before (black) and after (red) electrodepositing Ag from 5 mM AgNO<sub>3</sub> in 0.1 M H<sub>2</sub>SO<sub>4</sub> at -0.5 V potential.



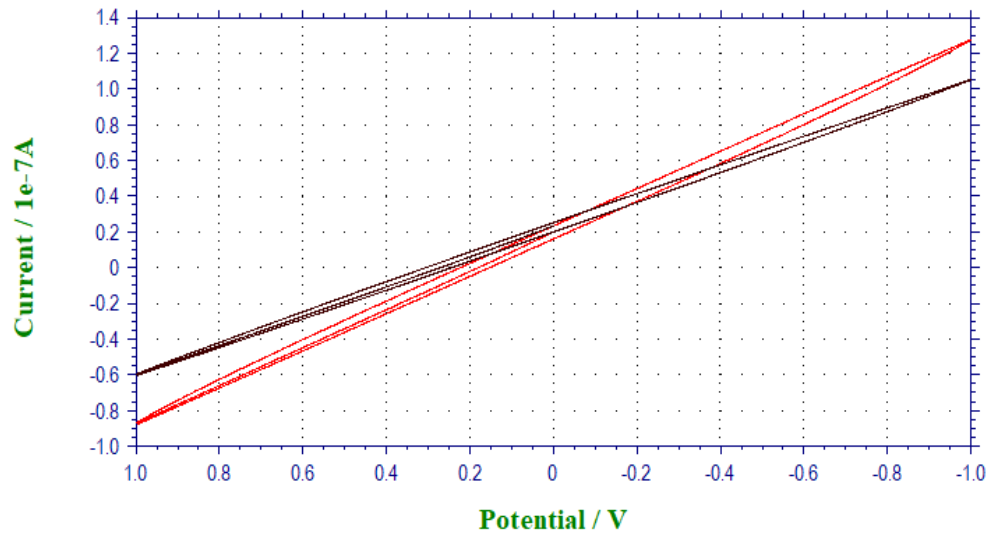
i-V curve obtained in air before (black) and after (red) electrodepositing Ag from 5 mM AgNO<sub>3</sub> in 0.1 M H<sub>2</sub>SO<sub>4</sub> at -0.5 V potential.



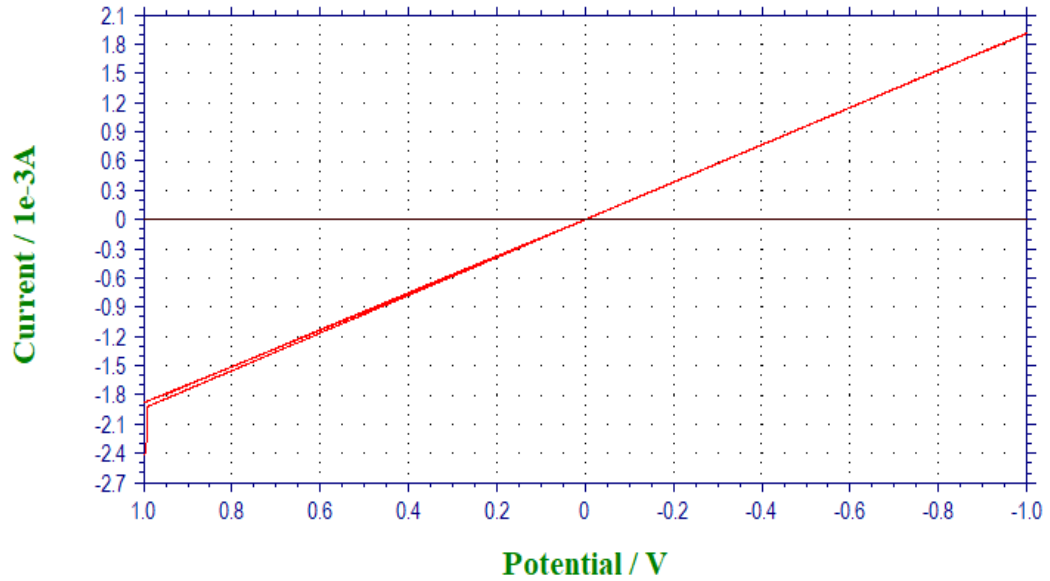
i-V curve obtained in air before (black) and after (red) electrodepositing Ag from 50 mM  $\text{AgNO}_3$  in 0.1 M  $\text{H}_2\text{SO}_4$  at -0.1 V potential.



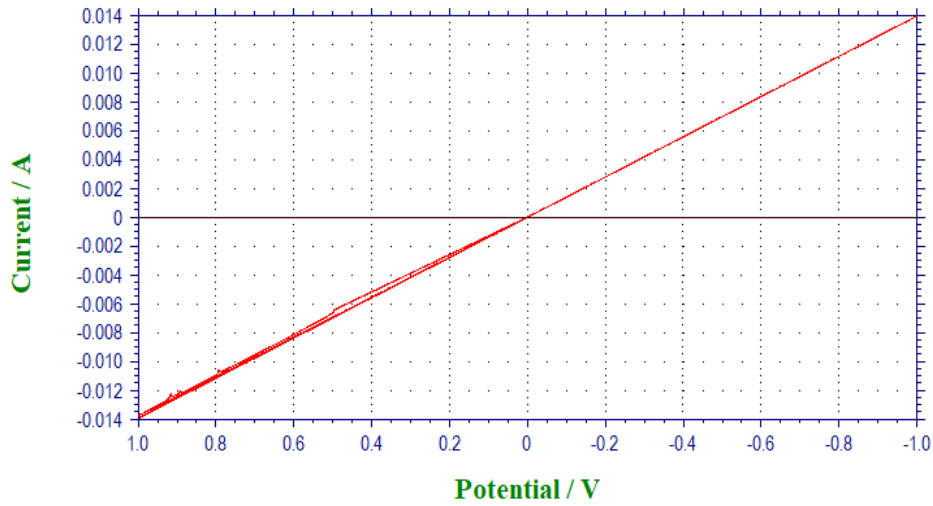
i-V curve obtained in air before (black) and after (red) electrodepositing Ag from 50 mM  $\text{AgNO}_3$  in 0.1 M  $\text{H}_2\text{SO}_4$  at -0.1 V potential.



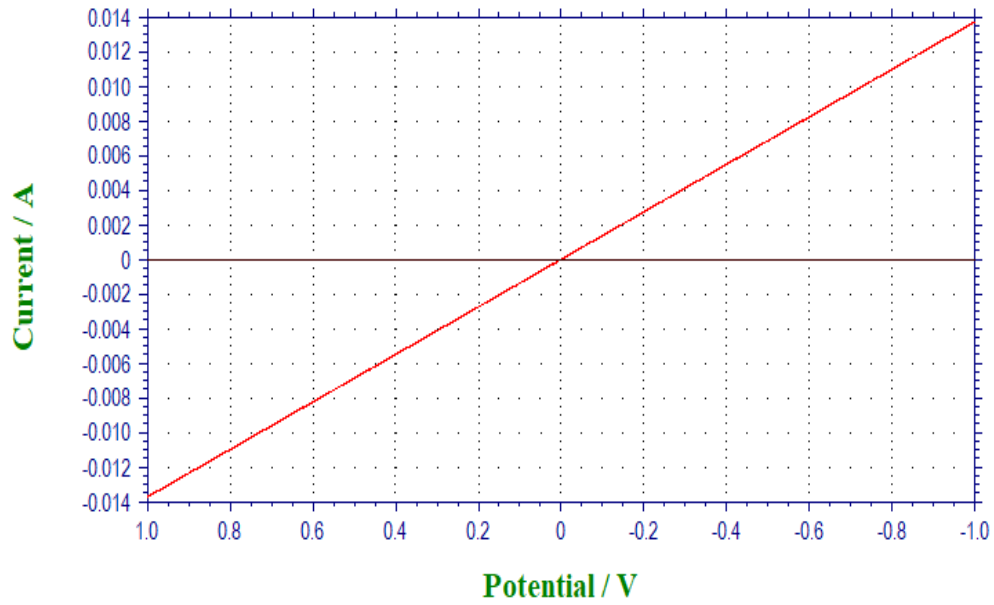
i-V curve obtained in air before (black) and after (red) electrodepositing Ag from 50 mM AgNO<sub>3</sub> in 0.1 M H<sub>2</sub>SO<sub>4</sub> at -0.2 V potential.



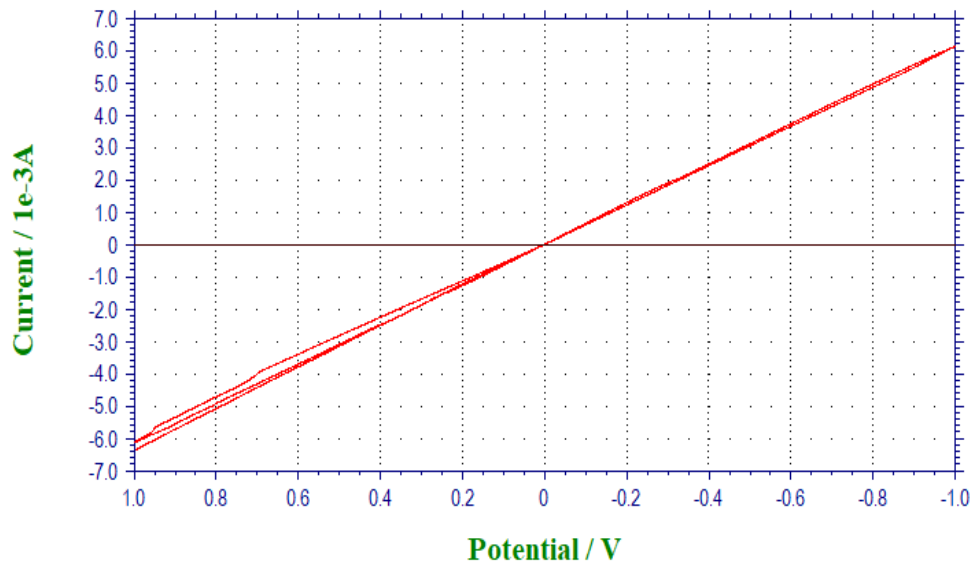
i-V curve obtained in air before (black) and after (red) electrodepositing Ag from 50 mM AgNO<sub>3</sub> in 0.1 M H<sub>2</sub>SO<sub>4</sub> at -0.2 V potential.



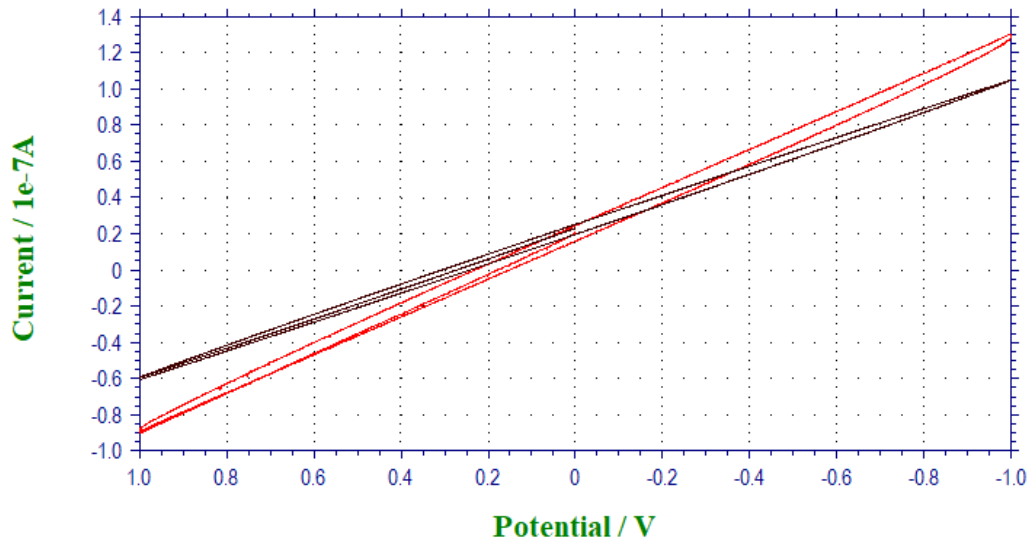
i-V curve obtained in air before (black) and after (red) electrodepositing Ag from 50 mM AgNO<sub>3</sub> in 0.1 M H<sub>2</sub>SO<sub>4</sub> at -0.3 V potential.



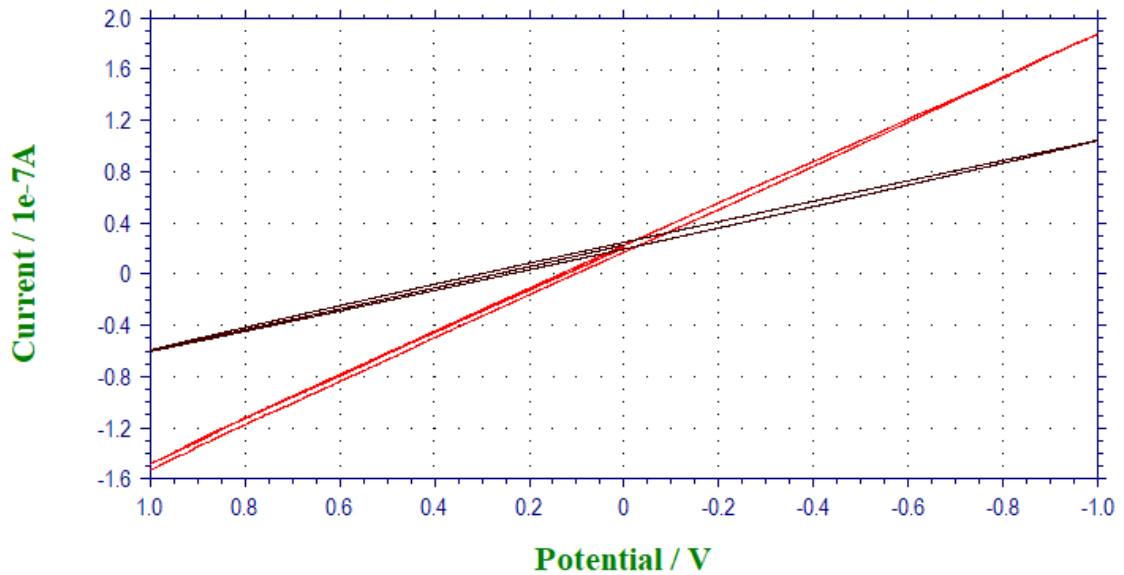
i-V curve obtained in air before (black) and after (red) electrodepositing Ag from 50 mM AgNO<sub>3</sub> in 0.1 M H<sub>2</sub>SO<sub>4</sub> at -0.3 V potential.



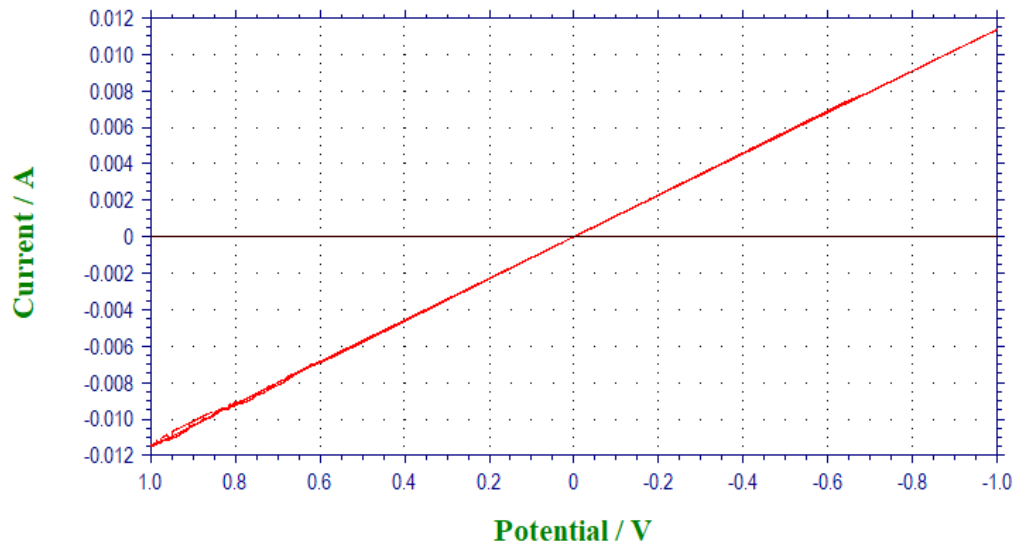
i-V curve obtained in air before (black) and after (red) electrodepositing Ag from 50 mM AgNO<sub>3</sub> in 0.1 M H<sub>2</sub>SO<sub>4</sub> at -0.4 V potential.



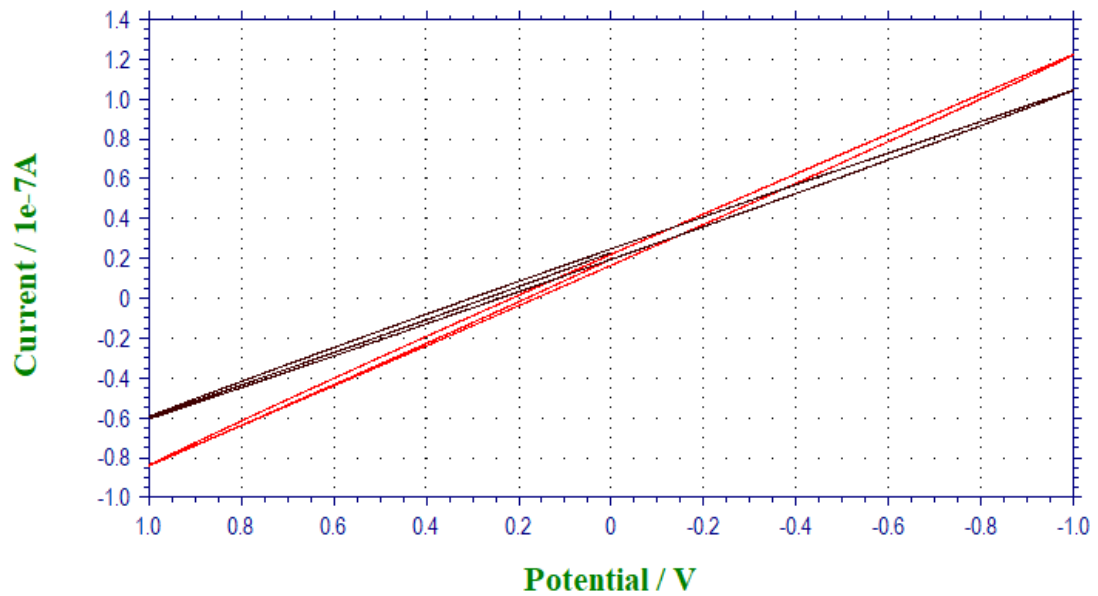
i-V curve obtained in air before (black) and after (red) electrodepositing Ag from 50 mM AgNO<sub>3</sub> in 0.1 M H<sub>2</sub>SO<sub>4</sub> at -0.4 V potential.



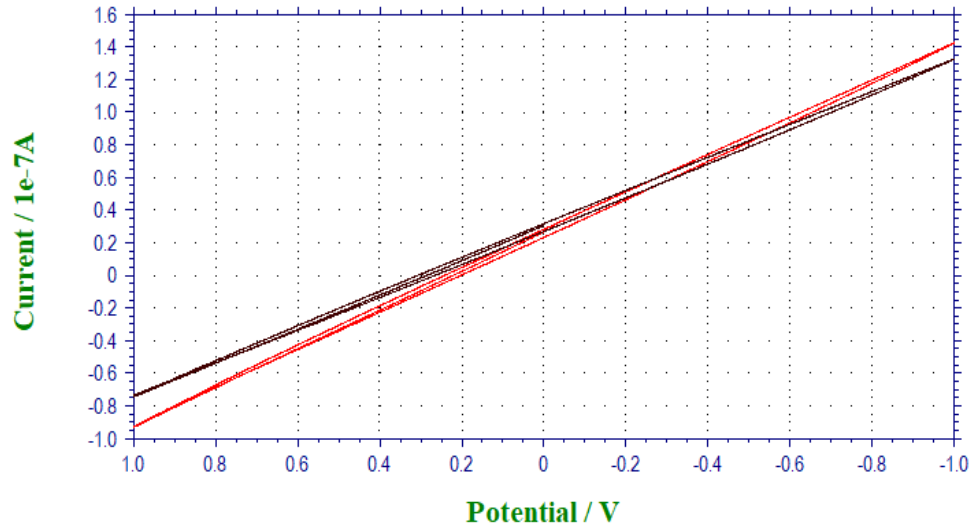
i-V curve obtained in air before (black) and after (red) electrodepositing Ag from 50 mM AgNO<sub>3</sub> in 0.1 M H<sub>2</sub>SO<sub>4</sub> at -0.5 V potential.



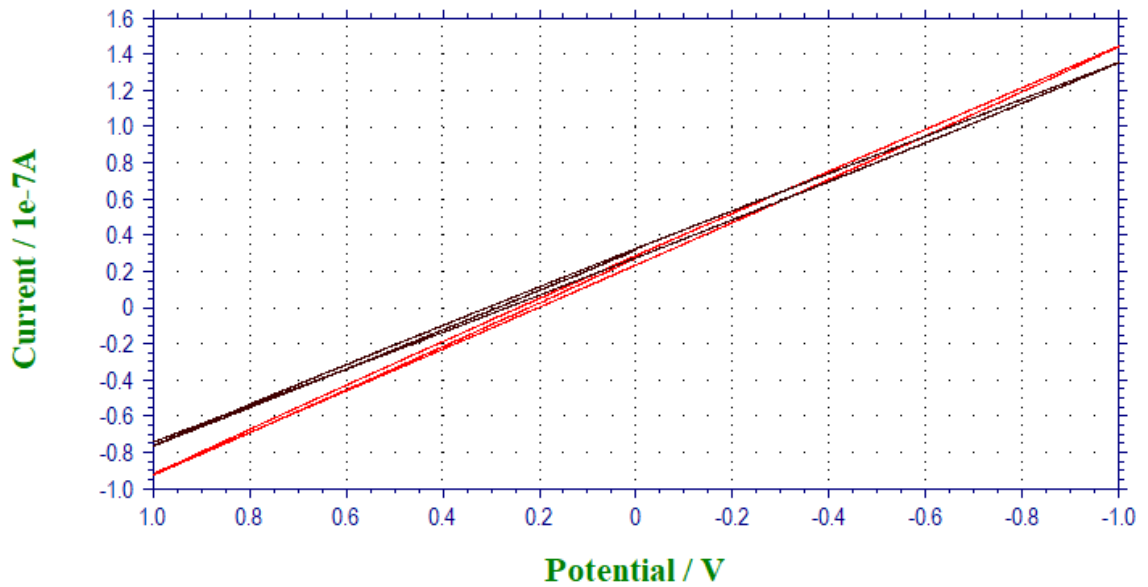
i-V curve obtained in air before (black) and after (red) electrodepositing Ag from 50 mM AgNO<sub>3</sub> in 0.1 M H<sub>2</sub>SO<sub>4</sub> at -0.5 V potential.



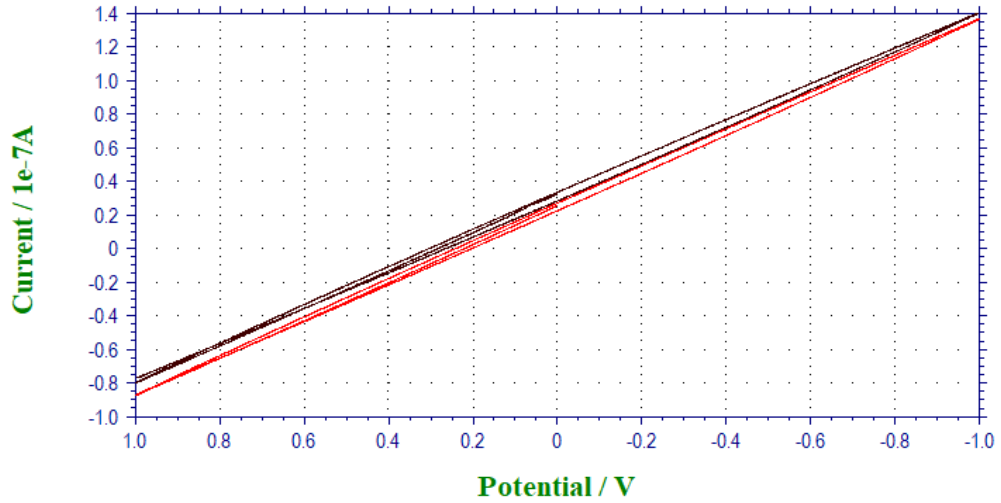
i-V curve obtained in air before (black) and after (red) electrodepositing Pd from 0.5 mM  $K_2PdCl_4$  in 0.1 M  $H_2SO_4$  at +0.1 V potential.



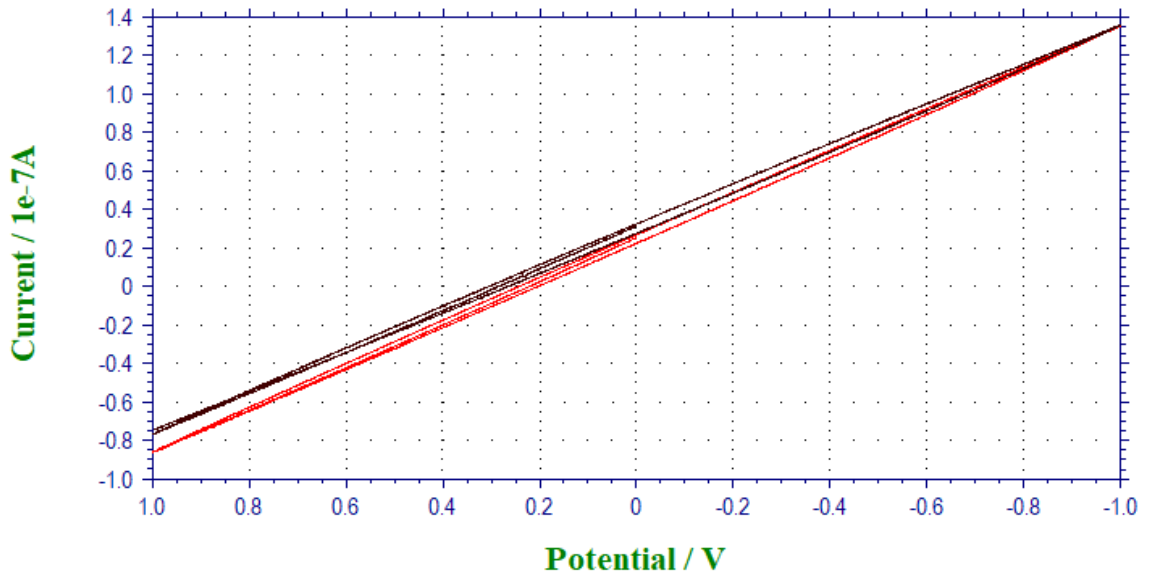
i-V curve obtained in air before (black) and after (red) electrodepositing Pd from 0.5 mM  $K_2PdCl_4$  in 0.1 M  $H_2SO_4$  at +0.1 V potential.



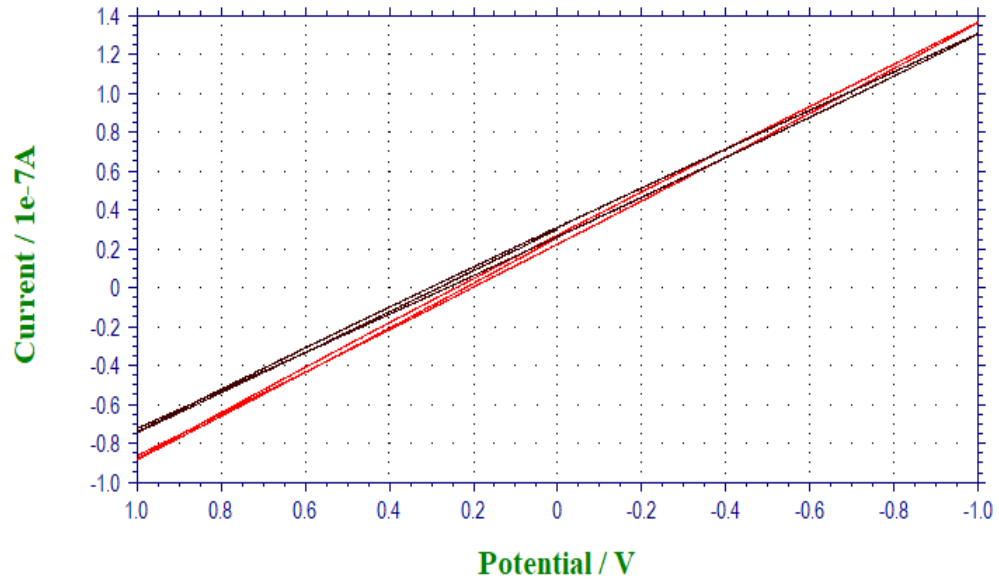
i-V curve obtained in air before (black) and after (red) electrodepositing Pd from 0.5 mM  $K_2PdCl_4$  in 0.1 M  $H_2SO_4$  at 0.0 V potential.



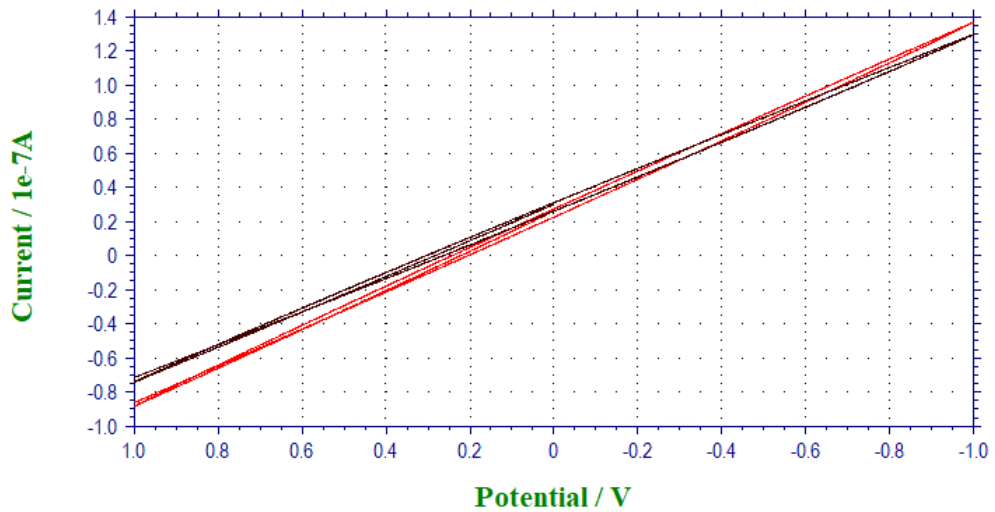
i-V curve obtained in air before (black) and after (red) electrodepositing Pd from 0.5 mM  $K_2PdCl_4$  in 0.1 M  $H_2SO_4$  at 0.0 V potential.



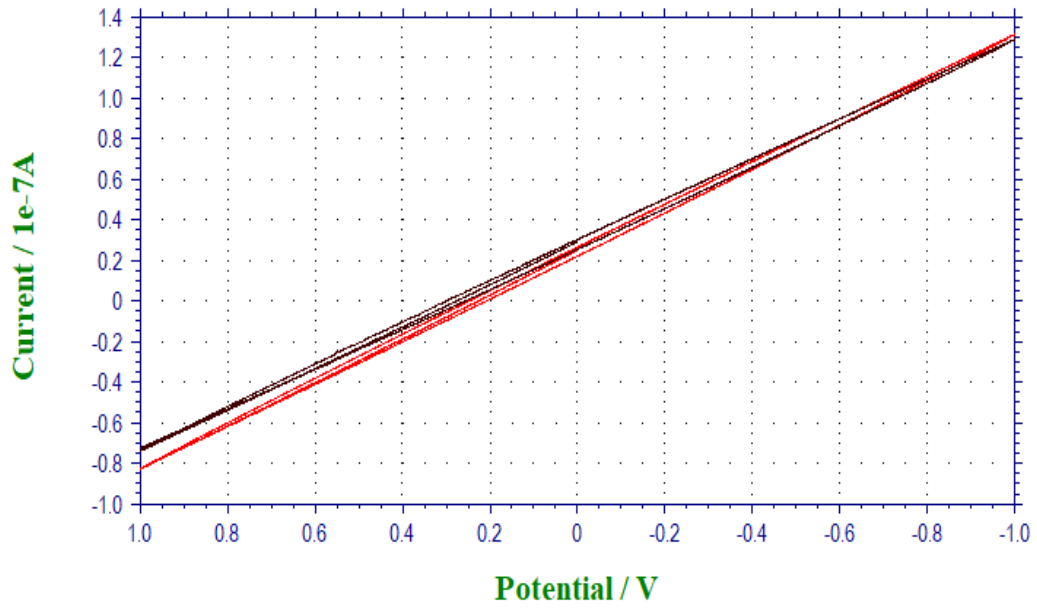
i-V curve obtained in air before (black) and after (red) electrodepositing Pd from 0.5 mM  $K_2PdCl_4$  in 0.1 M  $H_2SO_4$  at -0.1 V potential.



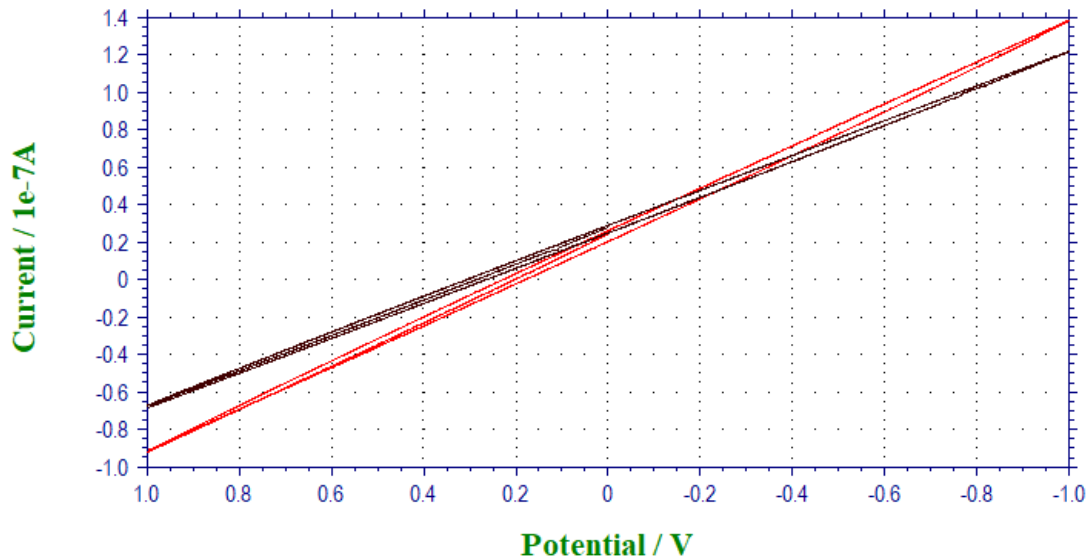
i-V curve obtained in air before (black) and after (red) electrodepositing Pd from 0.5 mM  $K_2PdCl_4$  0.1 M  $H_2SO_4$  at -0.1 V potential.



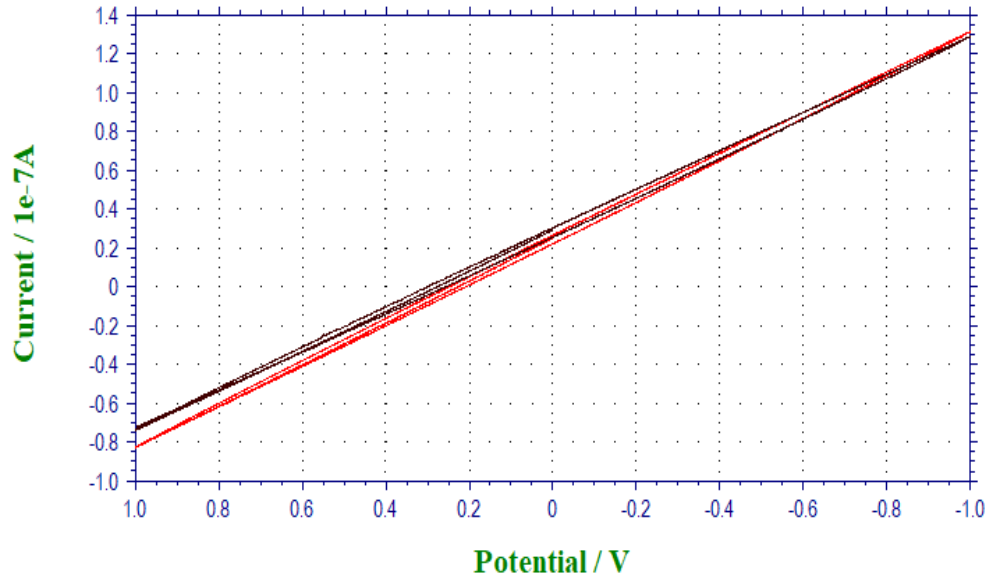
i-V curve obtained in air before (black) and after (red) electrodepositing Pd from 0.5 mM  $K_2PdCl_4$  in 0.1 M  $H_2SO_4$  at -0.2 V potential.



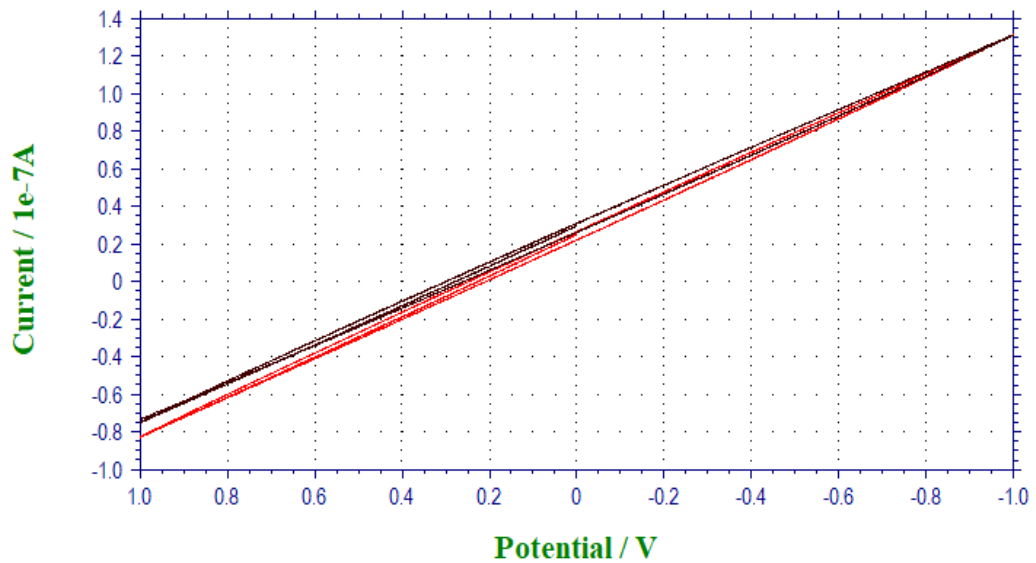
i-V curve obtained in air before (black) and after (red) electrodepositing Pd from 0.5 mM  $K_2PdCl_4$  in 0.1 M  $H_2SO_4$  at -0.2 V potential.



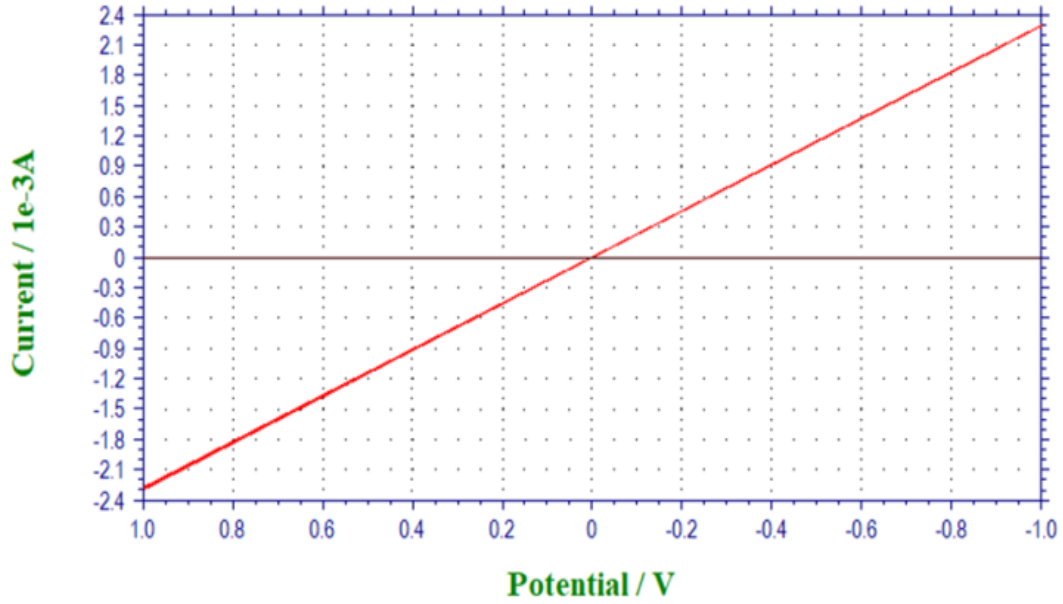
i-V curve obtained in air before (black) and after (red) electrodepositing Pd from 0.5 mM  $K_2PdCl_4$  in 0.1 M  $H_2SO_4$  at -0.3 V potential.



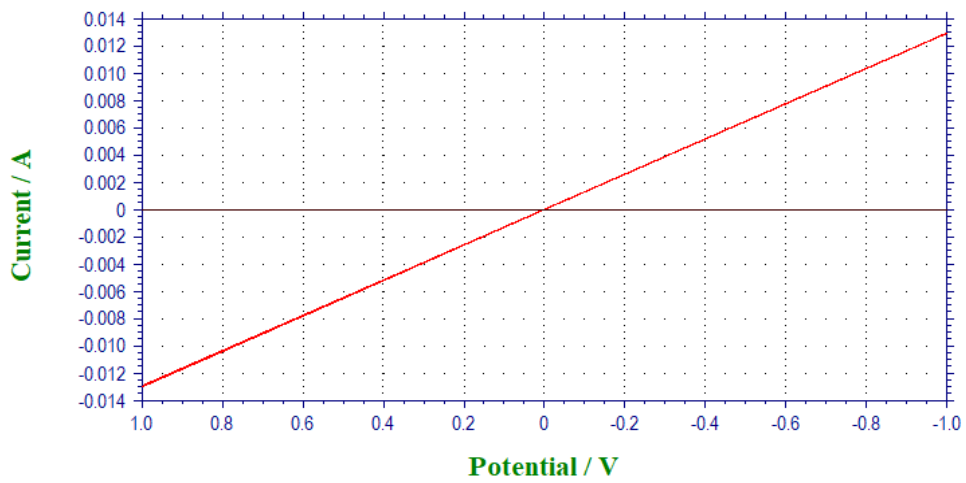
i-V curve obtained in air before (black) and after (red) electrodepositing Pd from 0.5 mM  $K_2PdCl_4$  in 0.1 M  $H_2SO_4$  at -0.3 V potential.



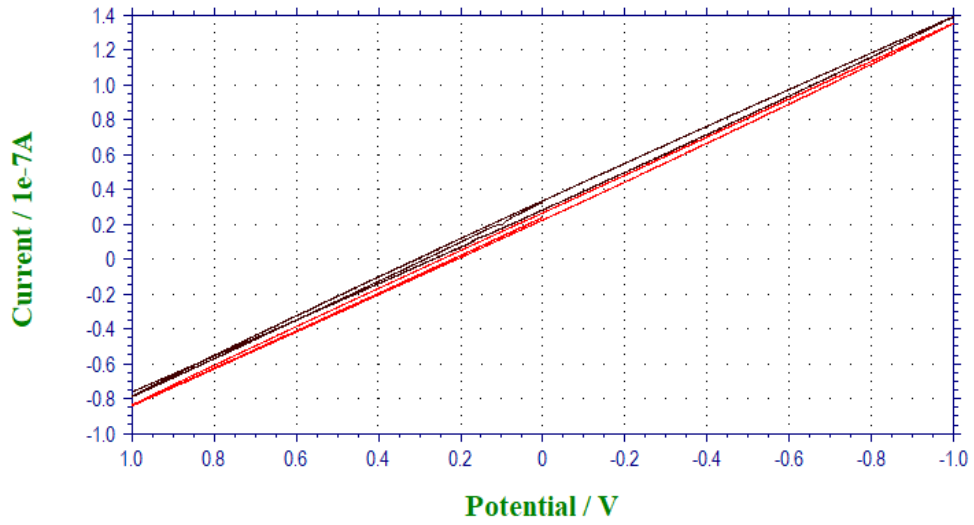
i-V curve obtained in air before (black) and after (red) electrodepositing Pd from 5 mM  $K_2PdCl_4$  in 0.1 M  $H_2SO_4$  at +0.1 V potential.



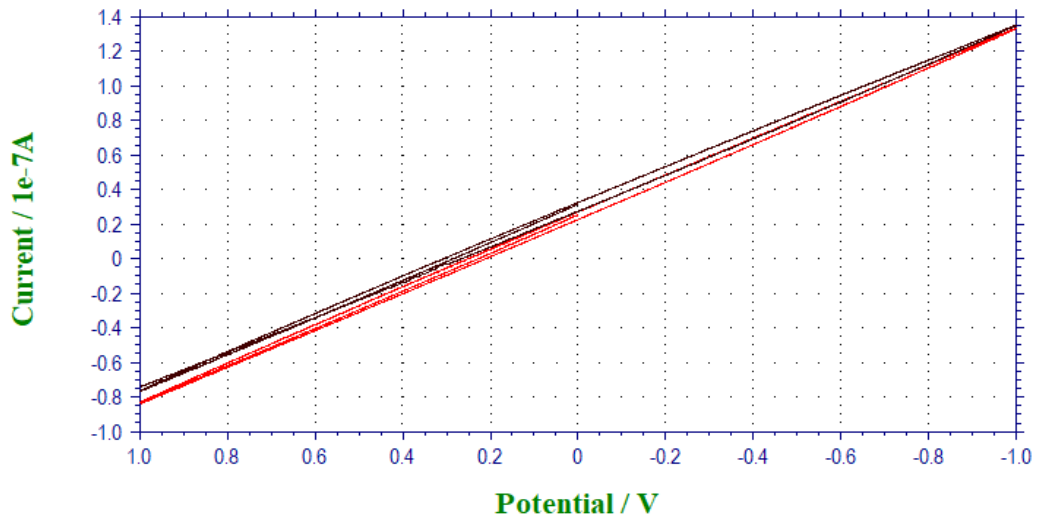
i-V curve obtained in air before (black) and after (red) electrodepositing Pd from 5 mM  $K_2PdCl_4$  in 0.1 M  $H_2SO_4$  at +0.1 V potential.



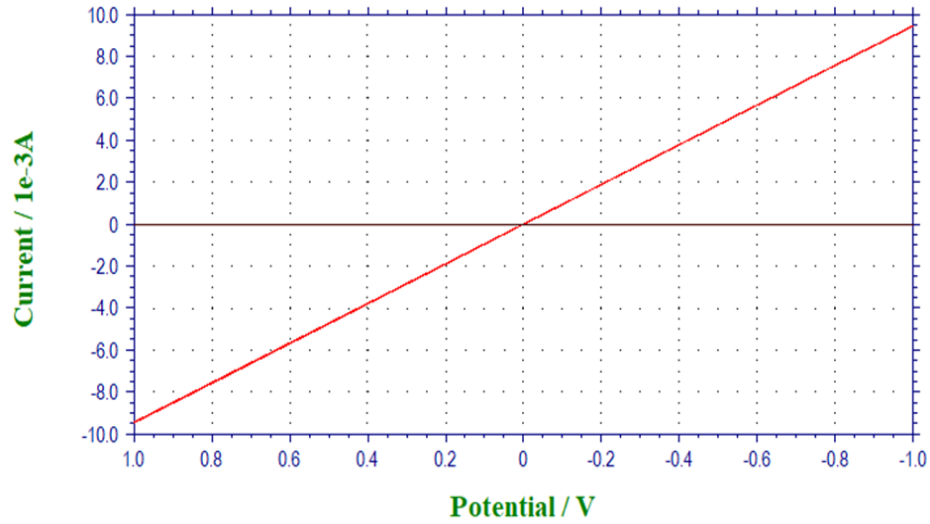
i-V curve obtained in air before (black) and after (red) electrodepositing Pd from 5 mM  $K_2PdCl_4$  in 0.1 M  $H_2SO_4$  at 0.0 V potential.



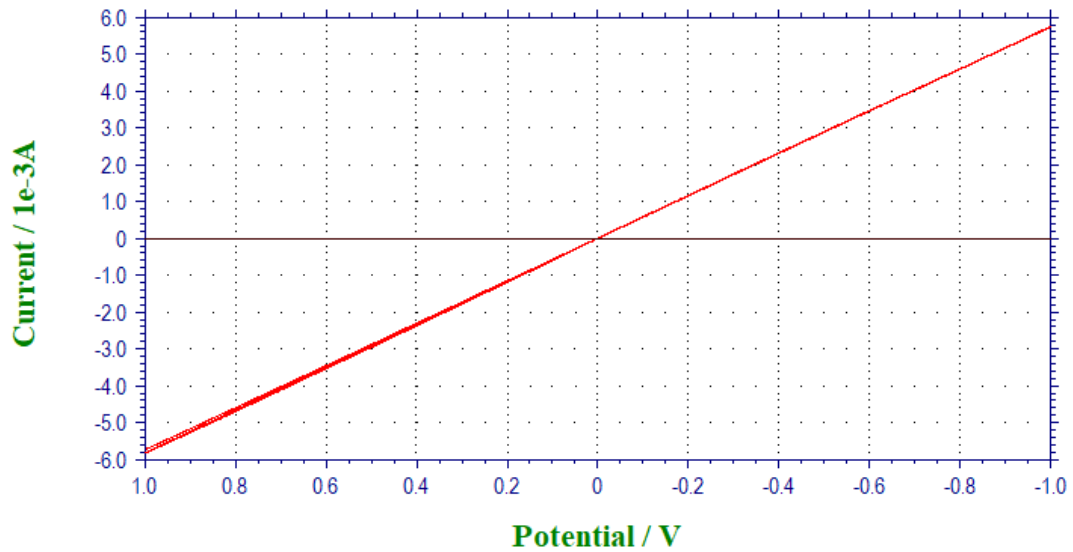
i-V curve obtained in air before (black) and after (red) electrodepositing Pd from 5 mM  $K_2PdCl_4$  in 0.1 M  $H_2SO_4$  at 0.0 V potential.



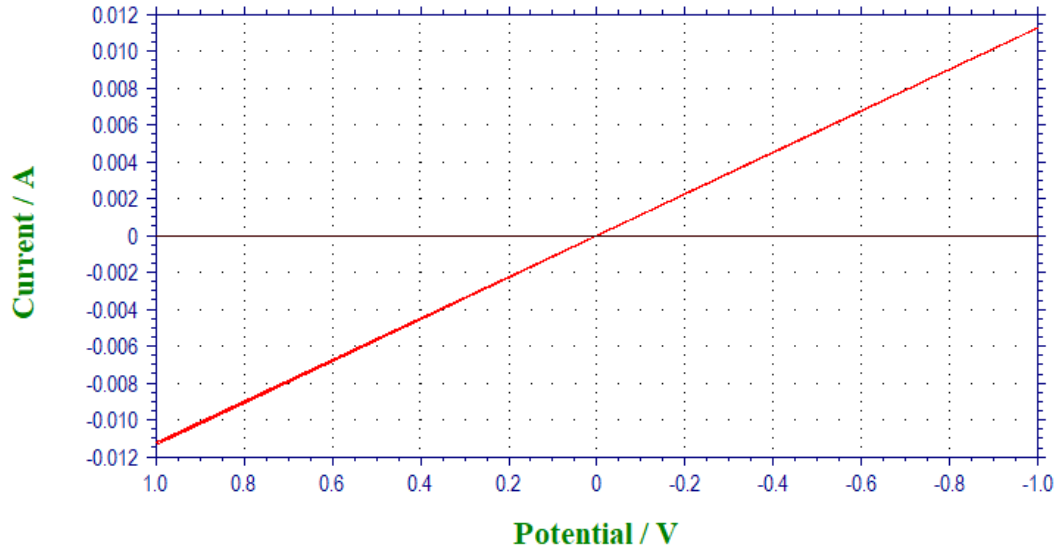
i-V curve obtained in air before (black) and after (red) electrodepositing Pd from 5 mM  $\text{K}_2\text{PdCl}_4$  in 0.1 M  $\text{H}_2\text{SO}_4$  at -0.1 V potential.



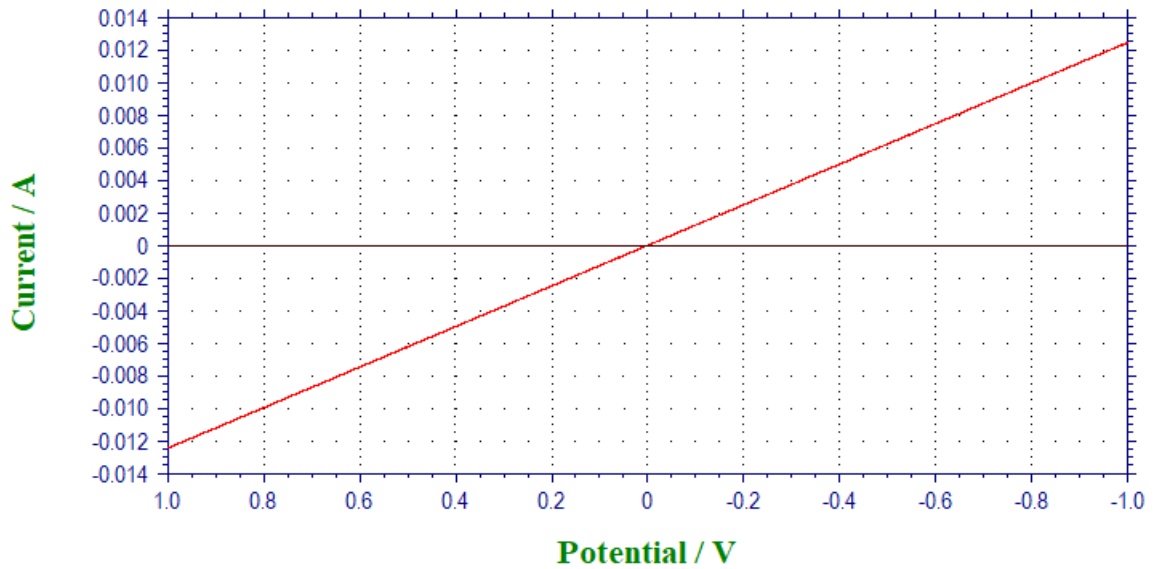
i-V curve obtained in air before (black) and after (red) electrodepositing Pd from 5 mM  $\text{K}_2\text{PdCl}_4$  in 0.1 M  $\text{H}_2\text{SO}_4$  at -0.1 V potential.



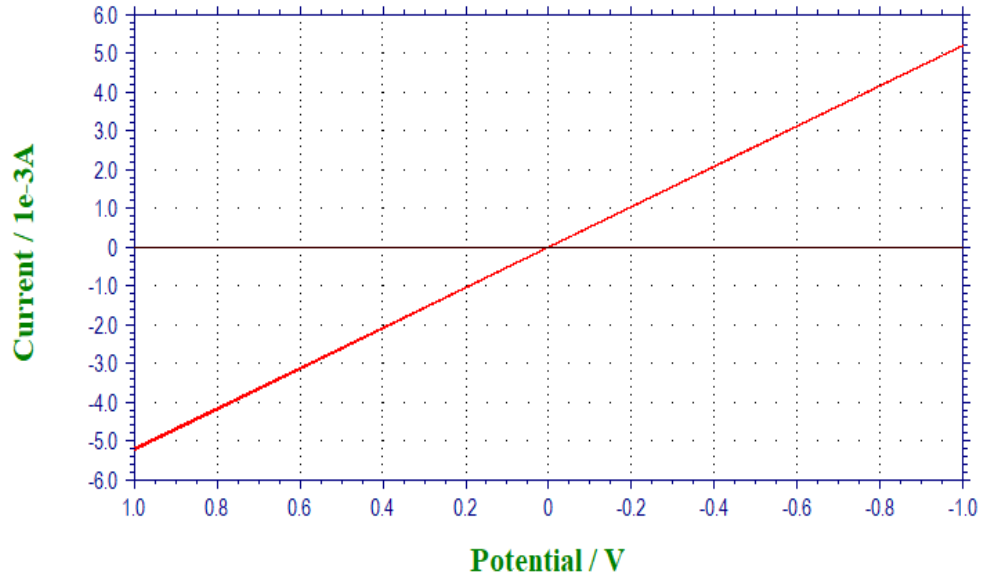
i-V curve obtained in air before (black) and after (red) electrodepositing Pd from 5 mM  $K_2PdCl_4$  in 0.1 M  $H_2SO_4$  at -0.2 V potential.



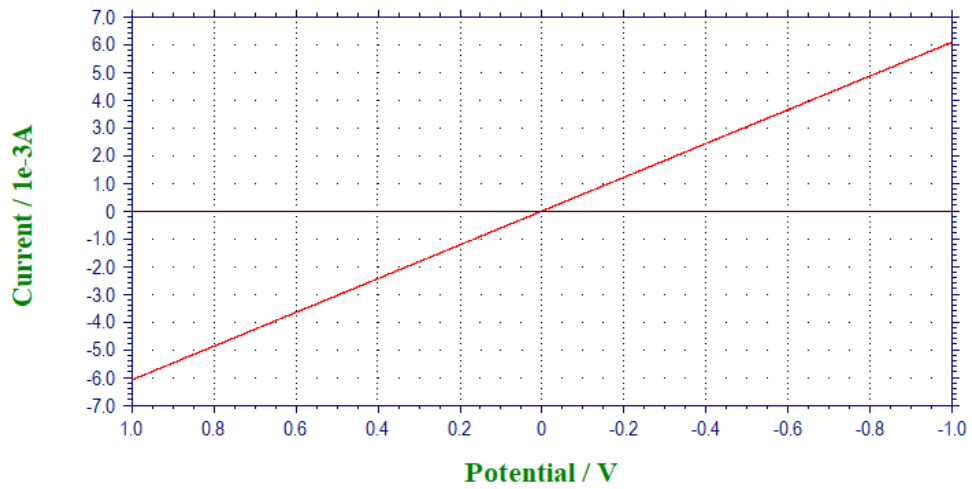
i-V curve obtained in air before (black) and after (red) electrodepositing Pd from 5 mM  $K_2PdCl_4$  in 0.1 M  $H_2SO_4$  at -0.2 V potential.



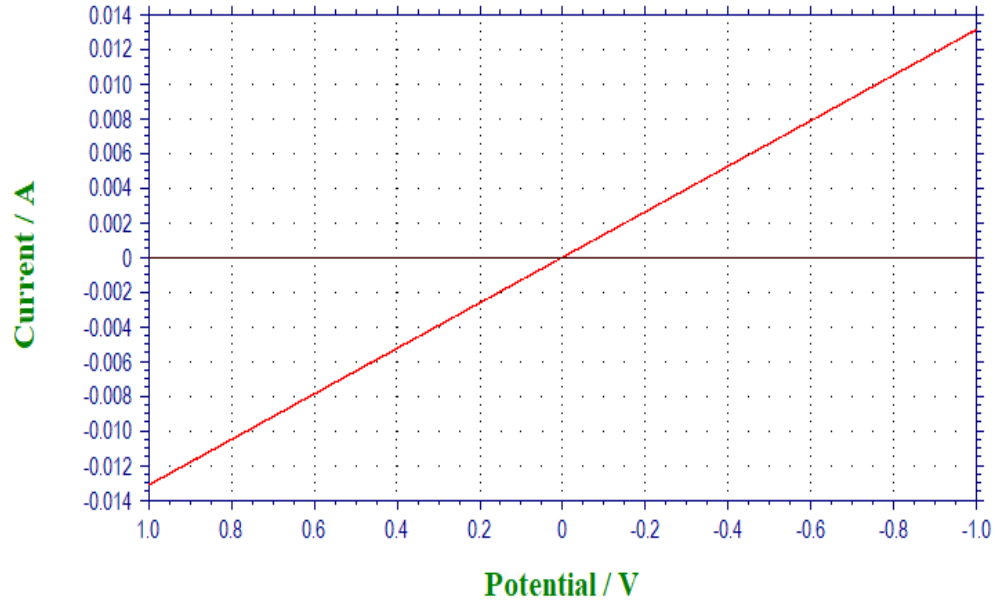
i-V curve obtained in air before (black) and after (red) electrodepositing Pd from 5 mM  $K_2PdCl_4$  in 0.1 M  $H_2SO_4$  at -0.3 V potential.



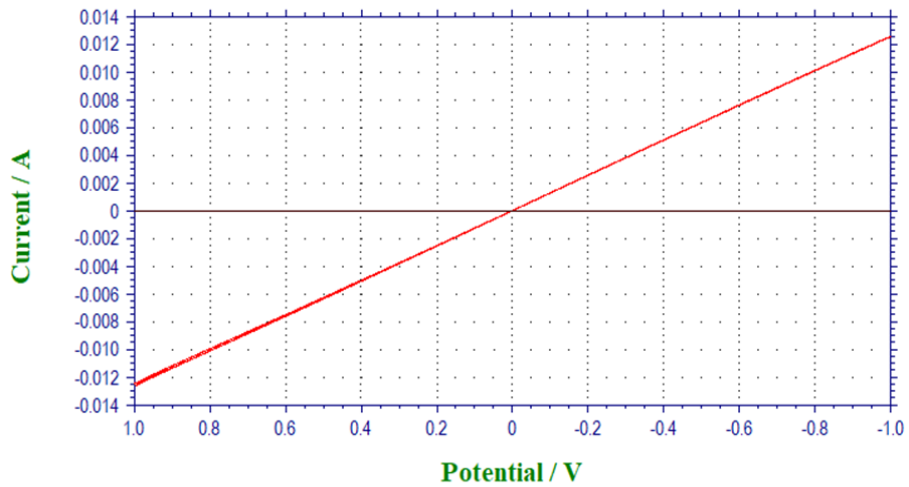
i-V curve obtained in air before (black) and after (red) electrodepositing Pd from 5 mM  $K_2PdCl_4$  in 0.1 M  $H_2SO_4$  at -0.3 V potential.



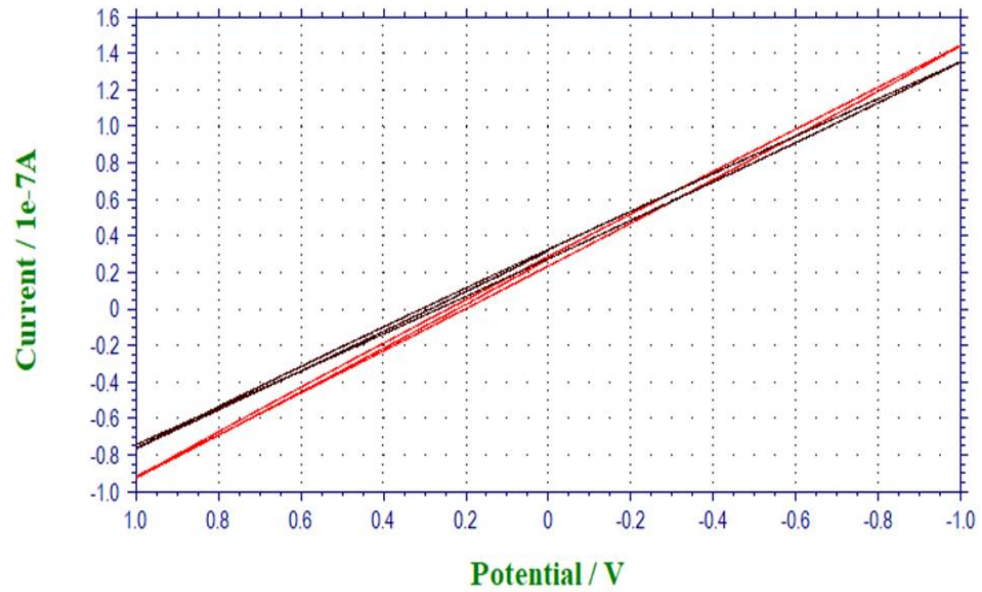
i-V curve obtained in air before (black) and after (red) electrodepositing Pd from 50 mM  $K_2PdCl_4$  in 0.1 M  $H_2SO_4$  at +0.1 V potential.



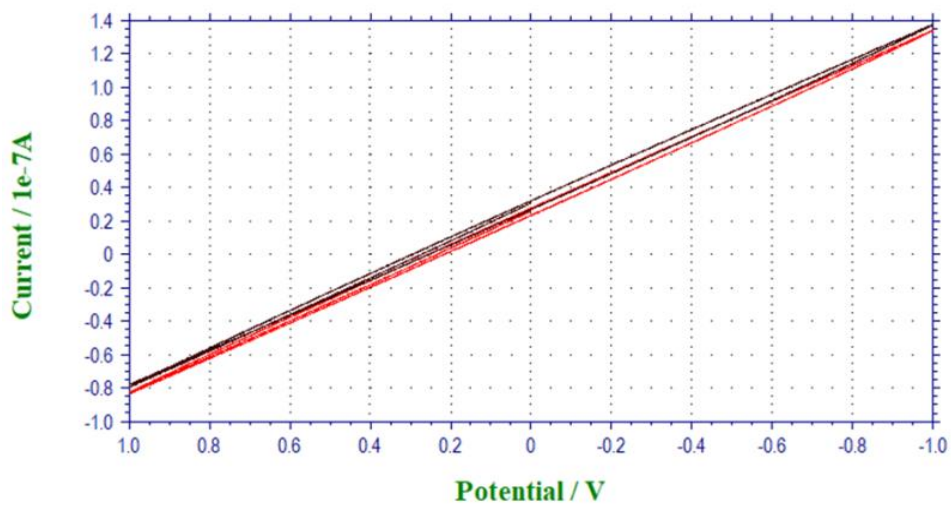
i-V curve obtained in air before (black) and after (red) electrodepositing Pd from 50 mM  $K_2PdCl_4$  in 0.1 M  $H_2SO_4$  at +0.1 V potential.



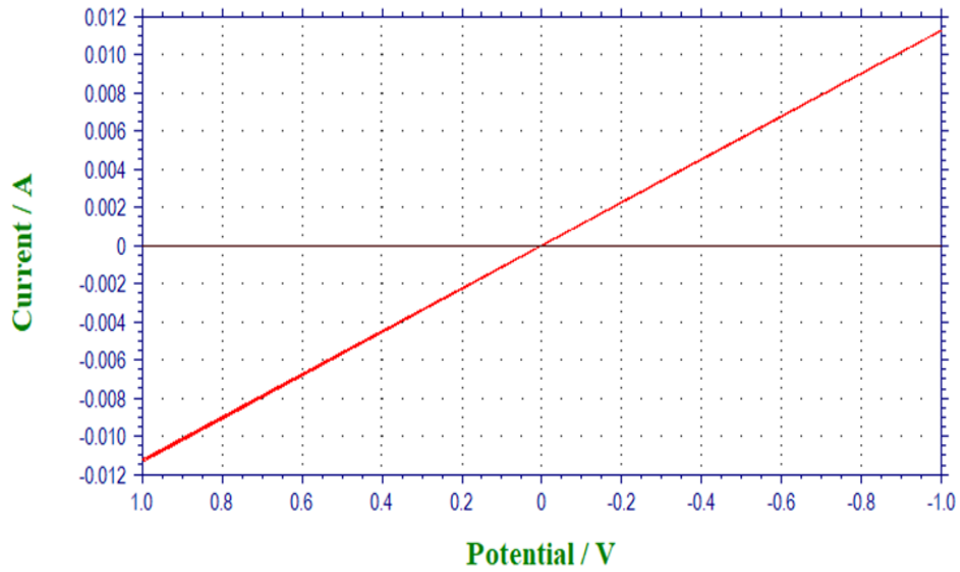
i-V curve obtained in air before (black) and after (red) electrodepositing Pd from 50 mM  $K_2PdCl_4$  in 0.1 M  $H_2SO_4$  at 0.0 V potential.



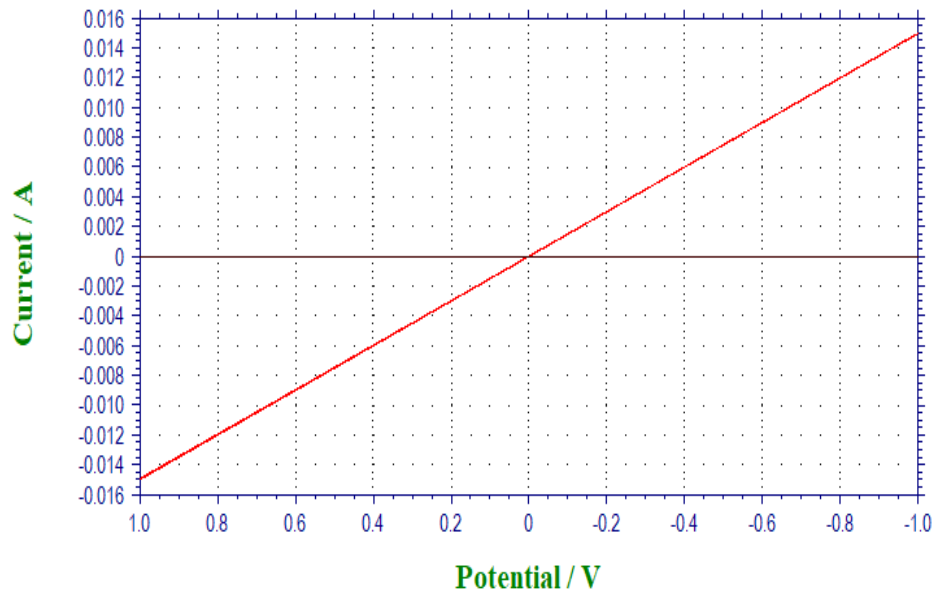
i-V curve obtained in air before (black) and after (red) electrodepositing Pd from 50 mM  $K_2PdCl_4$  in 0.1 M  $H_2SO_4$  at 0.0 V potential.



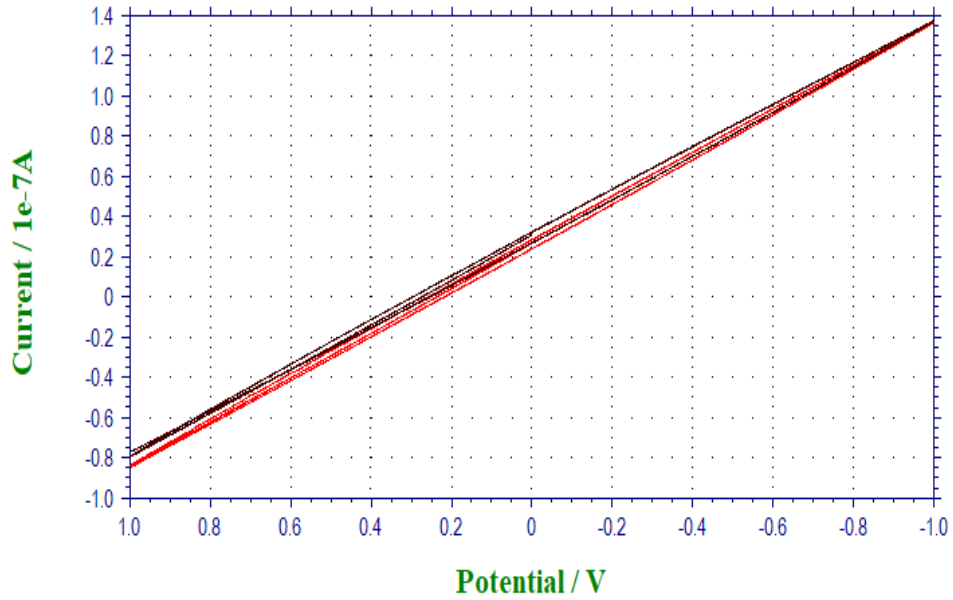
i-V curve obtained in air before (black) and after (red) electrodepositing Pd from 50 mM  $K_2PdCl_4$  in 0.1 M  $H_2SO_4$  at -0.1 V potential.



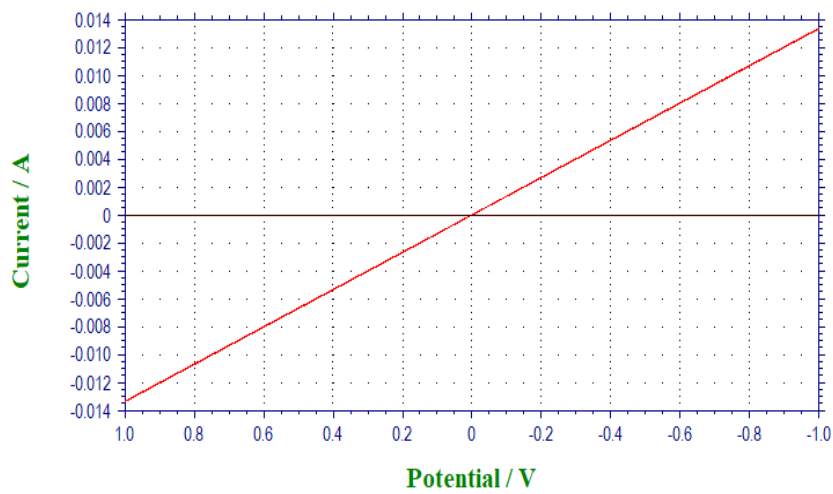
i-V curve obtained in air before (black) and after (red) electrodepositing Pd from 50 mM  $K_2PdCl_4$  in 0.1 M  $H_2SO_4$  at -0.1 V potential.



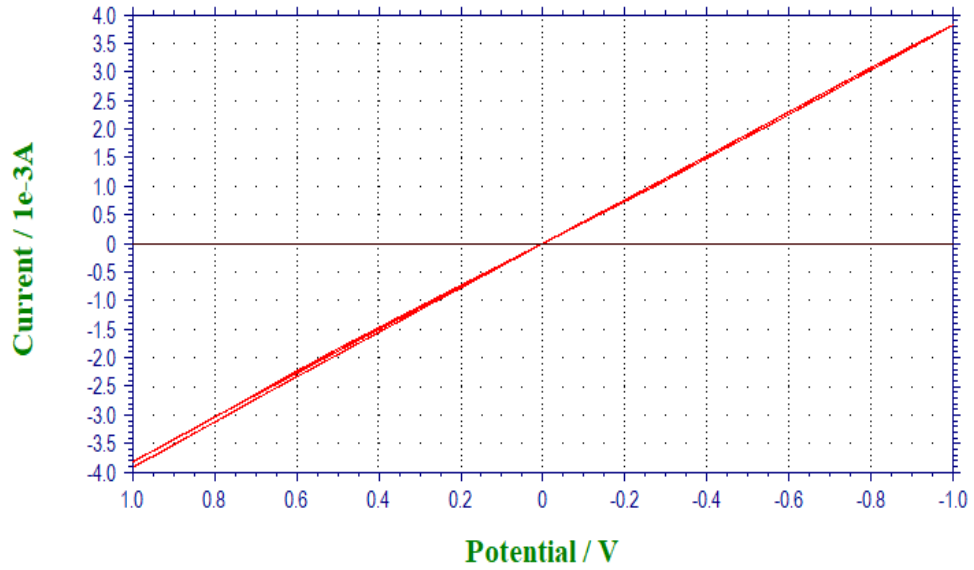
i-V curve obtained in air before (black) and after (red) electrodepositing Pd from 50 mM  $K_2PdCl_4$  in 0.1 M  $H_2SO_4$  at -0.2 V potential.



i-V curve obtained in air before (black) and after (red) electrodepositing Pd from 50 mM  $K_2PdCl_4$  in 0.1 M  $H_2SO_4$  at -0.2 V potential.



i-V curve obtained in air before (black) and after (red) electrodepositing Pd from 50 mM  $K_2PdCl_4$  in 0.1 M  $H_2SO_4$  at -0.3 V potential.



i-V curve obtained in air before (black) and after (red) electrodepositing Pd from 50 mM  $K_2PdCl_4$  in 0.1 M  $H_2SO_4$  at -0.3 V potential.

